SANDIA REPORT
SAND2020-5906
Printed August 2020

Sandia National Laboratories

Mechanical testing of PH13-8Mo H950 Steel for Xue-Wierzbicki Fracture Criterion Determination at 20° C and -40° C

Philip J. Noell, Priya R. Pathare, Zachary Casias, Todd Huber, John Laing, Jay D. Carroll

Prepared by
Sandia National Laboratories
Albuquerque, New Mexico
87185 and Livermore,
California 94550

Issued by Sandia National Laboratories, operated for the United States Department of Energy by National Technology & Engineering Solutions of Sandia, LLC.

Available to DOE and DOE contractors from
U.S. Department of Energy
Office of Scientific and Technical Information
P.O. Box 62
Oak Ridge, TN 37831

Telephone: (865) 576-8401
Facsimile: (865) 576-5728
E-Mail: reports@osti.gov
Online ordering: http://www.osti.gov/scitech

Available to the public from
U.S. Department of Commerce
National Technical Information Service
5301 Shawnee Rd
Alexandria, VA 22312

Telephone: (800) 553-6847
Facsimile: (703) 605-6900
E-Mail: orders@ntis.gov
Online order: https://classic.ntis.gov/help/order-methods/

ABSTRACT

Mechanical testing was conducted to collect the data needed to build a Xue-Wierzbicki (XW) fracture model for PH13-8 Mo H950 stainless steel (PH 13-8 SS). This model is intended for use in structural analysis of this material between room temperature and -40° C. Tests were performed on four different specimen geometries such that a range of stress states were characterized at room temperature and -40° C. Tensile tests on R5 tensile specimens were also performed to assess material anisotropy. Fracture toughness test were also conducted. The fracture toughness of this material at -40° C was 68% of the room-temperature value. Material strength generally increased with decreasing temperature while the opposite trend was observed for ductility. These trends were most pronounced for specimens with the largest stress triaxialities.

CONTENTS

LIST OF FIGURES

LIST OF TABLES

This page left blank

ACRONYMS AND DEFINITIONS

Abbreviation	Definition
DIC	Digital Image Correlation
TD	Tensile Direction
XW	Xue-Wierzbicki
ASTM	American Society for Testing and Materials
CT	Compact Tension
EDM	Electro-discharge Machining
EBSD	Electron backscatter diffraction
SEM	Scanning electron microscope
IPF	Inverse pole figure
ECCI	Electron Channeling Contrast Imaging

1. INTRODUCTION

Mechanical testing was conducted to collect the data needed to build a Xue-Wierzbicki (XW) [1] fracture model for PH13-8 Mo H950 stainless steel (PH 13-8 SS). This model is intended for use in structural analysis of this material between room temperature and -40° C. To calibrate the XW model, four parameters must be determined by testing specimens having the following loading conditions:

- two specimens with minimal ductility loss from a deviatoric stress state (Lode parameters of 1) but different stress triaxialities,
- pure shear (a stress triaxiality near 0.33), and
- transverse plane strain (a Lode parameter near 0).

These loading conditions can be accomplished by performing mechanical tests on specimens with different geometries. The four specimens used in this study to meet these conditions are pictured in **Figure 1-1**. The geometries of these specimens are identical to those described in reference [1]. Engineering drawings of all four specimens are provided in Appendix A. The average stress triaxiality (η) and average lode parameter (ξ) for each of these specimen designs are listed in **Table *1-1***. These values are all taken from calculations performed in reference [1]. The names of each specimen type are provided in **Table *1-1***. All specimen geometries were tested at both room temperature and at -40° C.

Table 1-1. The average stress triaxiality and Lode parameter for the six kinds of specimens tested in this study are listed. These values are taken from reference [1].

Specimen Name	η	ξ
3mm Notch	0.93	1.0
9mm Notch	0.63	1.0
Flat-groove	0.61	0.097
Shear specimen	0.0124	0.055
R5 radial	0.4	1.0
R5 parallel	0.4	1.0

All four of the specimen types described in the previous paragraph were extracted from a cylinder of PH 13-8 SS parallel to the length of the cylinder. A reference layout drawing is provided in Appendix A. To determine if the mechanical properties of this material varied between the parallel and the radial direction (see **Figure 1-2** for definitions of these terms), 18 unnotched round bars were also extracted, half having the tensile direction (TD) parallel to the circumference of the cylinder and the other half having the TD parallel to the long axis of the cylinder. These bars met the specification for R5 tensile bars from ASTM specification E8-16 [2] and will be referred to as R5-radial and R5-parallel. The η and ξ values associated with this specimen geometry are also provided in **Table *1-1***. Both kinds of R5 specimens were tested at both room temperature and at -40° C.

Figure 1-1. Examples of all the test specimens investigated in this study, excepting compact tension specimens, are shown. The specimens are, left to right: R5, flat-groove, 9mm notch, 3mm notch, and shear specimens.

To determine the fracture toughness of this material at both room temperature and at -40° C, compact tension (CT) specimens were also tested. Specimens were fabricated from the material in accordance with ASTM specification 399-17 [3]. An engineering drawing of this specimen type is provided in Appendix A.

The following sections describe:

- the material, mechanical methods, and microscopy methods,
- the results, both mechanical data and fractography, for each specimen type, and
- a brief discussion of these results with conclusions.

The results section contains representative plots of stress *versus* strain for each sample type. Plots of stress *versus* strain for all tested specimens are provided in Appendix B.

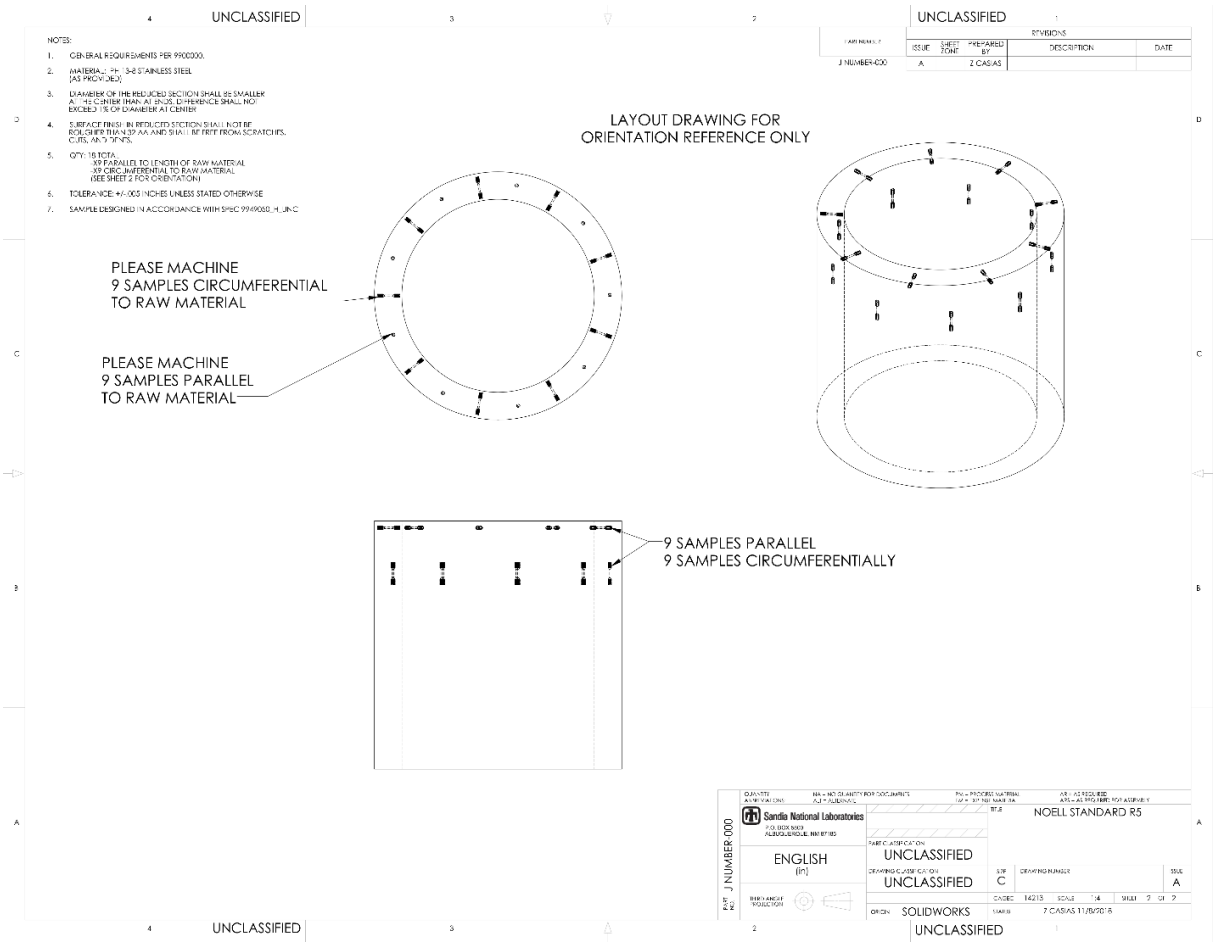

Figure 1-2. The layout of the specimens used in this study relative to the circumference and length of the cylinder from which they were extracted is shown. All specimens except the R5 radial specimen were extracted with the loading axis parallel to the length of this cylinder.

2. MATERIAL AND METHODS

2.1. Material

A PH13-8Mo H950 stainless steel was used in this study. This is a martensitic, precipitation-hardened stainless steel. Following the H950 heat treatment, the yield strength and ultimate strength of this material are typically ≈205 and ≈220 ksi, respectively, and the ductility is ≈10% [4]. The minimum mechanical properties for PH13-8Mo H950 stainless steel are summarized in Table 2-1. Based on the results of the tensile tests described in subsequent sections, this material meets the ASM specification AMS5629H for PH13-8Mo H950 [5]. For consistency, all test samples were fabricated from a single cylinder of this material. Samples were extracted using wire electro-discharge machining (EDM) and subsequently machined.

Table 2-1. PH13-8Mo H950 specification minimum material properties.

Ultimate Strength	220 ksi
Yield Stress	205 ksi
Modulus of Elasticity	28.3*10^3 ksi
Poisson's Ratio	0.28
Reduction of Area	45% longitudinal, 35% transverse
Elongation	10%

2.2. Mechanical Test Methods

All specimens were tested in uniaxial tension using an MTS® servo hydraulic load frame (SN645 01851 Four Post Frame 2B). One Tovey Engineering Inc. 60kip loadcell (SN114832A) was used to measure force on each of the samples. The load cell was subranged for specific tests to give more force precision. The subrange for each test is documented in Table 2-2 below along with the crosshead displacement rate, camera type, and lens arrangement.

Table 2-2. Table of testing criterion used to test each type of specimen. The same loadcell and LVDT was used for each sample. The loadcell was subranged to provide more precision at smaller loads.

Specimen Name	Load Cell Subrange (kip)	Displacement Rate (mm/sec)	Camera (MPx) (FLIR/PointGrey)	Lens Setup (Navitar Lens)
3mm Notch	20	.008	12	12x, 2x adapter, .25x lens
9mm Notch	20	.001	2.3	12x, 1x adapter, .25x lens
Flat-groove	20	.003	2.3	12x, 1x adapter, .25x lens
Shear specimen	5	.012	12	12x,1x adapter, .25x lens
R5 radial	5	.012	2.3	12x, 1x adapter, .25x lens

Specimen Name	Load Cell Subrange (kip)	Displacement Rate (mm/sec)	Camera (MPx) (FLIR/PointGrey)	Lens Setup (Navitar Lens)
R5 parallel	5	.012	2.3	12x, 1x adapter, .25x lens

An environmental chamber attached to the load frame was used to perform testing at -40° C. Liquid nitrogen was pumped into the chamber and temperature was controlled using an Applied Test System™ temperature controller, see **Figure 2-1**. Samples were preloaded to a small amount of force and left to cool for 20-30 min. Actuator displacement was monitored until the displacement stabilized to assure that the load train had equilibrated to the oven temperature.

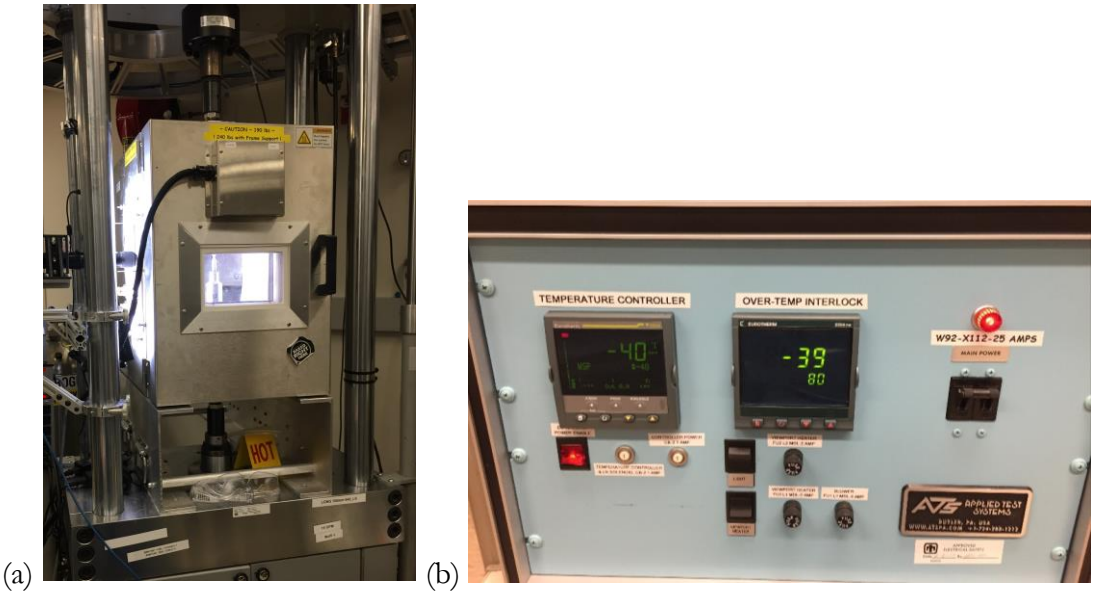

Figure 2-1. Images of the load frame used to perform tensile testing (left) and the ATS temperature controller used to control the temperature within the test chamber (right) are shown.

Strain was measured during testing using digital image correlation (DIC) with Correlated Solutions Vic Gauge 2® software. Images were taken using a FLIR/PointGrey camera and Navitar lenses. The specific hardware setups are cataloged in Table 2-2. Samples were preloaded to 20-50lbs, held for .5 sec to trigger the DAQ and the cameras, and then pulled in tension to failure. The cameras and DAQ were digitally controlled to start and stop by the procedure. Vic Gauge 2D® software allows the user to create up to two virtual extensometers. Strain is then measured across these extensometers throughout testing. For all specimens except the R5 specimens, two virtual extensometers were used during testing. The location of the virtual extensometers used for each specimen are reported in subsequent sections. Full-field strain measurements were subsequently measured for select samples using Vic 2D® software.

For most samples, during the cold temperature testing, frost, air currents, and thermal gradients created significant optical noise, causing noise in strain data, see *e.g.* Figure 3-28. This was particularly pronounced for the elastic regime. The cold temperatures also caused the speckle coating to crack when the samples were pulled. This caused the paint to chip away making full field correlation lose tracking during the test. Despite these challenges, useful data was still obtained from

tests at cold temperatures, though with a slightly lower strain resolution than during room-temperature testing.

Samples were speckled for DIC using a silicon ceramic spray paint. A white base coat was first applied followed by a black speckle coat for contrast. Dimensional measurements were taken before speckling the samples. Gauge diameters were measured using Mitutoyo calipers (serial number B17177394). Diameters and subsequent area measurements for individual specimens are reported in Sections 2.1.1 – 2.1.6.

The following subsections describe the specific mechanical test methods used to test each of the specimen types.

The extensometer length used to test each specimen varied slightly specimen to specimen. The lengths of extensometers were measured after testing each specimen. These extensometer lengths are summarized for the R5, 9mm notch and 3mm notch specimens in Table 2-3. Extensometer lengths are not included for the 3mm and 9mm notch specimens for which force *versus* displacement curves are provided in the appendix.

Table 2-3. The extensometer lengths for the R5, 9mm notch and 3mm notch specimens are summarized excepting the 3mm and 9mm notch specimens for which force *versus* displacement data are included in the appendix.

R5 Rad	Extensometer Length (mm)	R5 Par	Extensometer Length (mm)	3mm	Extensometer Length (mm)	9mm	Extensometer Length (mm)
10	16.68	1	16.22	1	-	1	-
11	15.53	2	16.10	2	7.60	2	23.86
12	15.52	3	16.14	3	7.41	3	23.96
13	15.48	4	15.60	4	-	4	-
14	15.49	5	15.51	5	7.83	5	22.76
15	15.60	6	15.51	6	7.79	6	19.21

2.2.1. 3mm Notch Specimens

The extensometer locations and the image setup for the 3mm samples are displayed in **Figure 2-2**. Images of the test setup used for 3mm notch samples are provided in **Figure 2-3**. Samples were loaded in tension at a displacement rate of .008 mm/sec using a servo hydraulic MTS load frame. Two ½-20 UNF threaded grips were used to pull the 3mm samples in tension. A sacrificial sample was first tested to check the procedure and to establish an appropriate displacement rate and camera rate. Samples 1-3 were tested at 22°C and samples 4-6 were tested at -40°C. Strain measurements reported in subsequent sections for the 3mm notch specimen are based off strain measurements from the long extensometer (see **Figure 2-2**). The approximate length of the extensometers used to test these specimens was 7.6 mm. The dimensions of all 3mm notch specimens tested are provided in **Table *2-4***.

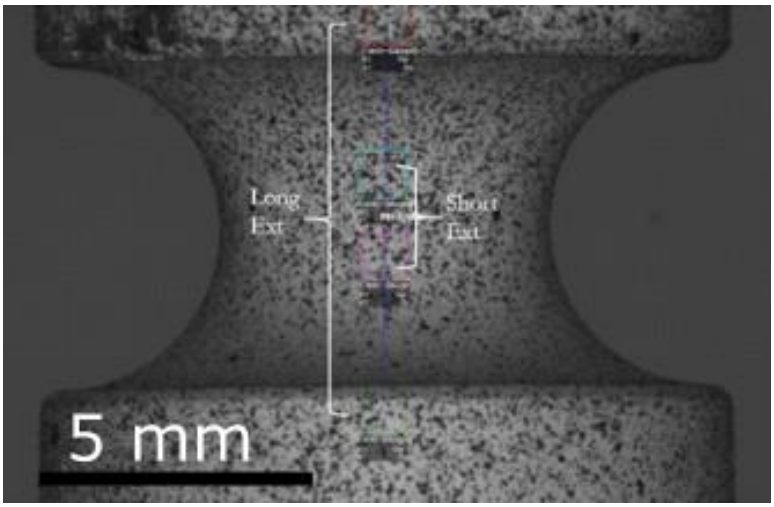

Figure 2-2. The location of short and long virtual extensometers for 3mm notch specimens are shown.

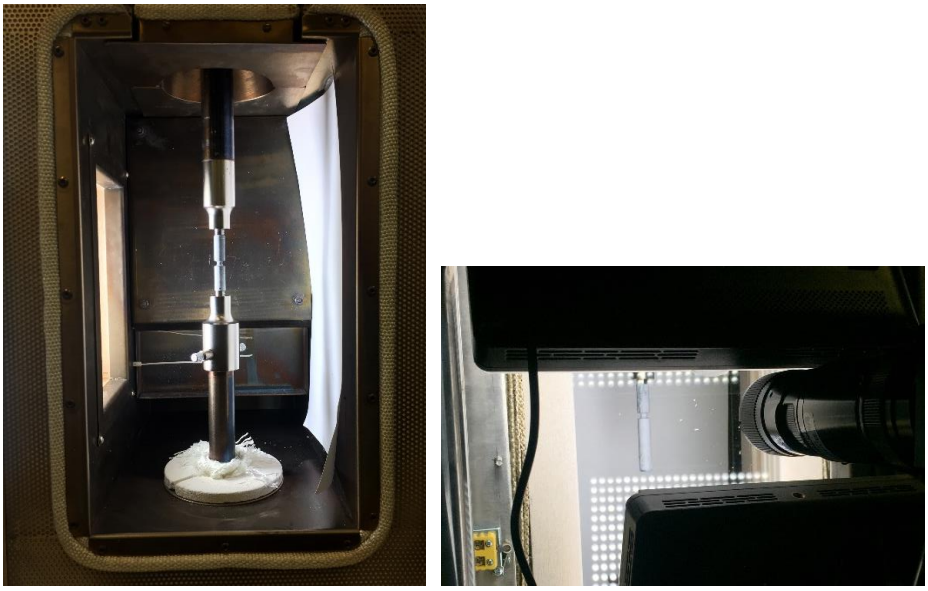

Figure 2-3. Images of the test setup for the 3mm notch samples are shown (chamber door removed for photos).

Table 2-4. The dimensions of 3mm notch specimens are summarized.

3mm Sample #	Gauge Diameter (mm)	Area (mm^2)
Sample 01	6.00	28.27
Sample 02	5.99	28.18
Sample 03	6.00	28.27
Sample 04	6.00	28.27
Sample 05	5.99	28.18

3mm Sample #	Gauge Diameter (mm)	Area (mm^2)
Sample 06	5.99	28.18

2.2.2. 9mm Notch Samples

The extensometer locations and the image setup for the 9mm notch samples are displayed in **Figure 2-4** and **Figure 2-5**. Samples were loaded in tension at a displacement rate of .01 mm/sec using a servo hydraulic MTS load frame. ½-20 UNF grips were also used to test the 9mm samples. One sample (Sample 07) was first tested to check the procedure and establish an appropriate displacement rate and camera rate. Samples 1-3 were tested at 22° C and samples 4-6 were tested at -40° C. Strain measurements reported in this study for the 9mm notch specimen were made using the long extensometer. The approximate length of this extensometer is 22 mm. The dimensions of all 9mm notch specimens tested are provided in **Table *2-5***.

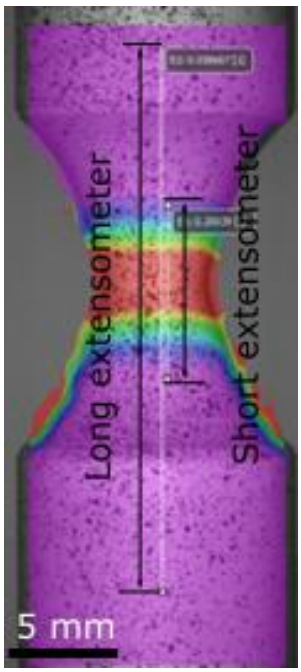

Figure 2-4. The locations of extensometers for the 9mm notch samples are shown.

Table 2-5. The dimensions of 9mm notch specimens are summarized.

9mm Sample #	Gauge Diameter (mm)	Area (mm^2)
Sample 01	5.94	27.71
Sample 02	5.95	27.81
Sample 03	5.94	27.71
Sample 04	5.95	27.81
Sample 05	5.95	27.81
Sample 06	5.94	27.71

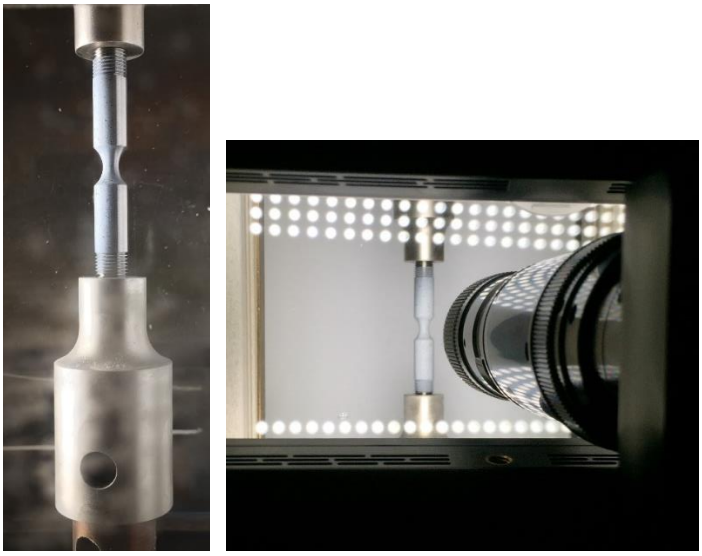

Figure 2-5. Images of the test setup for the 9mm notch samples are shown (chamber door removed for photos).

2.2.3. Flat Groove Samples

Pinch grips rated to 10 kip were installed in the load frame to test the flat groove samples. The extensometer locations and the setup for the flat groove samples are displayed below in **Figure 2-6** and **Figure 2-8**. Samples were loaded in tension at a displacement rate of .003 mm/sec using a servo hydraulic MTS load frame. One sample (Sample 07) was first tested to check the procedure and establish an appropriate displacement rate and camera rate. Samples 1, 2, 8 were tested at 22°C and samples 3-6 were tested at -40°C. All strain measurements reported in this study for this specimen are from the extensometer labelled as the "short extensometer" in **Figure 2-6**. The approximate length of this extensometer is 5.1 mm. The dimensions of the flat groove specimens tested in this study are reported in **Table *2-6***.

As **Figure 2-6** shows, strain was not applied uniformly to the flat groove specimens. Misalignment of the pinch grips created a slight bending moment in the samples. Evidence of this can be seen in the elastic loading region of flat groove specimens, see *e.g.* Figure 3-26. Because of this, the strain at failure for all flat groove specimens was typically ≈50% greater on the left side of the sample as on the right side of the sample. Average strain at failure values reported in this study were made using extensometers positioned in the center of the sample. However, to assess the evolution of strain across the sample, plots of stress *versus* strain and force *versus* displacement include data from three extensometers at the three locations shown in Figure 2-7.

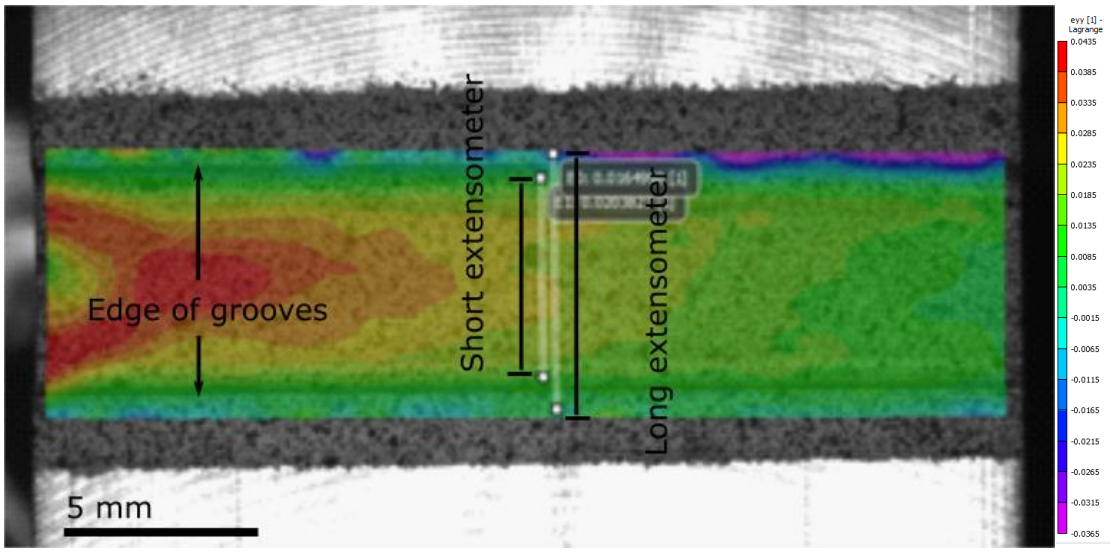

Figure 2-6. The locations of the two extensometers used to measure strain for the flat groove samples are shown overlaid on full-field strain data. Note the strain localization that can be seen on the left side of the sample (red "hotspot"). This was caused by misalignment of the grips and occurred in every specimen. This image was taken near failure.

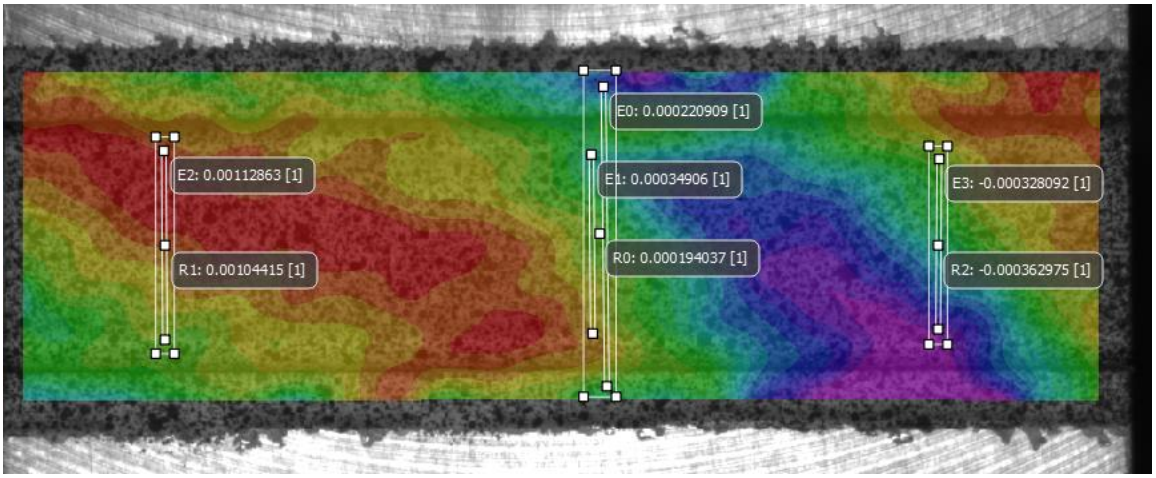

Figure 2-7. The locations of the three extensometers across the face of flat groove specimens used to make plots of stress versus strain and force versus displacement are shown. This image was taken in the elastic region failure.

Table 2-6. The dimensions of flat groove specimens are summarized.

Sample #	Width (mm)	Thickness (mm)	Area (mm^2)
Sample 01	25.38	.88	22.33
Sample 02	25.39	.85	21.58
Sample 03	25.39	.86	21.84
Sample 04	25.39	.86	21.83
Sample 05	25.38	.85	21.57

Sample #	Width (mm)	Thickness (mm)	Area (mm^2)
Sample 06	25.38	.84	21.32
Sample 08	25.40	.86	21.84

Figure 2-8. Images of the test setup for flat groove specimens are shown.

2.2.4. R5 Radial/Parallel

R5 samples were tested using ¼-28 UNF tension grips, see **Figure 2-10. The test setup used for R5 tensile specimens is shown.** for an image of the test setup. Strain was measured using DIC, see **Figure 2-9. The location of the extensometer used to measure strain across R5 specimens is shown.** for the location of the extensometer used to measure strain for R5 specimens. The approximate length of this extensometer is 16 mm. Samples were loaded in tension at a displacement rate of .012 mm/sec using a servo hydraulic MTS load frame. There were two batches of R5 samples. Nine were cut radially to the long axis of the tube, termed as radial samples, while the other 9 were cut with the loading axis parallel to the long axis of the tube, termed as parallel samples. See **Figure 1-2** for a reference drawing. R5 samples 01-09 were all parallel while R5 samples 10-18 were all radial. One sample, sample 07, was first tested to check the procedure and establish an appropriate displacement rate and camera rate. Samples 1-3 and 10-12 were tested at -40°C and samples 4-6 and 13-15 were tested at 22°C. The dimensions of all tested specimens are provided in **Table *2-7***.

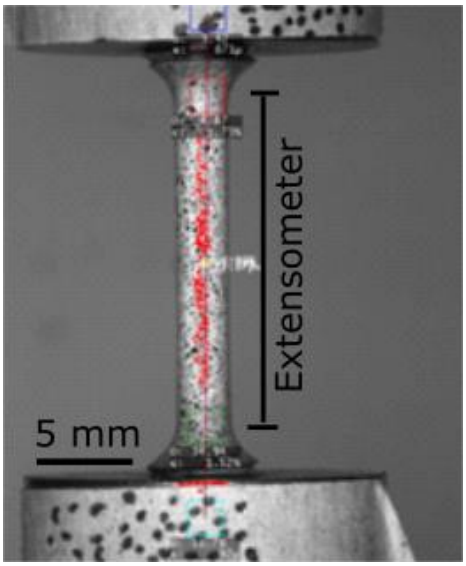

Figure 2-9. The location of the extensometer used to measure strain across R5 specimens is shown.

Table 2-7. The dimensions of R5 specimens are summarized.

R5 Sample #	Sample Type	Gauge Diameter (mm)	Area (mm^2)
Sample 01	Parallel	2.8	6.158
Sample 02	Parallel	2.81	6.202
Sample 03	Parallel	2.81	6.202
Sample 04	Parallel	2.81	6.202
Sample 05	Parallel	2.82	6.246
Sample 06	Parallel	2.82	6.246
Sample 10	Radial	2.81	6.202
Sample 11	Radial	2.81	6.202
Sample 12	Radial	2.81	6.202
Sample 13	Radial	2.8	6.158
Sample 14	Radial	2.81	6.202
Sample 15	Radial	2.8	6.158

Figure 2-10. The test setup used for R5 tensile specimens is shown.

2.2.5. Shear Sample

0.5" pin grips were used to test the shear samples. The test setup for shear samples is shown in **Figure 2-11**. The dimensions of the gauge region of all shear specimens are provided in **Table *2-8***. Strain was very challenging to accurately measure for shear samples. Strain measurements were very sensitive to the location of the extensometer. Moreover, the paint in the center of the gauge region of shear samples flaked off during testing at -40° C, adding significant noise to strain measurements of these samples. Because of this, only the average strain at failure values for shear samples are reported in this study. These values were measured using strain measurements from the region labelled in **Figure 2-12**.

DIC was also used to measure the relative displacement of shear samples. Displacement was measured across the length of the specimen using a virtual extensometer. This is shown in **Figure 2-13**. The length of this extensometer varied slightly specimen to specimen and was ≈52 mm long.

Samples were loaded in tension at a displacement rate of .012 mm/sec using a servo hydraulic MTS load frame. One sample (Sample 07) was first tested to check the procedure and establish an appropriate displacement rate and camera rate. Samples 1-3 were tested at 22°C and samples 4-6 were tested at -40°C.

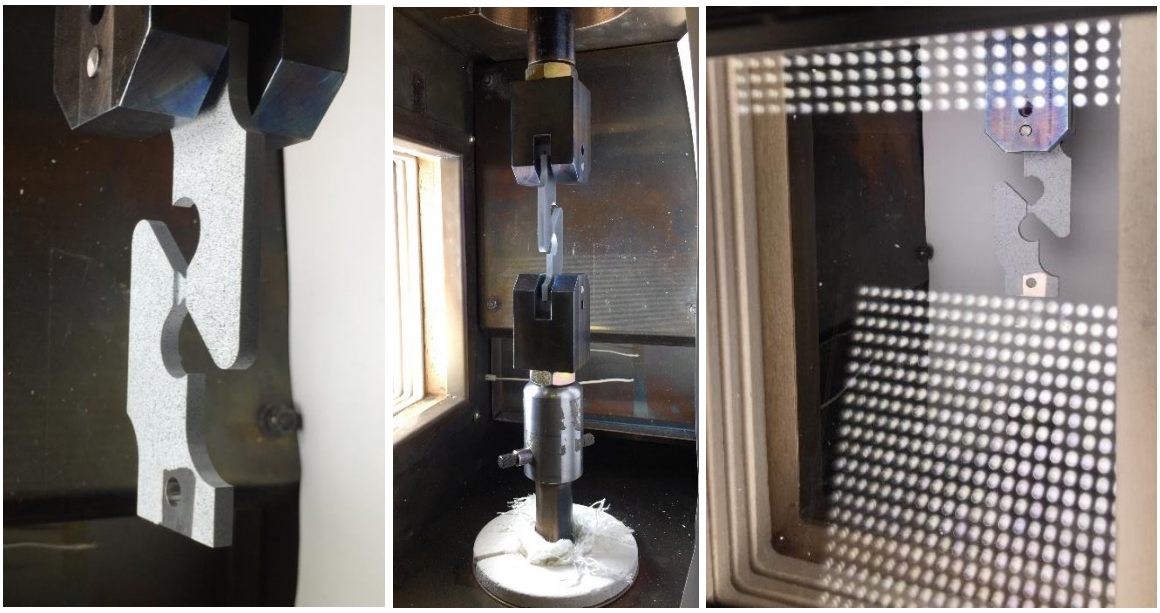

Figure 2-11. The test setup used for shear specimens is shown.

Table 2-8. The dimensions of shear specimens are summarized.

9mm Sample #	Width (mm)	Thickness (mm)	Area (mm^2)
Sample 01	1.61	4.74	7.6314
Sample 02	1.61	4.74	7.6314
Sample 03	1.61	4.74	7.6314
Sample 04	1.61	4.74	7.6314
Sample 05	1.61	4.74	7.6314
Sample 06	1.61	4.74	7.6314

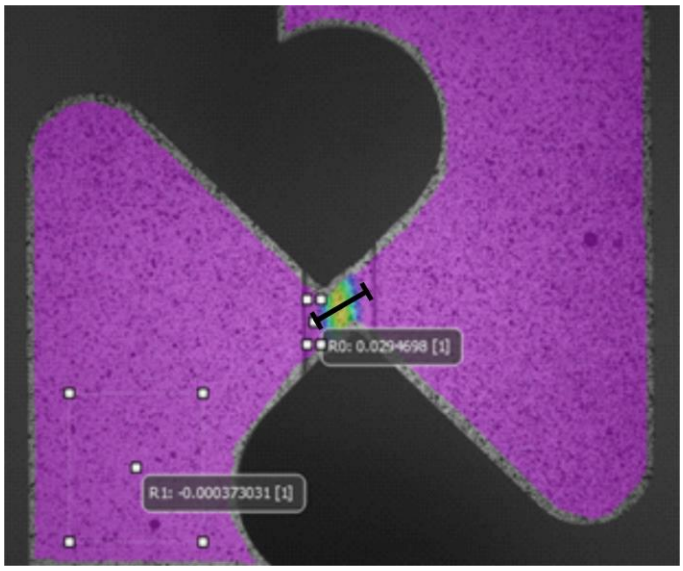

Figure 2-12. The location which specimen strain was measured using a virtual extensometer is shown.

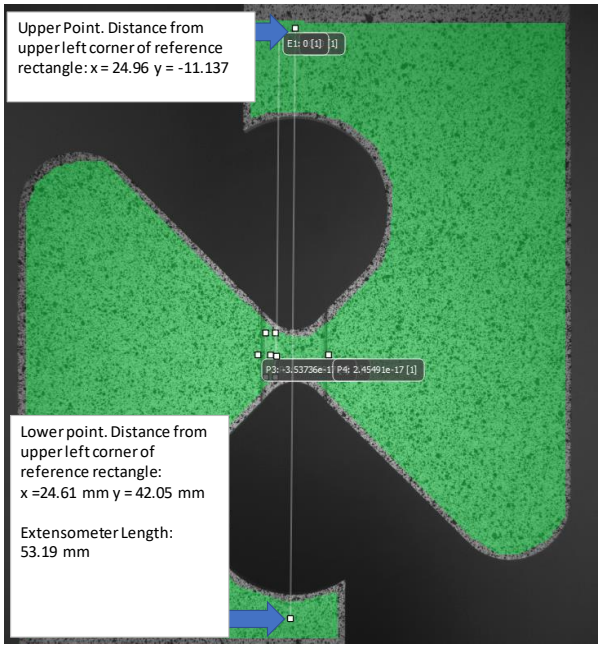

Figure 2-13. The location of the virtual extensometer that was used to measure specimen displacement is shown.

2.2.6. CT Sample

The fracture toughness of this material at both room temperature and -40° C was determined using ASTM standard designation E399-17 [3] for compact tension specimens. The equation for fracture toughness, K_{IC}, measured from CT specimens is:

$$K_{IC} = \frac{P_{IC}}{\sqrt{BB_N}\sqrt{W}} f\left(\frac{a}{W}\right)$$

where P_{IC} is the load at failure, a, W, and B are defined in Appendix A, and

$$f\left(\frac{a}{W}\right) = \frac{\left(2+\frac{a}{w}\right)\left[0.886 + 4.64\frac{a}{W} - 13.32\left(\frac{a}{W}\right)^2 + 14.72\left(\frac{a}{W}\right)^3 - 5.6(\frac{a}{W})^4\right]}{(1-\frac{a}{W})^{3/2}}$$

As specified by E399-17, fatigue pre-cracks were created using fatigue. Fatigue pre-cracks were produced in the CT specimens using an MTS load frame, Model 370.10 Serial: 10588202, with a 22 kip load cell installed, model: 661.20H-03, Serial: 120508A. Samples were fixtured using Material Testing Technology grips designed to meet ASTM.E0399 B=0.6 criteria. Fatigue cycling occurred at 3Hz under force-control. The maximum cycling load for each specimen and R-value are shown in Table 1. Note that ASTM.E0399.43 requires that the fatigue load applied to the sample should be no more than 80% of the room temperature K_{IC} of the material. This was the case for all samples. The first sample, sample CT 5, was used to initially estimate the K_{IC} of the material and was fatigued at a slightly higher load than the others.

Table 2-9. The fatigue load and R value used to produce fatigue cracks in the CT specimens are summarized.

Sample ID	Peak Fatigue Load (N)	R value
CT 1	5,785	0.1
CT 2	5,785	0.1
CT 3	5,785	0.1
CT 4	5,785	0.1
CT 5	6,675	0.1

Strain measurements collected via digital image correlation (DIC) were used to infer pre-crack length and halt fatigue cycling as needed. Correlated Solutions software VicGauge 2D v.528 was used to calculate strain on images provided by a Grasshopper3 GS3-U3-41C6M 1" Mono CMOS camera with a 2048x2048 pixel resolution and acquiring images at a rate 50 fps.

Two of the samples, samples CT 4 and 5, were subsequently elongated to failure at room-temperature using this load frame. The other three samples were tested at -40° C on the load frame that was used to test all other specimens. The same grips and methods were used on both frames. Changing frames should have no significant effect on K_{IC} measurements.

The pre-crack length, *a*, was measured for all CT specimens. Optical images collected by a Grasshopper3 GS3-U3-41C6M 1" Mono CMOS camera after the final fatigue cycle were used to measure the crack length at the surface of the sample on both sides of the sample. These values were subsequently averaged.

To test CT samples at -40° C, 0.25" pin CT grips were installed into the oven. Samples were loaded in tension at a displacement rate of .003 mm/sec using a servo hydraulic MTS load frame. One sample (Sample 01) was first tested to check the procedure and to establish an appropriate

displacement rate and camera rate. It was tested at .01 mm/s. Samples 2-3 were tested at a slower rate. There is no difference in results between the 2 different strain rates. All 3 were tested at -40°C. The maximum load and the length of the initial pre crack were used to determine K_{IC}.

Figure 2-14. The setup for performing fracture toughness tests is shown.

2.3. Microscopy Characterization Methods

Reduction in area was measured for R5, 3mm, and 9mm notch samples. These measurements were made using a Keyence IM-6700 Image Dimension measuring system (SN: Y5151050011) with Keyence IM 6225T (SN: 3C519002) Imaging Head. The diameters of unbroken specimens were averaged to give an overall initial diameter. The gauge diameter of broken samples was measured as illustrated in **Figure 2-15**. Areas were calculated from these diameters for reduction in area measurements.

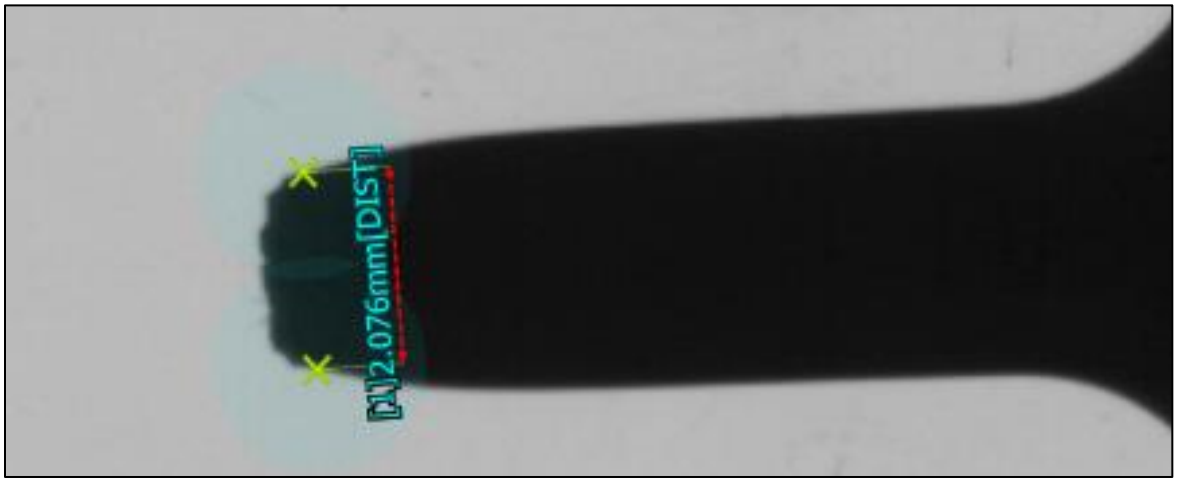

Figure 2-15. The method for measuring the diameter of fractured samples is illustrated for an R5 sample (Sample 11).

Optical images were taken of the fracture surface of samples using a Keyence VHX-500 Digital Microscope (SN:W5061060063) with a Keyence VH-ZST Multi Scan Optical Head (SN:5B10012). In addition to optical microscopy, select fracture surfaces were also characterized using a Zeiss Supra 55VP field emission SEM (scanning electron microscope). Representative specimens of all specimen types were tested at both room temperature and -40° C, except the CT specimens, which were chosen for SEM characterization. Additionally, four R5 samples were cross-sectioned and polished to the midplane for characterization in the SEM. Electron backscatter diffraction (EBSD) data were collected from the undeformed grip regions of these samples to evaluate the as-received microstructure of this material in both the parallel and radial directions. EBSD data were collected in the same Zeiss Supra 55VP SEM using Oxford HKL Aztec™ software. These EBSD data were processed using MTEX [6], an extension for MATLAB®. Grains were defined in MTEX by assigning neighboring points misoriented by less than 5° to the same grain and enforcing a minimum grain size of 10 adjacent points.

3. RESULTS

A summary of the average mechanical properties for all specimen types at 22° C and -40° C is provided in **Table *3-1***. The average reduction in area measurements for R5 specimens and 3mm and 9mm notch specimens are provided in ***Table 3-2***. The following sections provide results of microscopy characterization of the material microstructure, measurements of fracture toughness at 22° C and -40° C, and detailed results for each of the specimen types. Note that Appendices B, C, and D provide comprehensive results for all of the specimen types, including representative force *versus* displacement datasets in Appendix D for each of the specimen types.

Table 3-1. For each sample type tested in this study, the average ultimate tensile strength (UTS), ductility, yield strength (YS) and strain at YS are reported. Modulus of elasticity (E) is also reported for R5 specimens. Note that, for the shear specimens, average displacement at failure (mm) rather than ductility is provided.

Sample Name	Temp (°C)	UTS (MPa)	YS (MPa)	Ductility (%)	E (GPa)
3mm Notch	22	2070 ± 6.85	1850 ± 37.1	7.6 ± 0.76	-
	-40	2170 ± 15.4	1930 ± 30.9	2.6 ± 0.34	-
9mm Notch	22	1810 ± 1.84	1760 ± 1.42	5.6 ± 0.47	-
	-40	1900 ± 8.50	1820 ± 4.67	4.9 ± 0.83	-
Flat Groove	22	1740± 14.8	1500 ± 63.9	7.3 ± 0.10	-
	-40	1840 ± 6.83	1410 ± 52.9	7.7 ± 0.45	-
R5 Radial	22	1600 ± 6.43	1470 ± 13.0	12.1 ± 0.29	185 ± 1
	-40	1660 ± 7.80	1530 ± 31.8	11.9 ± 0.68	186 ± 5
R5 Parallel	22	1570 ± 16.0	1430 ± 22.7	12.8 ± 0.87	181 ± 2
	-40	1640 ± 3.72	1490 ± 7.88	12.0 ± 0.36	182 ± 4
Shear	22	950 ± 5.81	806 ± 11.2	2.25 ± 0.13	
	-40	1009 ± 3.81	847 ± 7.45	2.40 ± 0.13	

Table 3-2. The average reduction in area of R5 specimens and 3mm and 9mm notch specimens are summarized.

Sample Name	Temp (°C)	Average Reduction in Area (%)
R5 Parallel	22	57.4
	-40	55.0
R5 Radial	22	55.7
	-40	48.6
3mm	22	23.5

Sample Name	Temp (°C)	Average Reduction in Area (%)
	-40	5.75
9mm	22	42.8
	-40	31.6

3.1. Material Microstructure

Electron backscatter diffraction (EBSD) data from the undeformed grip regions of R5 radial and R5 parallel samples are presented in **Figure 3-1.** and **Figure 3-2**. Because all samples except the R5 radial samples were extracted with their loading direction parallel to the length of the cylinder, the microstructure shown in **Figure 3-2** is considered representative of the undeformed microstructure of all other specimens. In each figure, the EBSD data are plotted as an inverse pole figure (IPF) map colored with respect to the tensile direction (TD) and as an IPF relative to the TD. High-angle grain boundaries, defined as boundaries greater than 5°, are colored black in the IPF maps. Grains appear acicular with the long axis randomly oriented. The texture in the radial direction was diffuse. A weak <111> fiber parallel to the TD was observed in the parallel sample, indicating that all samples except the R5 radial samples had a weak <111> fiber parallel to the loading direction.

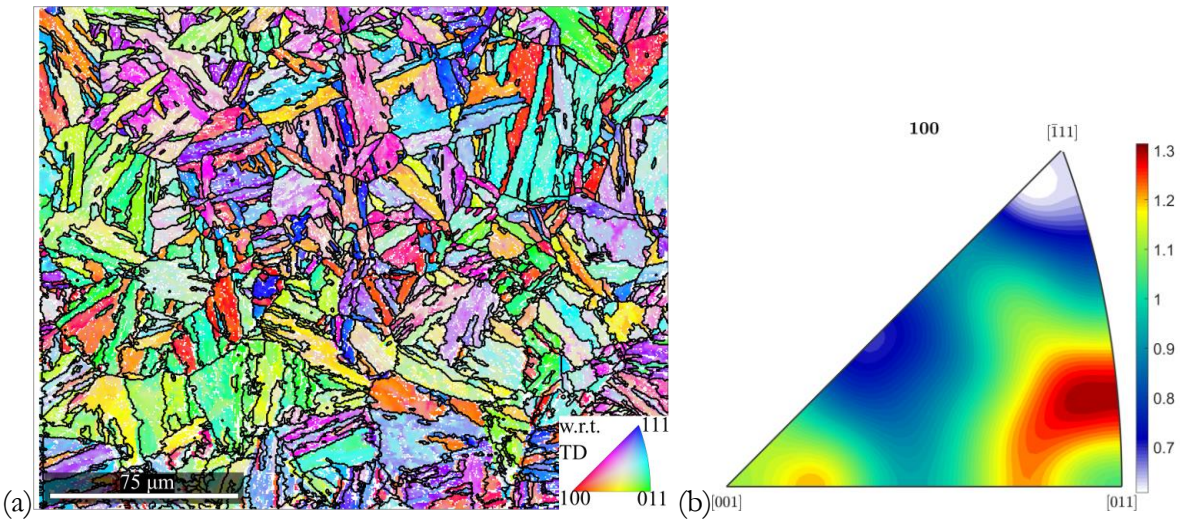

Figure 3-1. EBSD data from the grip region of an R5 radial specimen are plotted as an inverse pole figure (IPF) map colored with respect to the tensile direction and an IPF. High-angle (>5 °) grain boundaries are colored black in (a). The IPF plots the texture of the material relative to the tensile direction of the R5 radial sample as multiples of random.

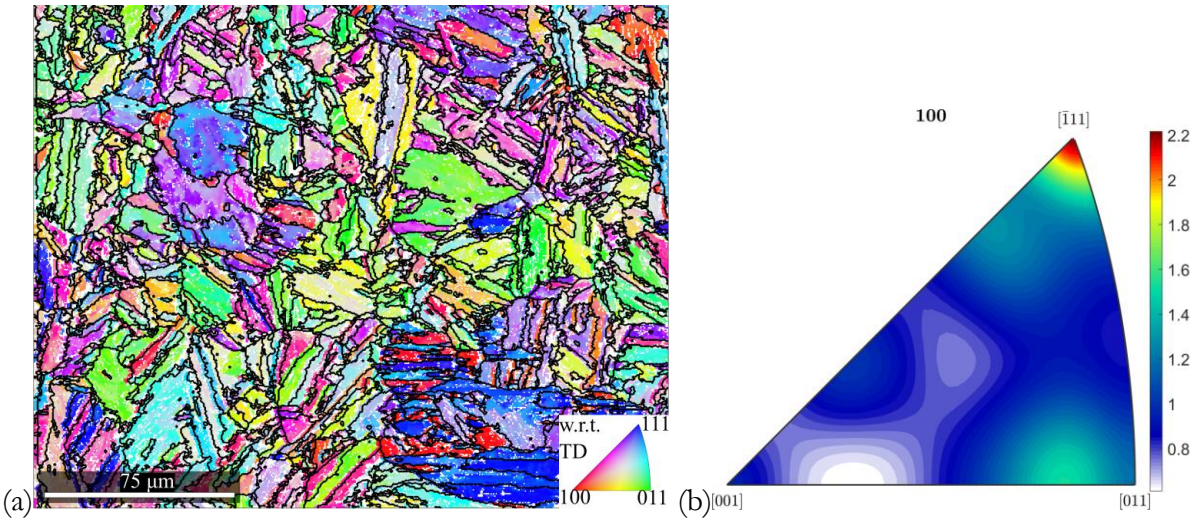

Figure 3-2. EBSD data from the grip region of an R5 parallel specimen are plotted as an inverse pole figure (IPF) map colored with respect to the tensile direction and an IPF. High-angle (>5 °) grain boundaries are colored black in (a). The IPF shows the texture of the material relative to the tensile direction of the R5 parallel sample as multiples of random.

3.2. Fracture Toughness Measurements

The testing temperature length of the precrack, maximum load held by the sample, and corresponding K_{IC} are provided for each of the 5 CT specimens tested. These measurements indicate that the fracture toughness of this material is significantly lower at -40° C than at room temperature. The average K_{IC} at room temperature and -40° C were 53.6 and 36.40 MPa$\sqrt{m}$, respectively. Images of a CT specimen before and after failure are shown in **Figure 3-3**.

Table 3-3. The measured maximum load and KIC for CT specimens tested at -40° C and 22° C are shown.

Sample Name	Temp (°C)	Total crack length (mm)	Max Load (N)	K_{IC} (MPa$\sqrt{m}$)
1	-40	14.68	8428	35.62
2	-40	14.53	8981	37.35
3	-40	14.68	8571	36.22
4	22	14.76	12383	54.42
5	22	14.83	11880	52.80

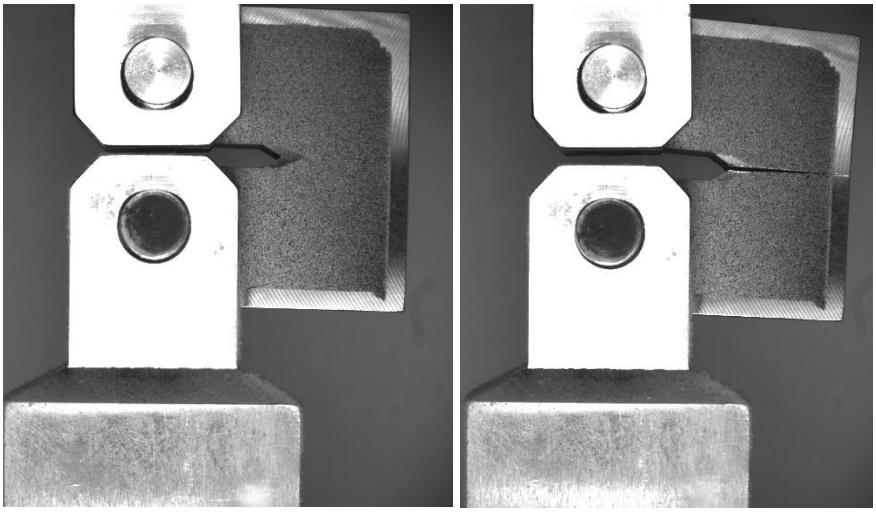

Figure 3-3. Pre-test and post-test images showing failure location, CT, -40°C, Sample 03

3.3. R5 Specimens

Typical plots of stress *versus* strain for R5 parallel samples tested at 22° C and -40° C are provided in Figure 3-4 and Figure 3-5. Typical plots of stress *versus* strain for R5 radial samples tested at 22° C and -40° C are provided in Figure 3-6 and Figure 3-7. As these figures and

Table ***3-1*** show, the modulus of elasticity, UTS, and YS of R5 radial samples were 2-3% greater than that of R5 parallel samples. This is a small, but measurable difference based on the number of samples tested. These different values may be caused by differences in crystallographic texture relative to the TD in the two sample types. Assuming slip along the {110} family of planes, the Schmid factor of the <111> fiber is the smallest of any orientation. As shown in Figure 3-1. and Figure 3-2, this texture component was stronger in the parallel samples than in the radial samples.

Testing temperature affected the mechanical behavior of R5 radial and parallel samples. The YS and UTS of both radial and parallel R5 samples increased with decreasing testing temperature, see

Table ***3-1*** and Figure 3-4 to Figure 3-7. Ductility did not change significantly with decreasing testing temperature.

Reduction in area measurements for R5 samples are provided in **Table *3-2*** (average values for each specimen type and temperature) and **Table *3-4*** (all values). These tables indicate that the reduction in area of R5 samples decreased with testing temperature.

Figure 3-8 shows images of a R5 sample tested at 22° C before and after testing. Full-field strain fields measured using DIC are overlaid on images of samples tested at 22° C and -40° C in Figure 3-9. The images in Figure 3-9 were taken immediately before fracture. The full-field strain data in these images show the strain localization in a neck in both samples.

After testing, the fracture surfaces of representative R5 samples were characterized optically and using an SEM. The fracture surface of each sample was typical of classic cup and cone fracture. This can be seen in the SEM images of the fracture surfaces of radial samples tested at 22° C and -40° C provided in Figure 3-10 and Figure 3-11. Ductile dimples can be seen in the center of both specimens while shear dimples were observed along the shear lip of both samples. These SEM

images are typical of the fracture surfaces of R5 parallel samples tested at 22° C and -40° C. Optical images of the fracture surfaces of radial and parallel samples tested at 22° C and -40° C are provided in Appendix C. No significant differences were observed between the fracture surfaces of any of the samples.

R5 radial and parallel samples tested at both temperatures were also cross-sectioned to characterize damage beneath the fracture surface. Representative images of cross-sectioned R5 radial samples tested at 22° C and -40° C are provided in Figure 3-12 and Figure 3-13. In both samples, voids were observed up to 500 μm below the fracture surface. The high-magnification images of the fracture surface also indicate that failure occurred by void nucleation, growth, and coalescence. The images in Figure 3-12 and Figure 3-13 are typical of the R5 parallel samples tested at 22° C and -40° C, which are provided in Appendix C.

Table 3-4. The reduction in area measurements for R5 specimens are summarized.

Sample #	Type	Temp (°C)	Initial Diameter (mm)	Initial Area (mm^2)	Final Diameter (mm)	Final Area (mm^2)	Reduction in Area (%)
1	Parallel	-40	2.86	6.40	1.77	2.46	61.7
2	Parallel	-40	2.86	6.40	1.95	3.00	53.2
3	Parallel	-40	2.86	6.40	2.01	3.18	50.3
4	Parallel	22	2.86	6.40	1.94	2.95	54.0
5	Parallel	22	2.86	6.40	1.89	2.80	56.3
6	Parallel	22	2.86	6.40	1.868	2.74	57.2
7	Parallel	22	2.86	6.40	1.76	2.41	62.2
10	Radial	-40	2.86	6.40	1.96	3.02	52.8
11	Radial	-40	2.86	6.40	2.08	3.39	47.1
12	Radial	-40	2.86	6.40	2.10	3.47	45.8
13	Radial	22	2.86	6.40	1.91	2.87	55.1
14	Radial	22	2.86	6.40	1.84	2.65	58.6
15	Radial	22	2.86	6.40	1.95	2.98	53.5

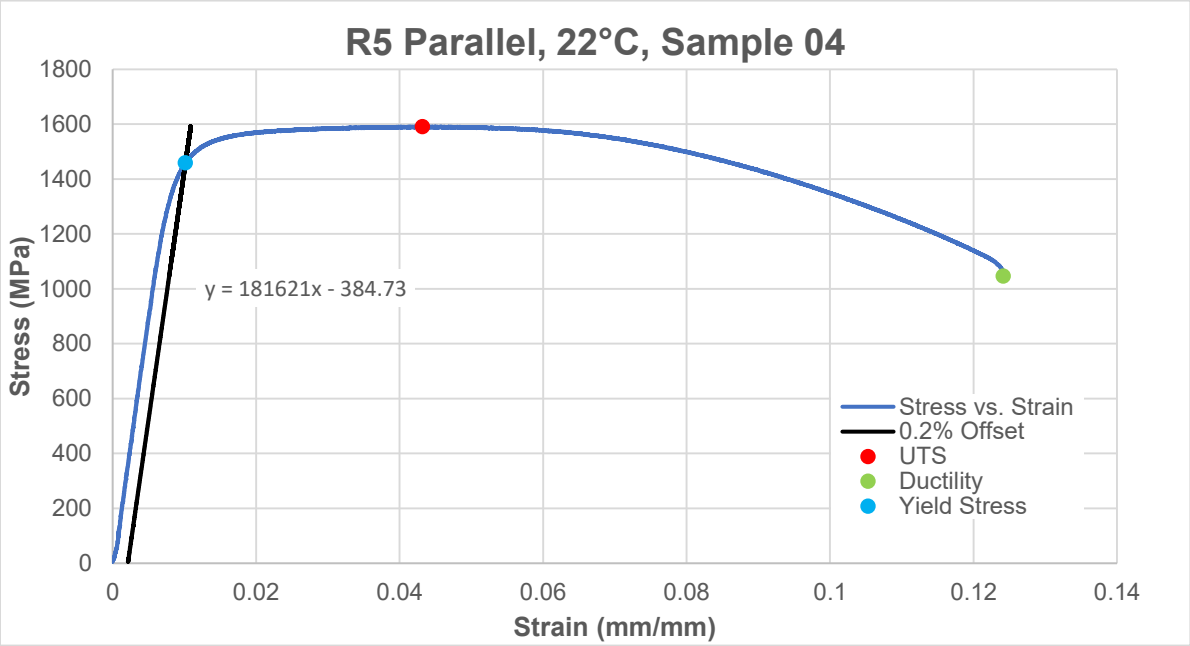

Figure 3-4. Stress vs. strain curve – R5 Parallel, 22°C, Sample 04.

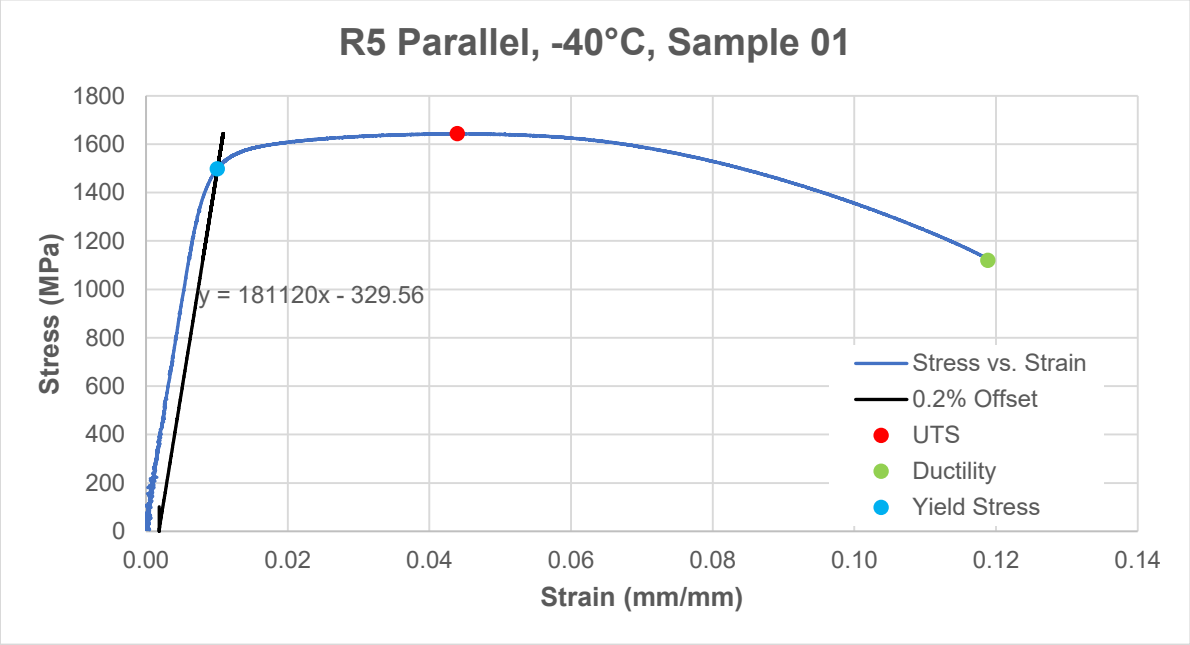

Figure 3-5. Stress-strain curve, R5 Parallel, -40°C, Sample 01.

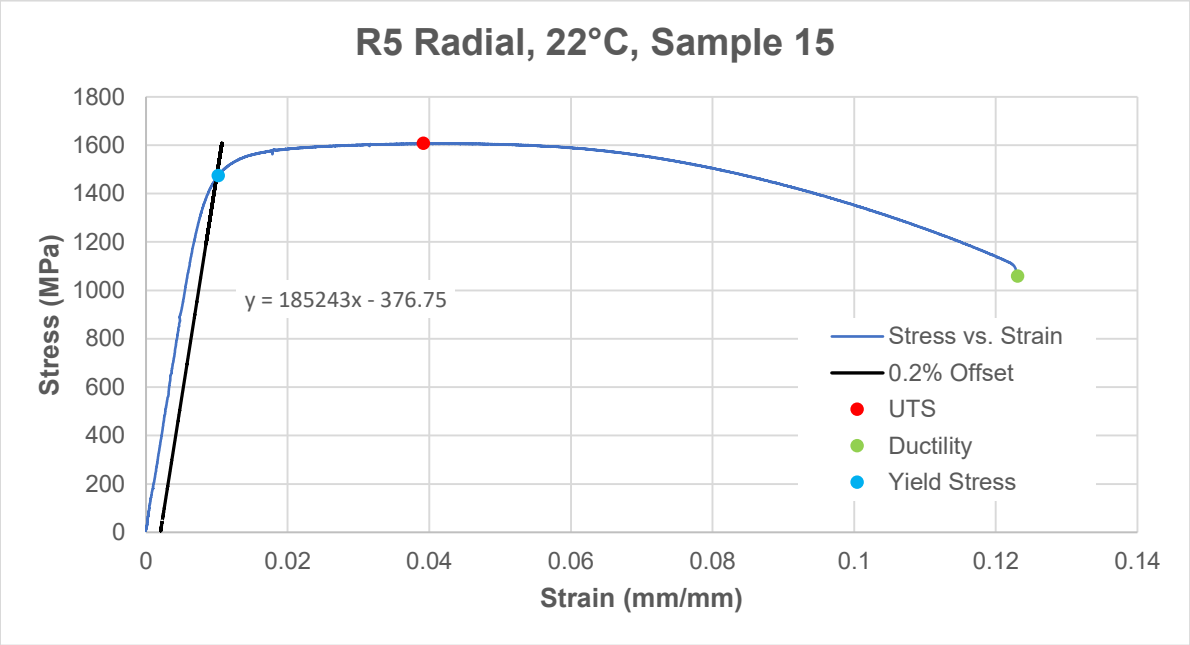

Figure 3-6. Stress-strain curve, R5 Radial, 22°C, Sample 15.

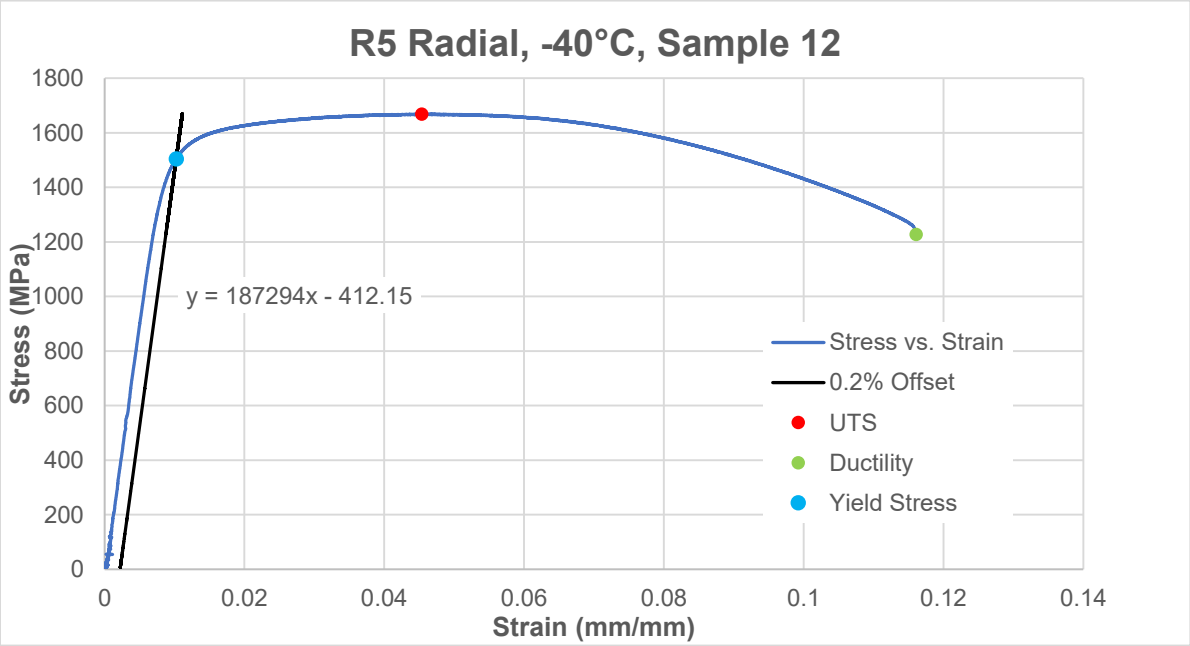

Figure 3-7. Stress-strain curve, R5 Radial, -40°C, Sample 12.

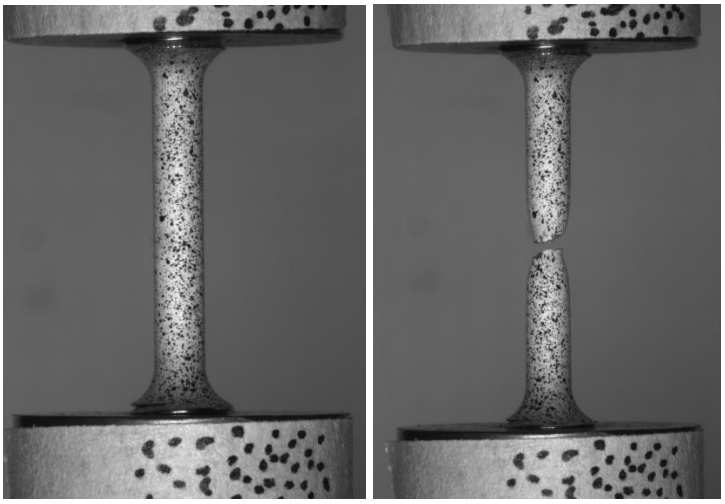

Figure 3-8. Pre-test and post-test images showing failure location, R5 Parallel, 22°C, Sample 07.

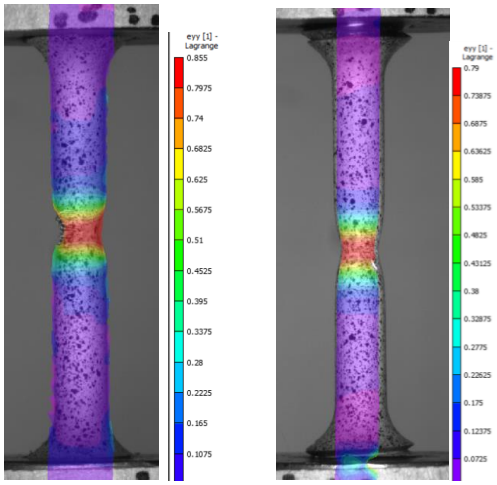

Figure 3-9. Final full field eyy strain measurements before failure for R5 samples tested at 22 °C, Sample 01 (Left) and-40°C, Sample 10 (Right). Strain localization in a neck can be seen for both samples. Note the different scales for strain, left: 85.5% to 0%, right: 80% to 0%.

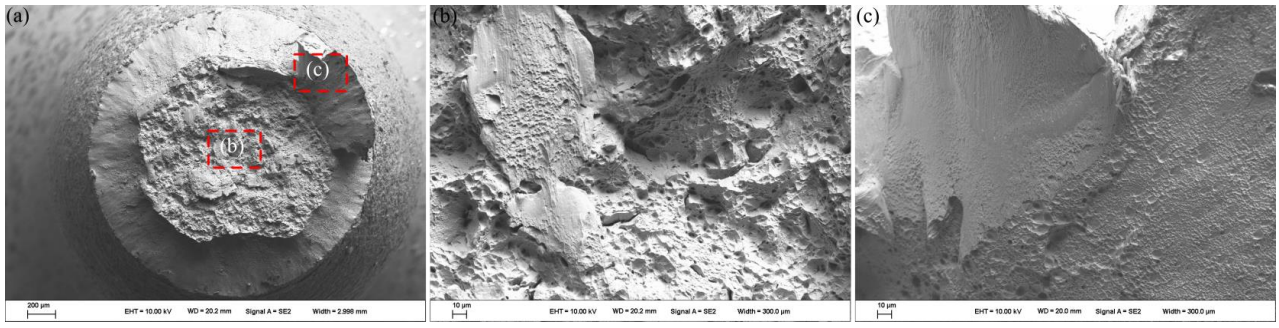

Figure 3-10. Secondary electron images of the fracture surface of a R5 radial sample tested at 22C are provided. A low-magnitude image of the entire fracture surface is show in (a). High-magnification images of the center (b) and shear lip (c) are also provided.

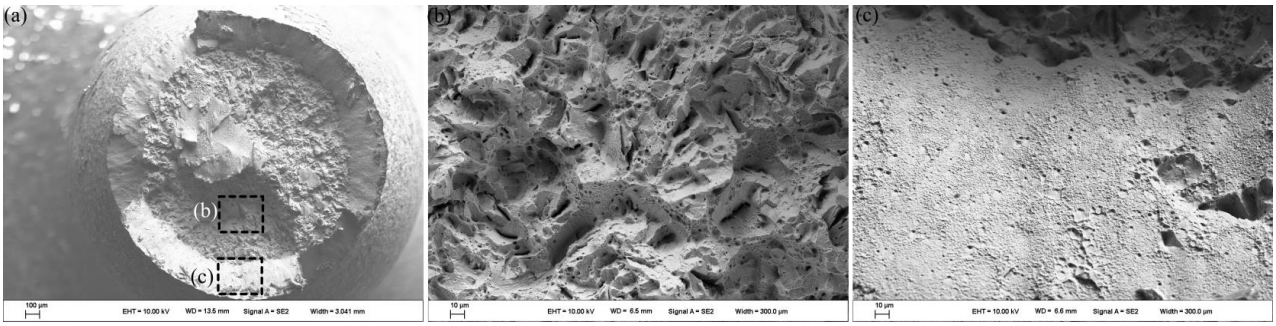

Figure 3-11. Secondary electron images of the fracture surface of a R5 radial sample tested at -40C are provided. A low-magnitude image of the entire fracture surface is show in (a). High-magnification images of the center (b) and shear lip (c) are also provided.

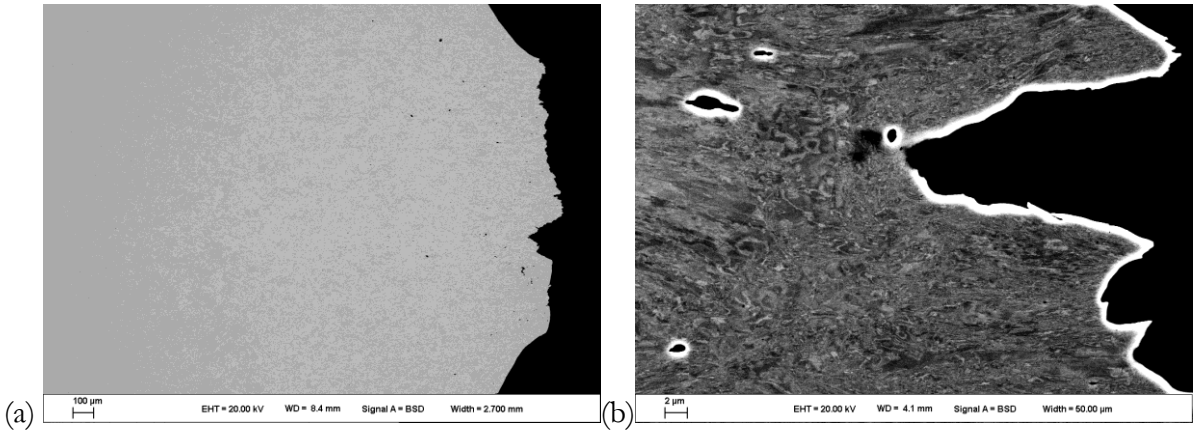

Figure 3-12. ECCI images of a cross-sectioned R5 radial sample tested at 22C are provided. The fracture surface can be seen on the right side of both images. (a) shows a low magnification image (the image width is 2.7 mm) and (b) shows a high magnification image (the image width is 0.05 mm). Voids near the fracture surface can be seen in both images.

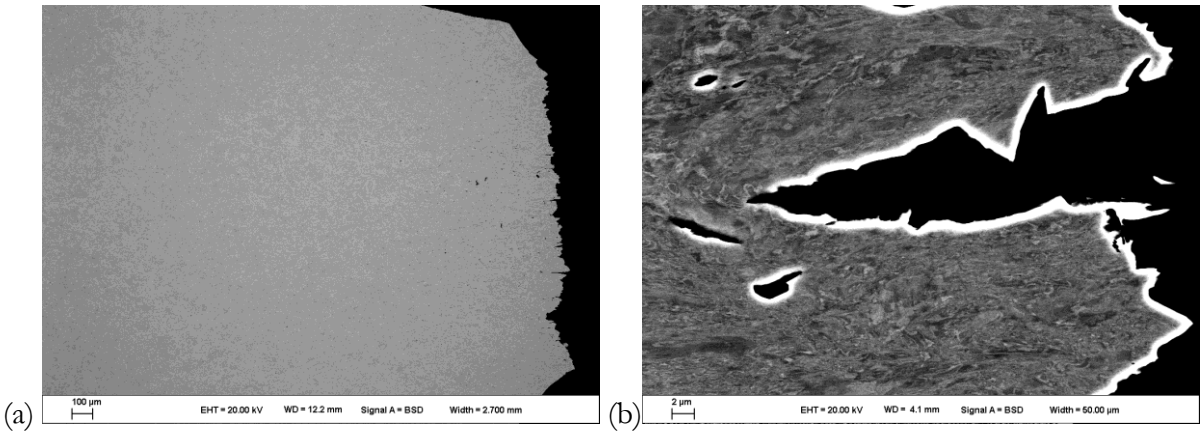

Figure 3-13. ECCI images of a cross-sectioned R5 parallel sample tested at -40C are provided. The fracture surface can be seen on the right side of both images. (a) shows a low magnification image (the image width is 2.7 mm) and (b) shows a high magnification image (the image width is 0.05 mm). Voids near the fracture surface can be seen in both images.

3.4. 3mm Notched Specimens

Typical plots of stress *versus* strain for 3mm notched specimens tested at 22° C and -40° C are provided in Figure 3-14 and Figure 3-15. Reduction in area measurements for all tested 3mm notch samples are provided in **Table *3-6***. The average reduction in area values for 3mm notch specimens tested at the two temperatures are provided in **Table *3-2***.

This specimen type exhibited significantly different mechanical behaviors at these two temperatures, see **Table *3-1***. The UTS and YS increased by 4 to 5% with decreasing temperature, but the ductility of samples tested at -40° C was approximately 1/3 of those of samples tested at 22° C. Reduction in area measurements also indicate that this specimen was significantly less ductile at -40° C than at 22° C.

Table 3-5. The reduction in area measurements for 3mm notch specimens are summarized.

Sample #	Temp (°C)	Initial Diameter (mm)	Initial Area (mm^2)	Final Diameter (mm)	Final Area (mm^2)	Reduction of Area (%)
1	22	5.98	28.1	5.24	21.5	23.3
2	22	5.98	28.1	5.20	21.2	24.4
3	22	5.98	28.1	5.25	21.7	22.8
4	-40	5.98	28.1	5.73	25.8	8.14
5	-40	5.98	28.1	5.80	26.4	5.82
6	-40	5.98	28.1	5.88	27.1	3.30

Figure 3-18 shows images of a 3mm notch specimen tested at 22° C before and after testing. Full-field strain fields measured using DIC are overlaid on images of specimens tested at 22° C and -40° C in Figure 3-19. The images in Figure 3-19 were taken immediately before fracture. These images show the significant differences in ductility between samples tested at 22° C and -40° C.

SEM images of fractured 3mm notched specimens tested at 22° C and -40° C are shown in Figure 3-16 and Figure 3-17. Optical images of the fracture surfaces of these specimens are provided in Appendix C. The fracture surface of 3mm notched samples tested at 22° C suggest ductile fracture. Specimens exhibited cup and cone fracture with ductile dimples in the center of the sample and shear dimples along the shear lip. Ductile dimples in these samples were similar to those observed in the center of R5 samples. While the fracture surfaces of samples tested at -40° C suggest ductile fracture at this temperature, several features are reminiscent of brittle failure. First, the shear lip on samples tested at -40° C was much smaller than that of samples tested at 22° C, compare Figure 3-16 and Figure 3-17. Second, facets reminiscent of transgranular fracture rather than dimples were seen in the center of the fracture surface of specimens tested at -40° C, as can be seen in the high magnification image provided in Figure 3-17.

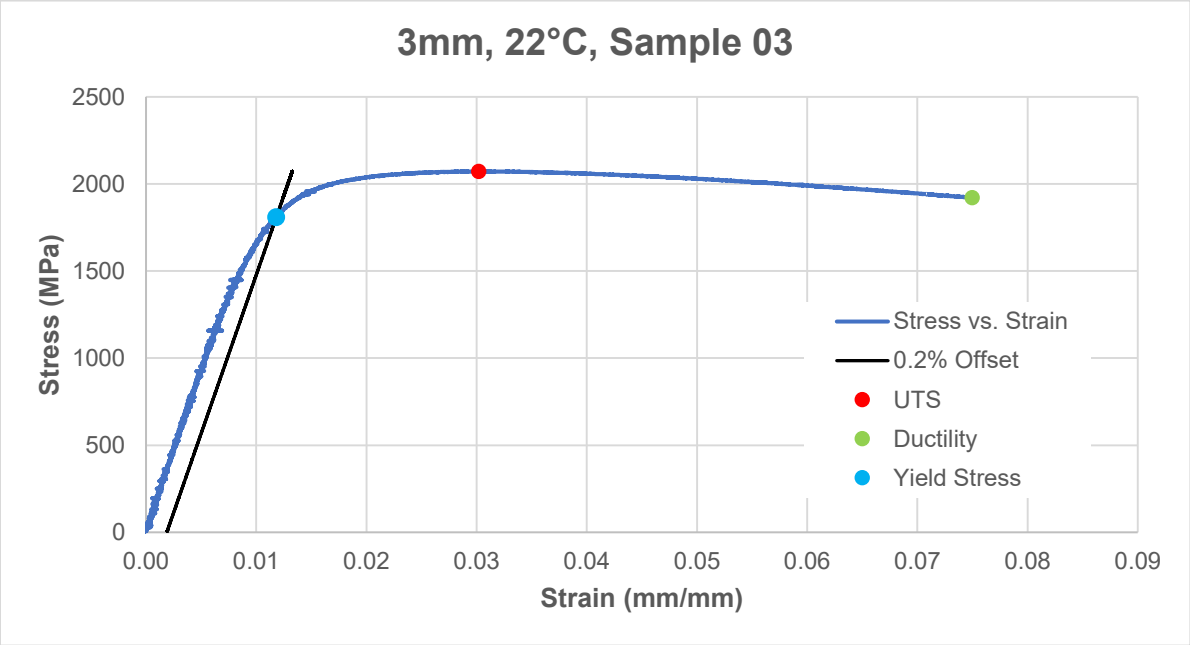

Figure 3-14. Stress-strain curve, 3mm, 22°C, Sample 03.

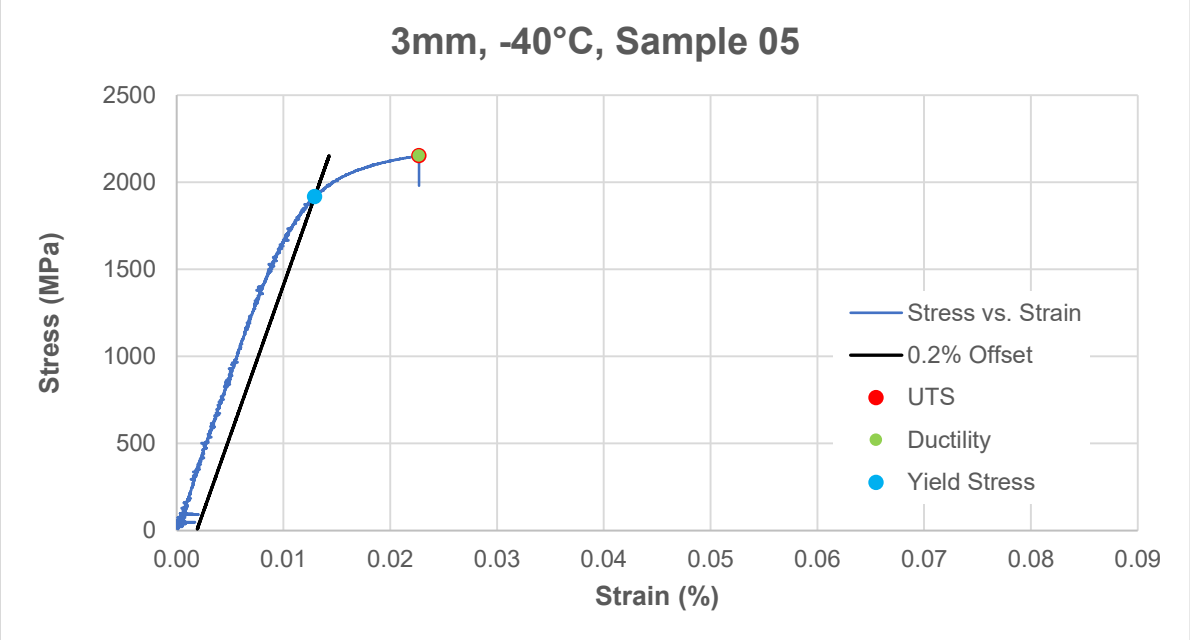

Figure 3-15. Stress-strain curve, 3mm, -40°C, Sample 05.

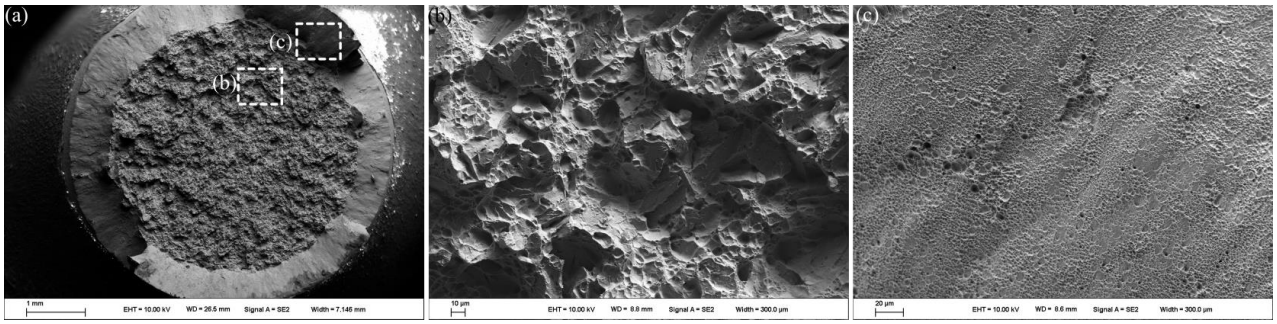

Figure 3-16. Secondary electron images of the fracture surface of a 3mm-notched sample tested at 22C are provided. A low-magnitude image of the entire fracture surface is show in (a). High-magnification images of the center (b) and shear lip (c) are also provided.

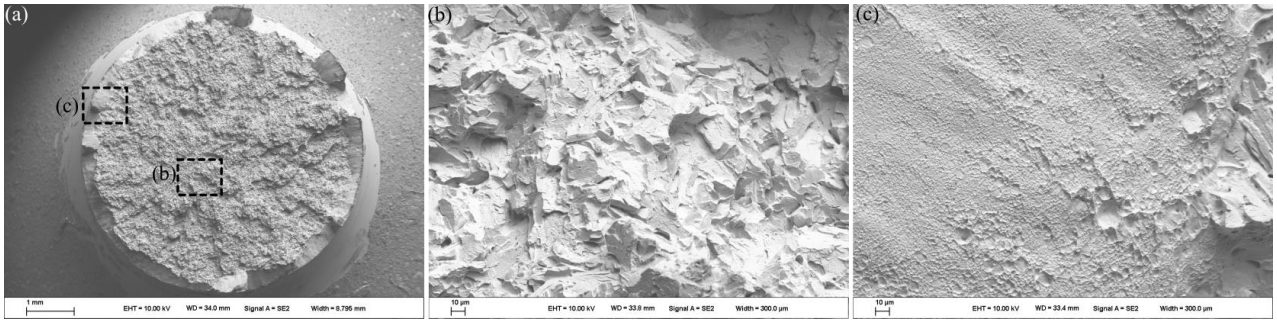

Figure 3-17. Secondary electron images of the fracture surface of a 3mm-notched sample tested at -40C are provided. A low-magnitude image of the entire fracture surface is show in (a). High-magnification images of the center (b) and shear lip (c) are also provided.

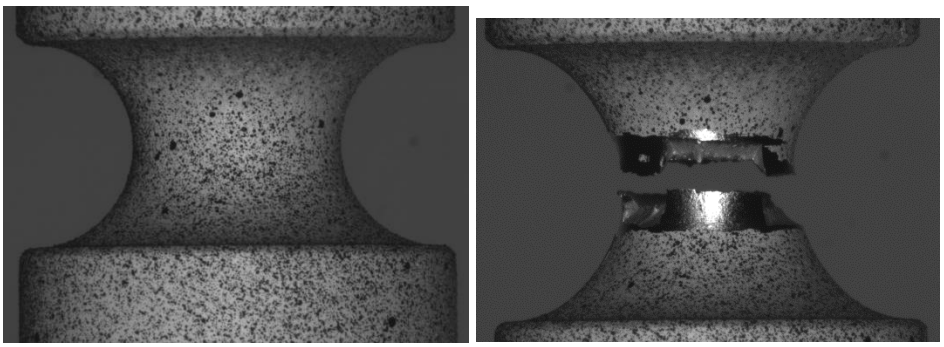

Figure 3-18. Pre-test and post-test images showing failure location, 3mm, 22°C, Sample 01.

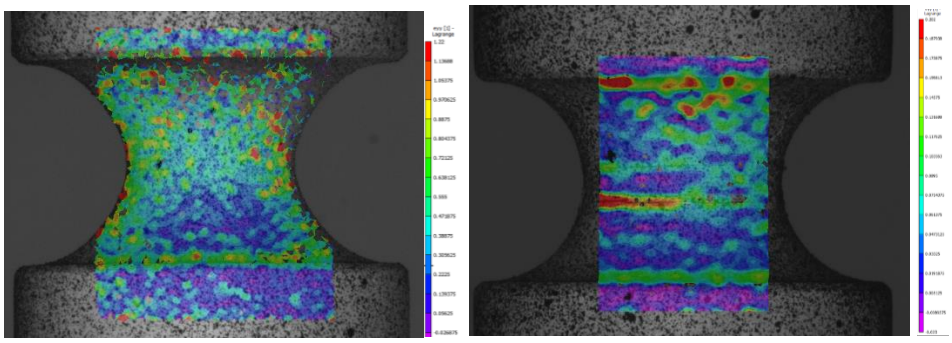

Figure 3-19. Full field eyy measurements immediately before failure, 22°C, Sample 01 (left) and -40°C, Sample 04 (Right). Note the different scales for strain, left: 122% to 0%, right: 20% to 0%.

3.5. 9mm Notched Specimens

Typical plots of stress *versus* strain for 9mm notched specimens tested at 22° C and -40° C are provided in Figure 3-20 and Figure 3-21. Reduction in area measurements for all tested 9mm notch samples are provided in Table 3-6. Similar to the 3mm notched specimens, the UTS and YS of specimens tested at -40° C was 3 to 5% greater. The ductility of 9mm notch samples tested at -40° C was slightly but measurably less than that of specimens tested at 22° C, see **Table 3-1**. Reduction in area of 9mm notch specimens tested at -40° C was also slightly but measurably less than that of specimens tested at 22° C.

Table 3-6. The reduction in area measurements for 9mm notch specimens are summarized.

Sample #	Temp (°C)	Initial Diameter (mm)	Initial Area (mm^2)	Final Diameter (mm)	Final Area (mm^2)	Reduction of Area (%)
1	22	5.98	28.1	4.64	16.9	39.8
2	22	5.98	28.1	4.39	15.1	46.2
3	22	5.98	28.1	4.54	16.2	42.3
4	-40	5.98	28.1	4.71	17.4	38.0
5	-40	5.98	28.1	5.13	20.7	26.4
6	-40	5.98	28.1	4.99	19.6	30.3

Figure 3-22 shows images of a 9mm notch specimen tested at 22° C before and after testing. Full-field strain fields measured using DIC are overlaid on images of specimens tested at 22° C and -40° C in Figure 3-23. The images in Figure 3-23 were taken immediately before fracture. These images show the differences in ductility between samples tested at 22° C and -40° C, *e.g.* the strain in the center of necked specimens before failure was ≈55% and ≈45% at 22° C and -40° C, respectively.

SEM images of fractured 9mm notched specimens tested at 22° C and -40° C are shown in Figure 3-24 and Figure 3-25. Optical images of the fracture surfaces of these specimens are provided in Appendix C. The fracture surfaces of both samples are characteristic of ductile, cup and cone fracture. Ductile dimples were observed in the center of the sample and shear dimples along the shear lip. Both ductile and shear dimples in these samples were similar to those observed in the R5

samples. No significant differences were observed between the fracture surfaces of 9mm notched specimens tested at 22° C and -40° C.

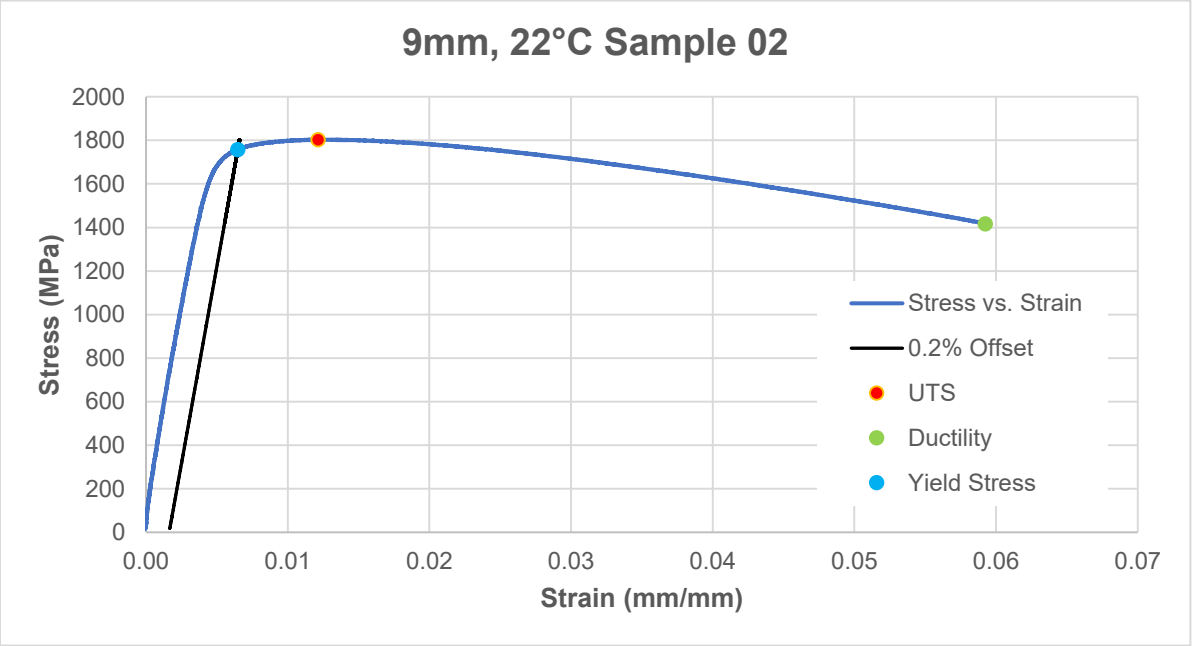

Figure 3-20. Stress-strain curve, 9mm, 22°C, Sample 02.

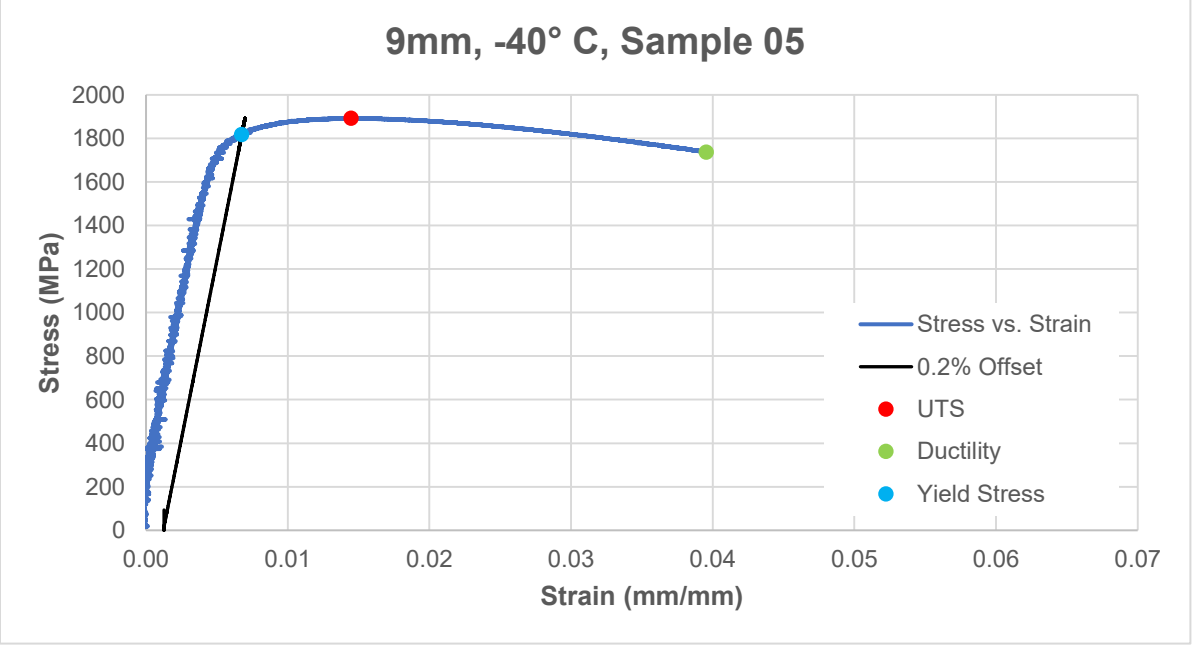

Figure 3-21. Stress-strain curve, 9mm, -40°C, Sample 05.

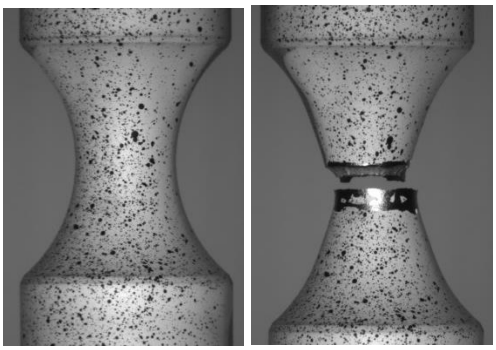

Figure 3-22. Pre-test and post-test images showing failure location 9mm, 22°C, Sample 01

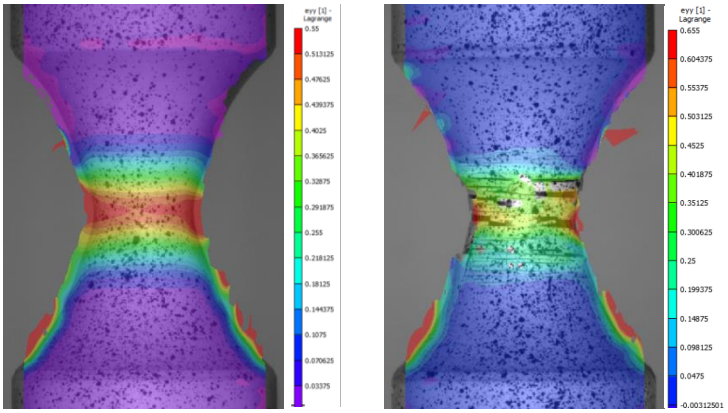

Figure 3-23. Full field strain (eyy) measurements for 9mm notch specimens immediately before failure, 22°C, Sample 01 (left) and -40°C, Sample 04 (Right). Note the different scales for strain, left: 122% to 0%, right: 20% to 0%. Paint chipping, likely caused by the cold temperature, can be seen for Sample 04. This created the elevated strain measurements (red areas) in full field strain measurements. The maximum strain in the center of the 9mm notch specimen tested at -40° C is ≈45%. Note the different scales for strain, left: 55% to 0%, right: 65.5% to 0%.

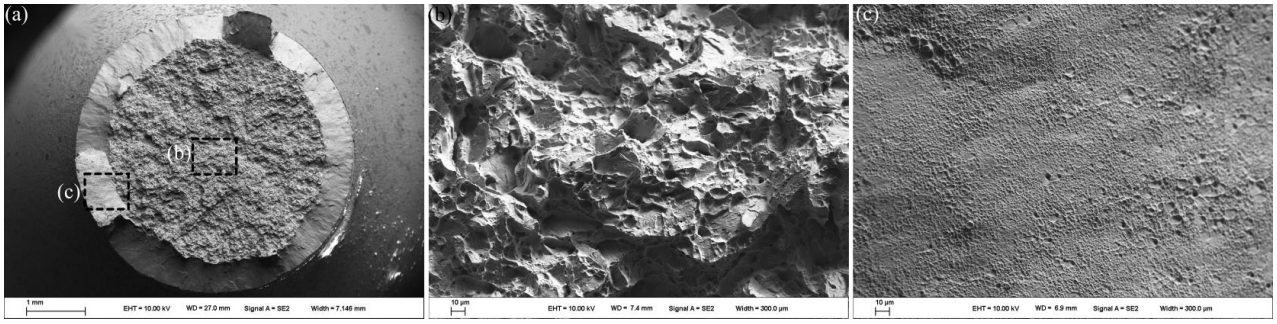

Figure 3-24. Secondary electron images of the fracture surface of a 9mm-notched sample tested at -40C are provided. A low-magnitude image of the entire fracture surface is show in (a). High-magnification images of the center (b) and shear lip (c) are also provided.

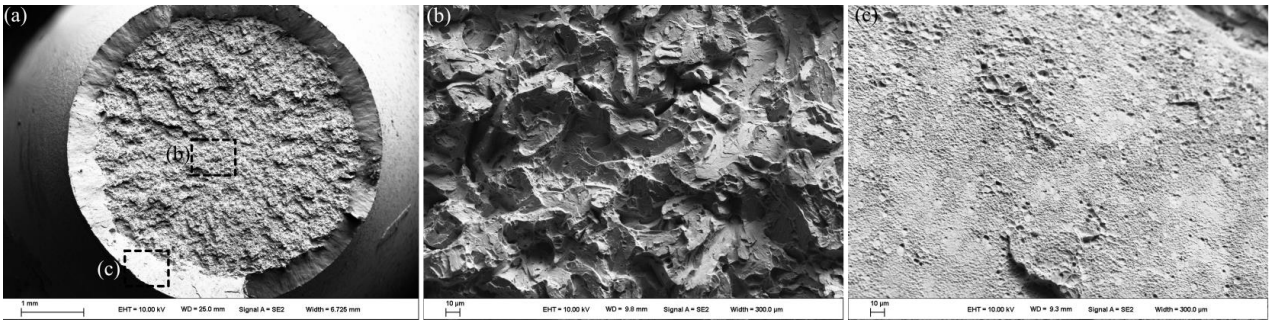

Figure 3-25. Secondary electron images of the fracture surface of a 9mm-notched sample tested at -40C are provided. A low-magnitude image of the entire fracture surface is show in (a). High-magnification images of the center (b) and shear lip (c) are also provided.

3.6. Flat-Grooved Plate Specimens

Typical plots of stress *versus* strain for flat-grooved plate specimens tested at 22° C and -40° C are provided in Figure 3-26 and Figure 3-28. Similar to other specimens, the UTS of specimens tested at -40° C was approximately 4% greater than that of specimens tested at 22° C. As Figure 3-27 and Figure 3-29 show, strain varied significantly across the width of the specimen. The difference between the strain measured on the left and right sides of the specimens was typically 3-4% strain for all specimens tested in this study. Similar distributions of strain were observed for samples tested at all temperatures.

Table 3-1 shows, the YS varied significantly (±4%) sample to sample, likely due to bending in the specimens caused by grip misalignment, see the Methods section for more details. Due to the extra scatter caused by misalignment, we cannot definitively conclude that there is a significant difference in YS or ductility between specimens tested at 22° C and -40° C.

Figure 3-30 shows images of a flat-groove sample tested at 22° C before and after testing. Full-field strain fields measured using DIC are overlaid on images of samples tested at 22° C and -40° C in Figure 3-31. The images in Figure 3-31 were taken immediately before fracture. The full-field strain data in these images show the strain localization on one side of the sample that occurred before fracture. Optical and SEM images of the fracture surface of flat-groove specimens tested at 22° C and -40° C are shown in Figure 3-32 to Figure 3-35. There appears to be little difference in fracture surfaces between samples tested at 22° C and -40° C.

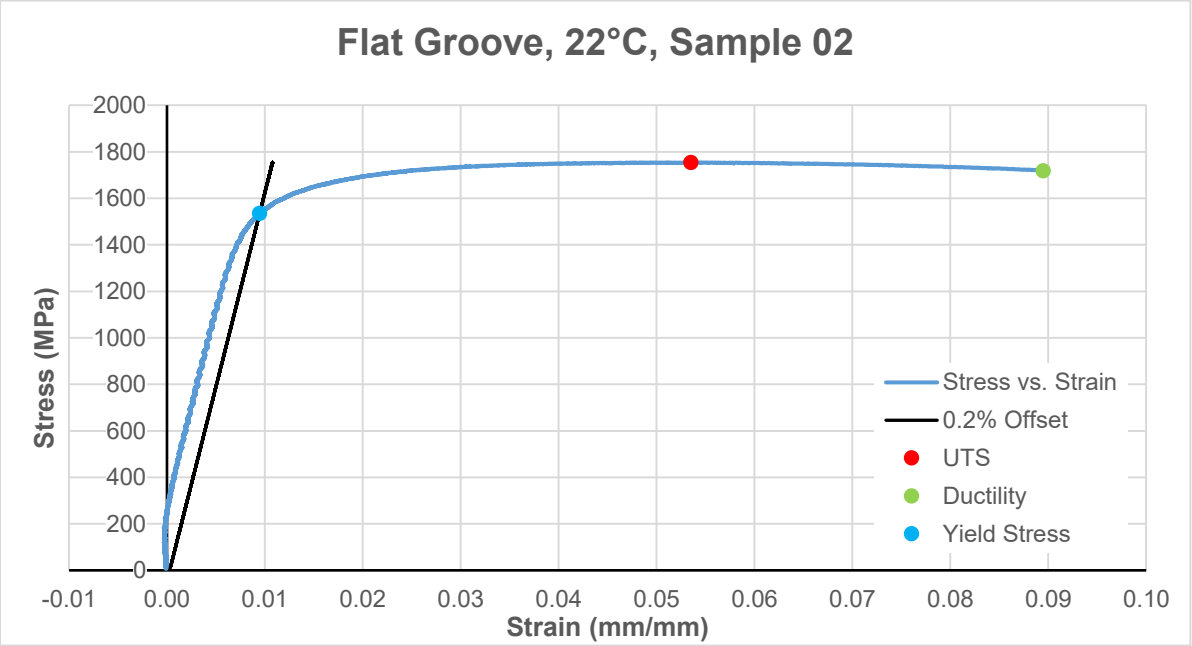

Figure 3-26. Stress-strain curve, Flat Groove, 22°C, Sample 02.

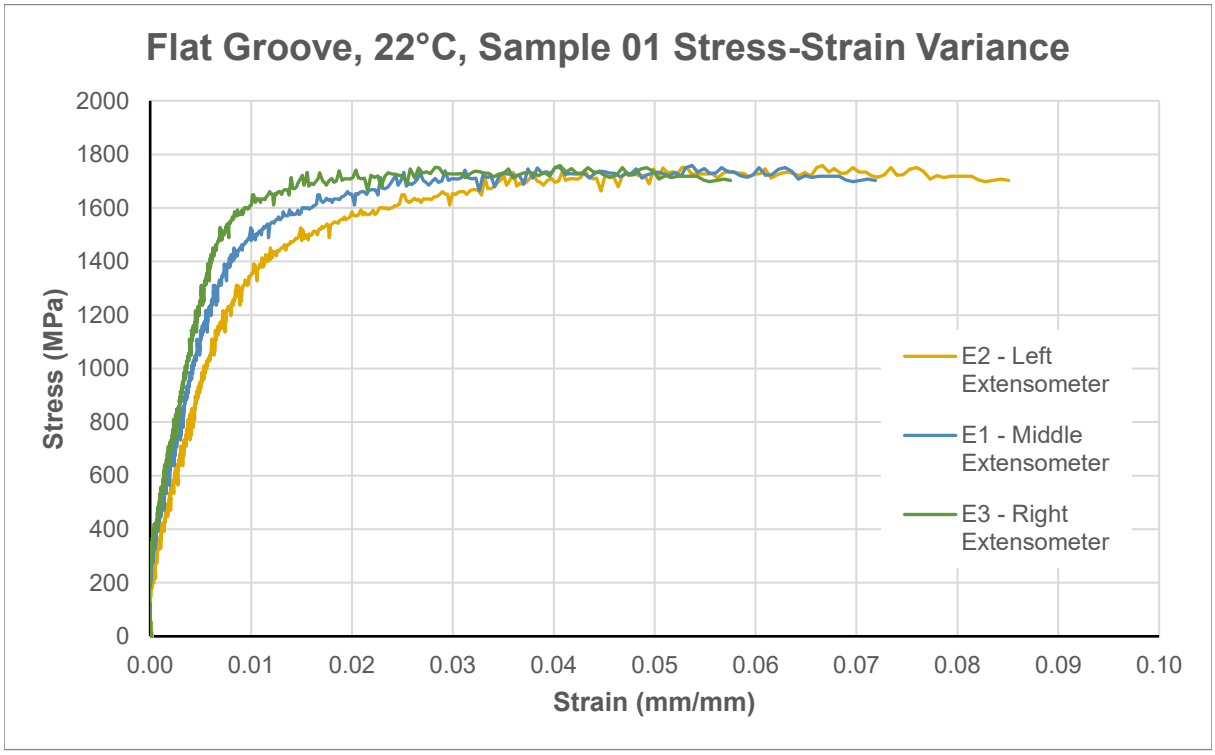

Figure 3-27. The distribution of strain across the sample measured using the extensometers shown in Figure 2-7 are provided for Flat Groove sample, 22°C, Sample 01.

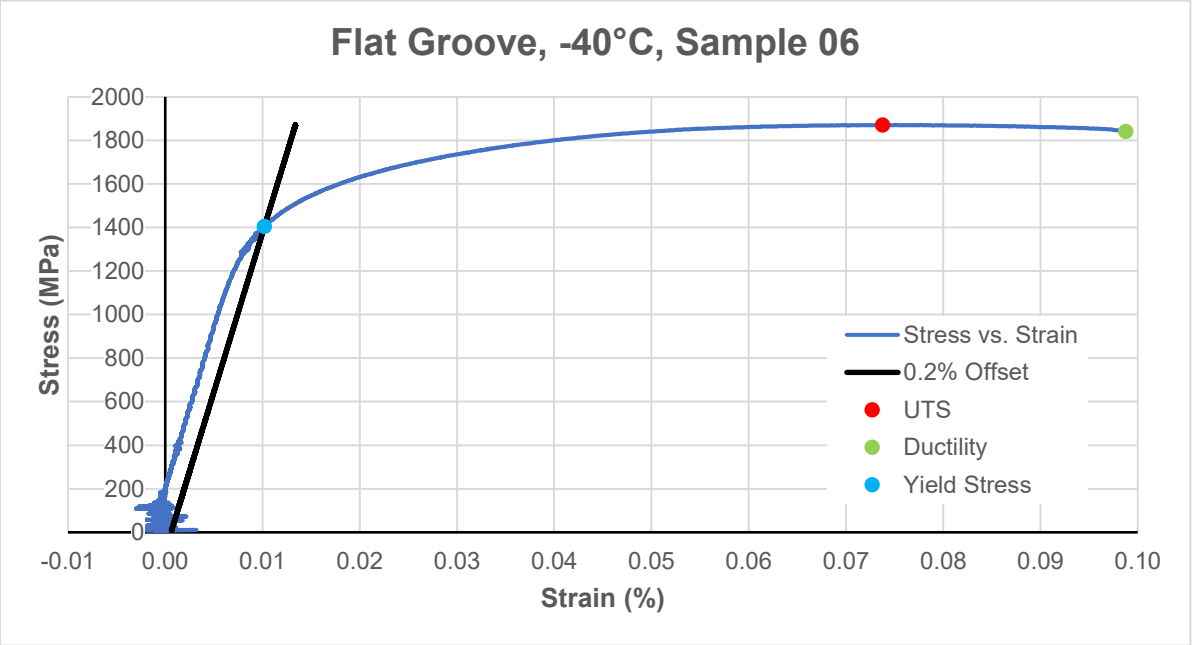

Figure 3-28. Stress-strain curve, Flat Groove, -40°C, Sample 06.

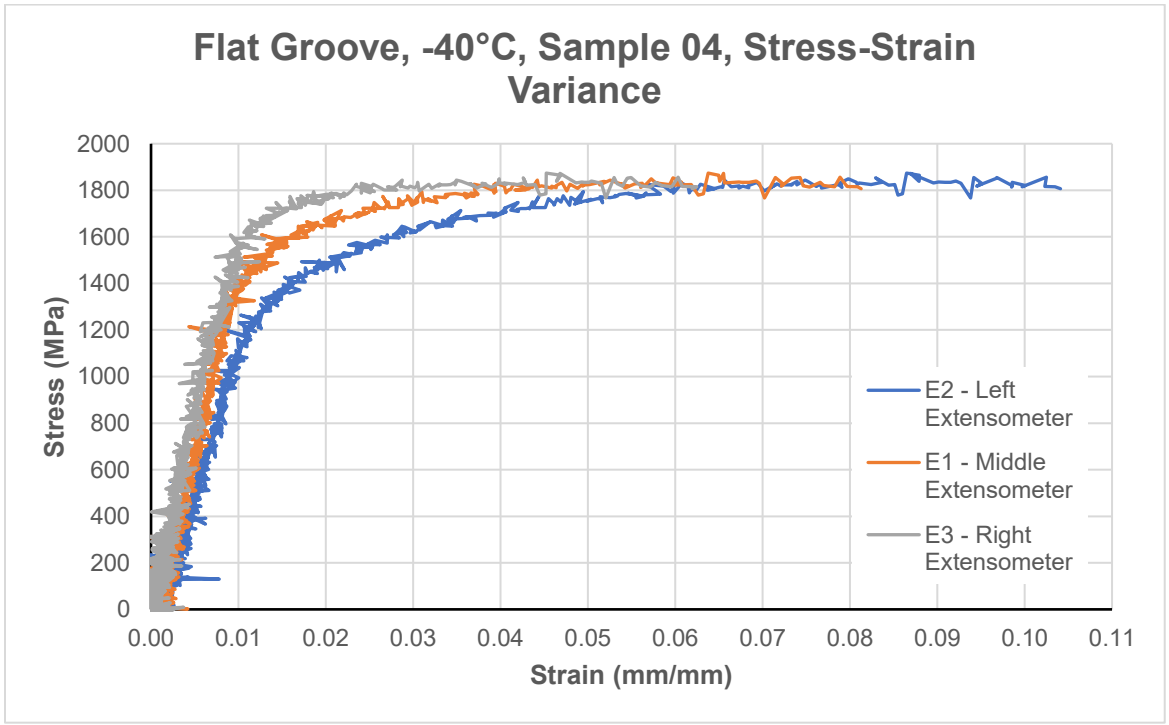

Figure 3-29. The distribution of strain across the sample measured using the extensometers shown in Figure 2-7 are provided for Flat Groove sample, -40°C, Sample 06.

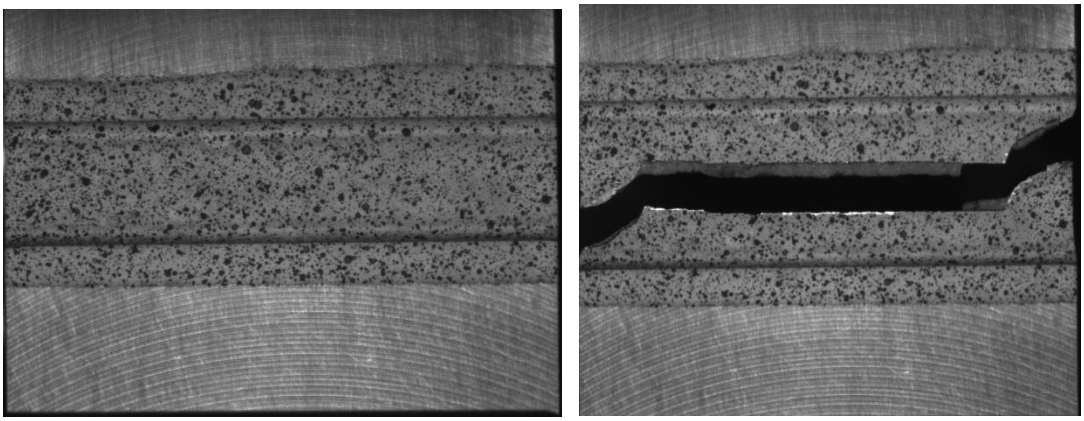

Figure 3-30. Pre-test and post-test images showing failure location Flat Groove, 22°C, Sample 08

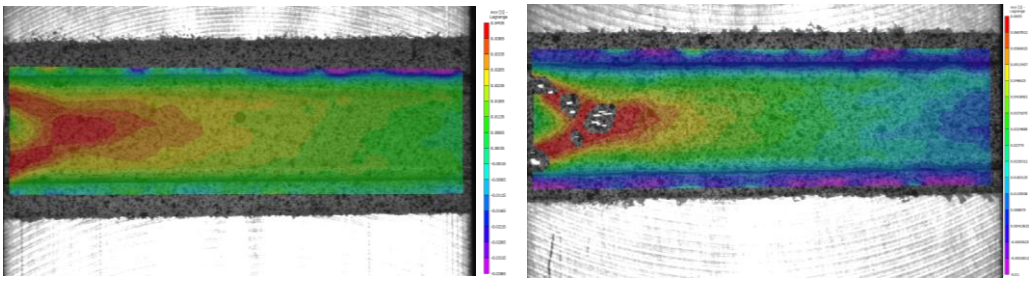

Figure 3-31. Full field strain (eyy) measurements for 9mm notch specimens immediately before failure, 22°C, Sample 01 (left) and -40°C, Sample 04 (Right). Paint chipped off Sample 04 because of the cold temperatures. Strain localizes on the left edge due to slight misalignment in the pinch grips. Note the different scales for strain, left: 4.4% to -3.7%, right: 6.6% to -1.0%. Negative strain measurements are from measurement noise.

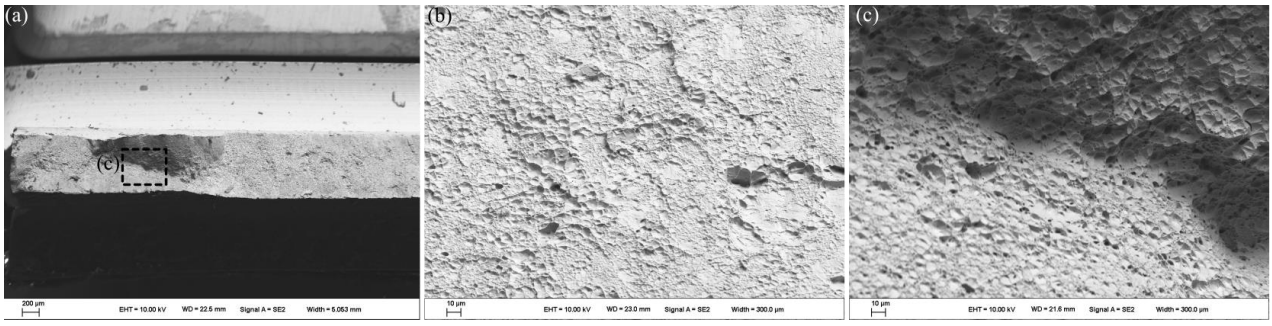

Figure 3-32. Secondary electron images of the fracture surface of a flat-grooved sample tested at 22° C are provided. A low-magnitude image of the left side of the fracture surface is show in (a). A high-magnification image of the center of the fracture surface is shown in (b). A high-magnification image of the left side of the fracture surface is shown in (c).

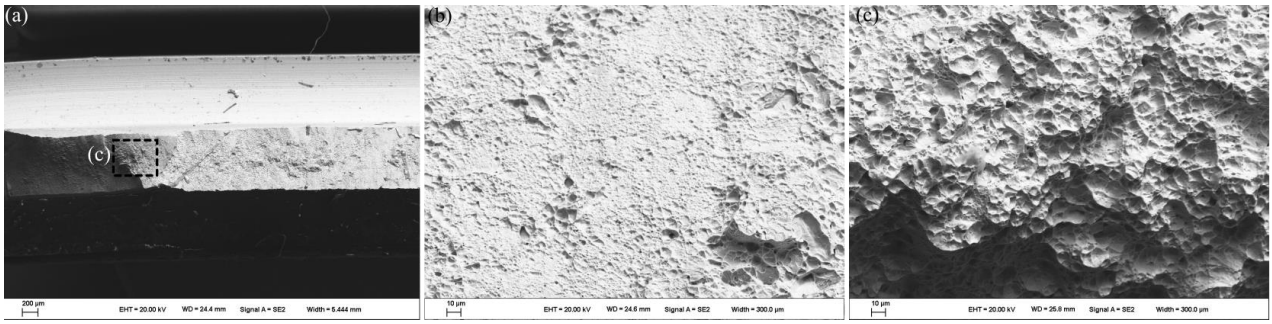

Figure 3-33. Secondary electron images of the fracture surface of a flat-grooved sample tested at -40° C are provided. A low-magnitude image of the left side of the fracture surface is show in (a). A high-magnification image of the center of the fracture surface is shown in (b). A high-magnification image of the left side of the fracture surface is shown in (c).

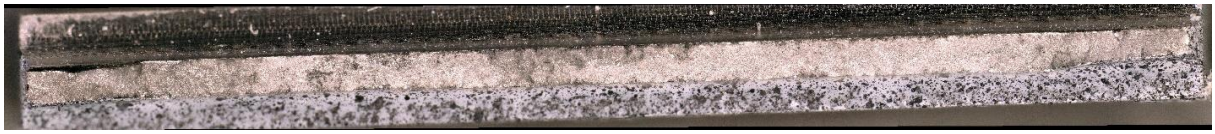

Figure 3-34. Fracture Surface – Flat Groove, 22°C, Sample 01

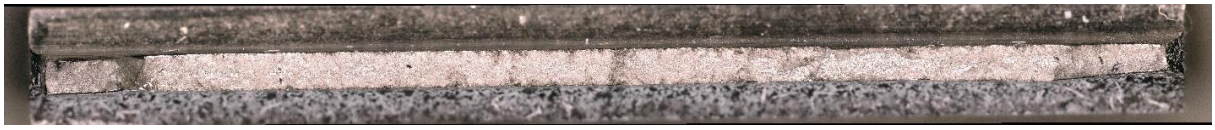

Figure 3-35. Fracture Surface – Flat Groove, -40°C, Sample 03

3.7. Shear Specimens

Typical plots of force *versus* displacement for shear samples tested at 22° C and -40° C are provided in Figure 3-36 and Figure 3-37. As discussed in the Methods section, ductility measurements were highly sensitive to the exact location at which the virtual extensometer was placed and plots of stress *versus* strain are thus not shown. The sensitivity of strain measurements to the location of the extensometer is the likely explanation for the significant variation observed between samples in ductility. The UTS and YS of shear specimens increased significantly with decreasing testing temperature. Measured specimen displacement also increased slightly with decreasing temperature, though no significant difference in strain at failure was observed as a function of temperature.

Figure 3-38 shows images of a shear specimen tested at 22° C before and after testing. Full-field shear strain measurements are overlaid on images of samples tested at 22° C and -40° C in Figure 3-39. The images in Figure 3-39 were taken immediately before fracture. SEM images of the fracture surface of shear specimens at 22° C and -40° C are shown in Figure 3-40 and Figure 3-41. Shear

dimples were observed across the fracture surfaces of both specimens. Optical images of the fracture surfaces of shear samples are provided in Appendix C.

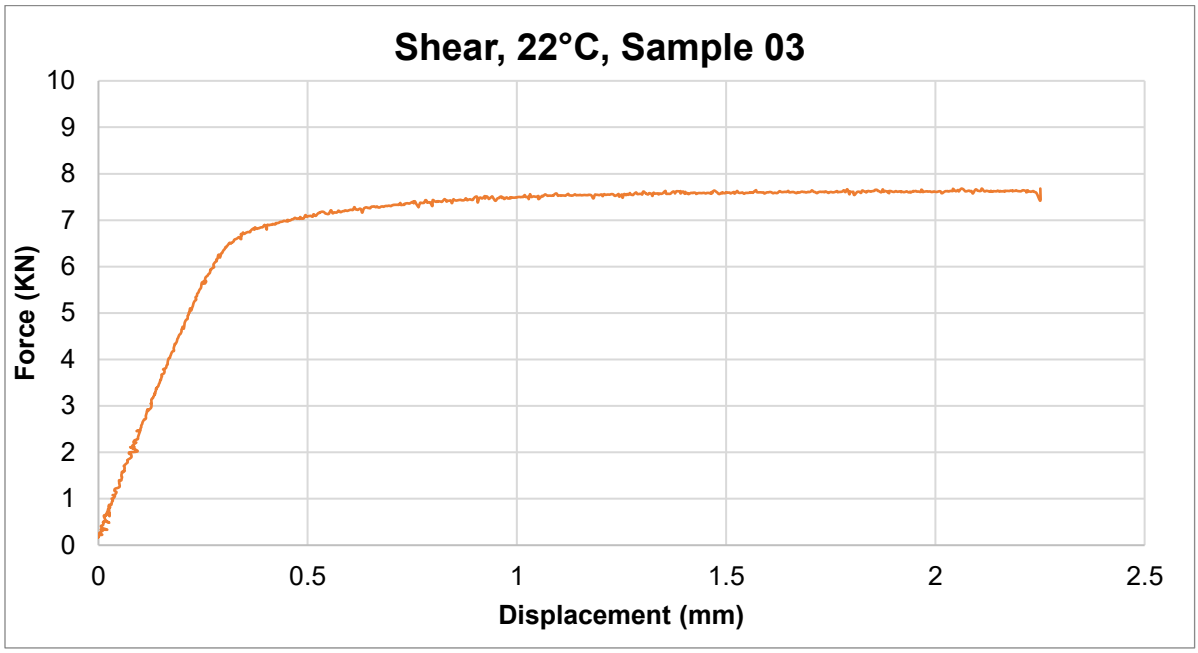

Figure 3-36. Force-displacement curve, Shear, 22°C, Sample 03.

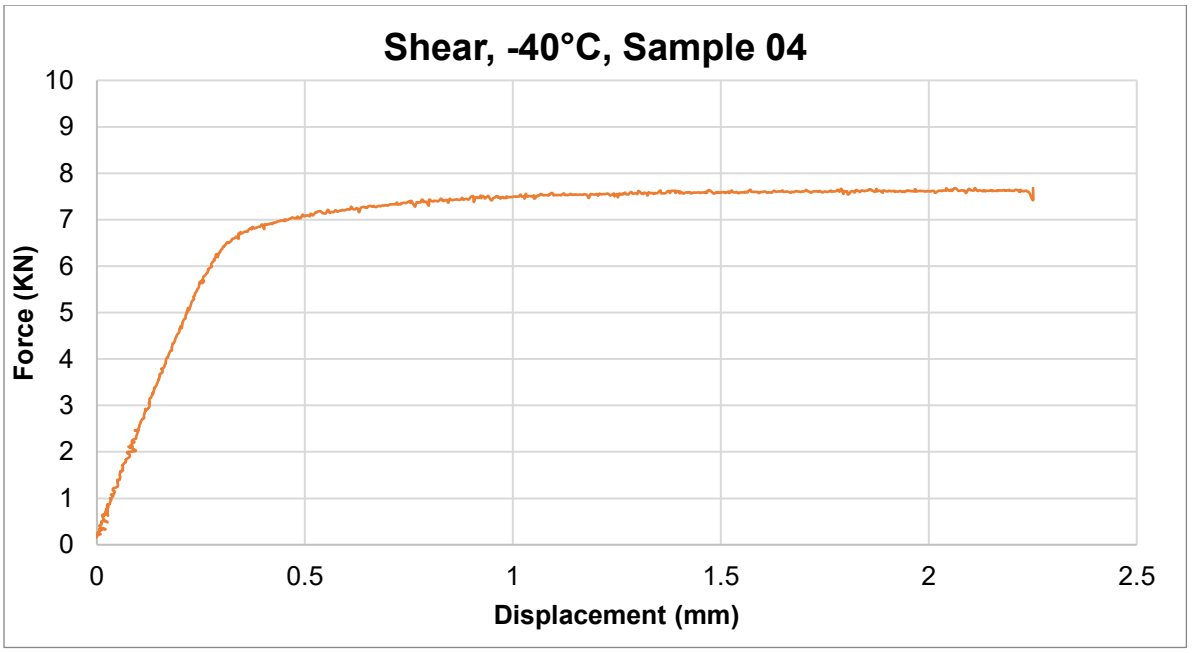

Figure 3-37. Force-displacement curve, Shear, -40°C, Sample 04.

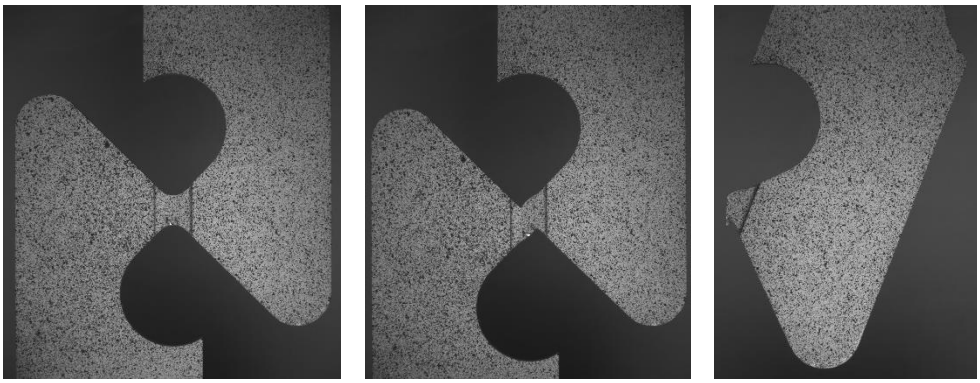

Figure 3-38. Pre-test and post-test images showing failure location of a shear sample, sample 2, tested at 22°C.

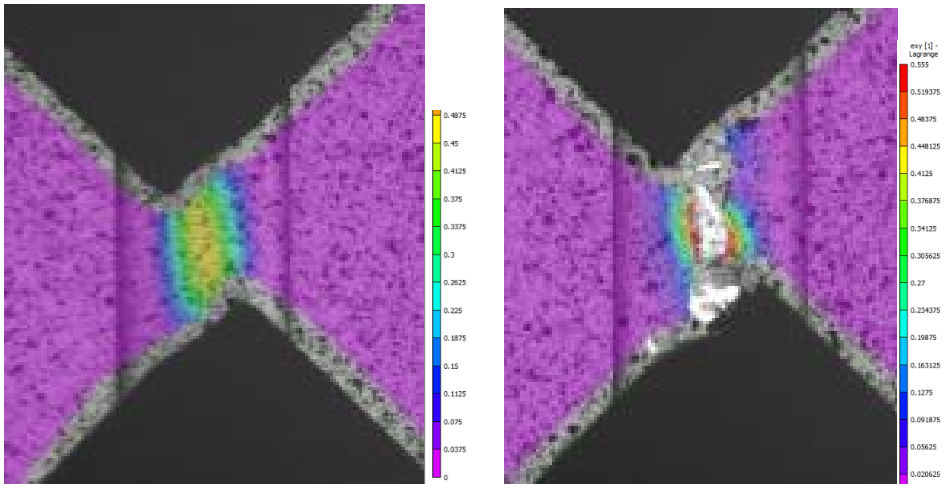

Figure 3-39. Full field strain (exy) measurements for shear specimens immediately failure, 22°C, Sample 01 (left) and -40°C, Sample 06 (Right). Paint chipping in the center of the sample tested at -40° C prevented the shear strain in the center of the sample immediately before failure from being evaluated. Note the different scales for strain, left: 48.8% to 0%, right: 55.5% to 0%.

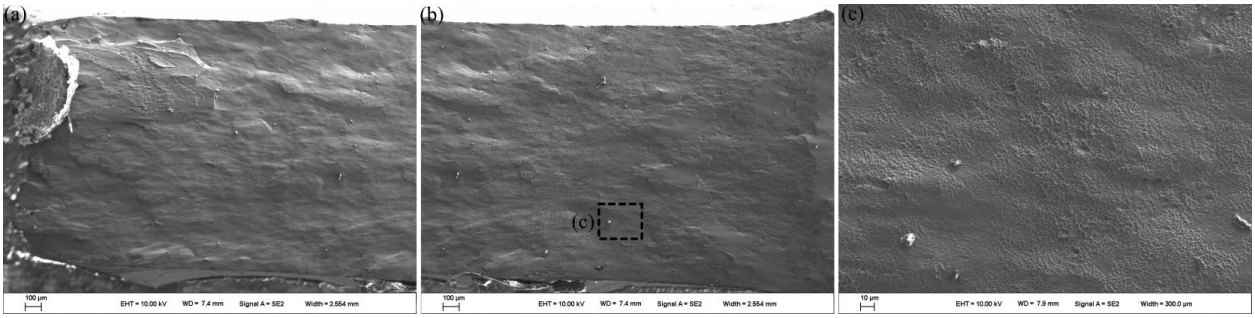

Figure 3-40. Secondary electron images of the fracture surface of a shear sample tested at -40C are provided. Low-magnitude images of the (a) left and (b) center of the fracture surface are shown. A high-magnification images of the center of the fracture surface is provided in (c).

[7]

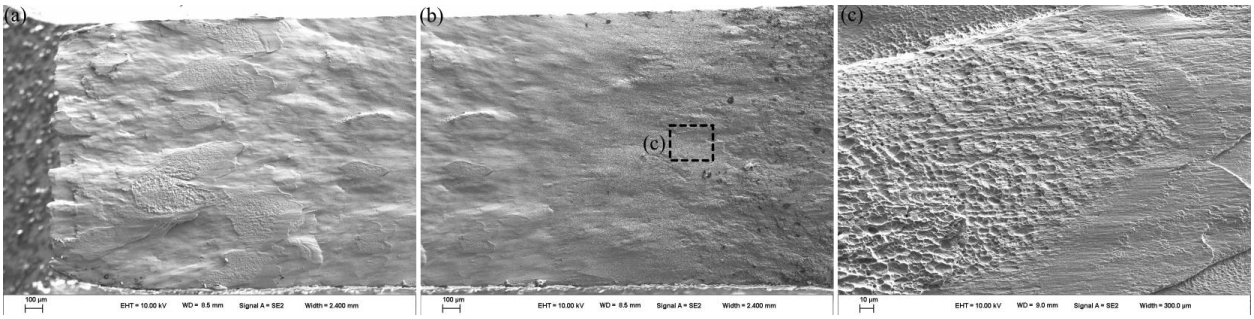

Figure 3-41. Secondary electron images of the fracture surface of a shear sample tested at 22C are provided. Low-magnitude images of the (a) left and (b) center of the fracture surface are shown. A high-magnification images of the center of the fracture surface is provided in (c).

4. DISCUSSION AND CONCLUSIONS

The goal of this project was to collect the data needed to build a Xue-Wierzbicki (XW) [1] fracture model for PH 13-8 SS for structural analysis between room temperature and -40° C. An initial study, documented in Sandia Report SAND2018-10921, was performed to build a XW model for PH 13-8 SS at room-temperature. The goal of this model was to assess any differences in the mechanical performance of this material between room temperature and -40° C. The two major takeaways from this study are:

1) The mechanical behavior reported in this study for PH 13-8 SS at room temperature was similar to that reported previously in SAND2018-10921, and
2) The fracture toughness and ductility of this material decreases significantly between 22° C (room temperature) and -40° C.

Regarding 2), the measured decrease in ductility depended on the loading conditions of the specimen.

The fracture toughness of this material at -40° C, 36.4 MPa√m, was 68% of the room-temperature fracture toughness, 53.6 MPa√m. Fracture surfaces of all samples tested at -40° C generally exhibited ductile dimples, including that of 3mm notch samples. The fracture surface of 3mm notch samples also included features typical of brittle cleavage, suggesting a combination of failure mechanisms. These data suggest that the ductile-to-brittle transition temperature for this material is near -40° C.

In general, decreasing testing temperature was associated with a 3-5% increase in UTS and YS and a negligible decrease in ductility. No change in ductility was observed for shear specimens and flat-groove specimens while slight decreases in ductility and reduction in area were measured for R5 and 9mm notch specimens. The ductility of 3mm notch specimens decreased significantly with testing temperature. The measured ductility and reduction in area of 3mm notch specimens tested at room temperature were nearly three and four times that of specimens tested at -40° C, respectively. Images of the fracture surfaces of 3mm notch specimens indicate a transition in fracture mechanism to one dominated by void nucleation, growth, and coalescence to a mix of brittle cleavage and void nucleation, growth, and coalescence. As discussed by Teirlinck *et al.* [7], fracture mechanisms depend on both testing temperature and loading conditions. For materials that undergo a transition from ductile to brittle fracture, the temperature at which this transition occurs increases with increasing stress triaxiality.

REFERENCES

1. Wierzbicki, T., et al., *Calibration and evaluation of seven fracture models.* International Journal of Mechanical Sciences, 2005. **47**(4-5): p. 719-743.
2. International, A., *Standard Test Methods for Tension Testing of Metallic Materials.* Standard Designation E8 -16, ASTM International, West Conshohocken, PA, 2016.
3. International, A., *Standard Test Method for Linear-Elastic Plane-Strain Fracture Toughness KIC of Metallic Materials.* Standard Designation E399-17, ASTM International, West Conshohocken, PA, 2017.
4. Hochanadel, P., et al., *Heat treatment of investment cast PH 13-8 Mo stainless steel: Part I. Mechanical properties and microstructure.* Metallurgical and Materials Transactions A, 1994. **25**(4): p. 789-798.
5. Internationa;, S., *AMS5629H Material Specification for 13Cr - 8.0Ni - 2.2Mo - 1.1Al.* AMS5629H.
6. Bachmann, F., R. Hielscher, and H. Schaeben. *Texture analysis with MTEX--free and open source software toolbox*. in *Solid State Phenomena*. 2010.
7. Teirlinck, D., et al., *Fracture mechanism maps in stress space.* Acta Metallurgica, 1988. **36**(5): p. 1213-1228.

APPENDIX A. ENGINEERING DRAWINGS OF TEST SPECIMENS

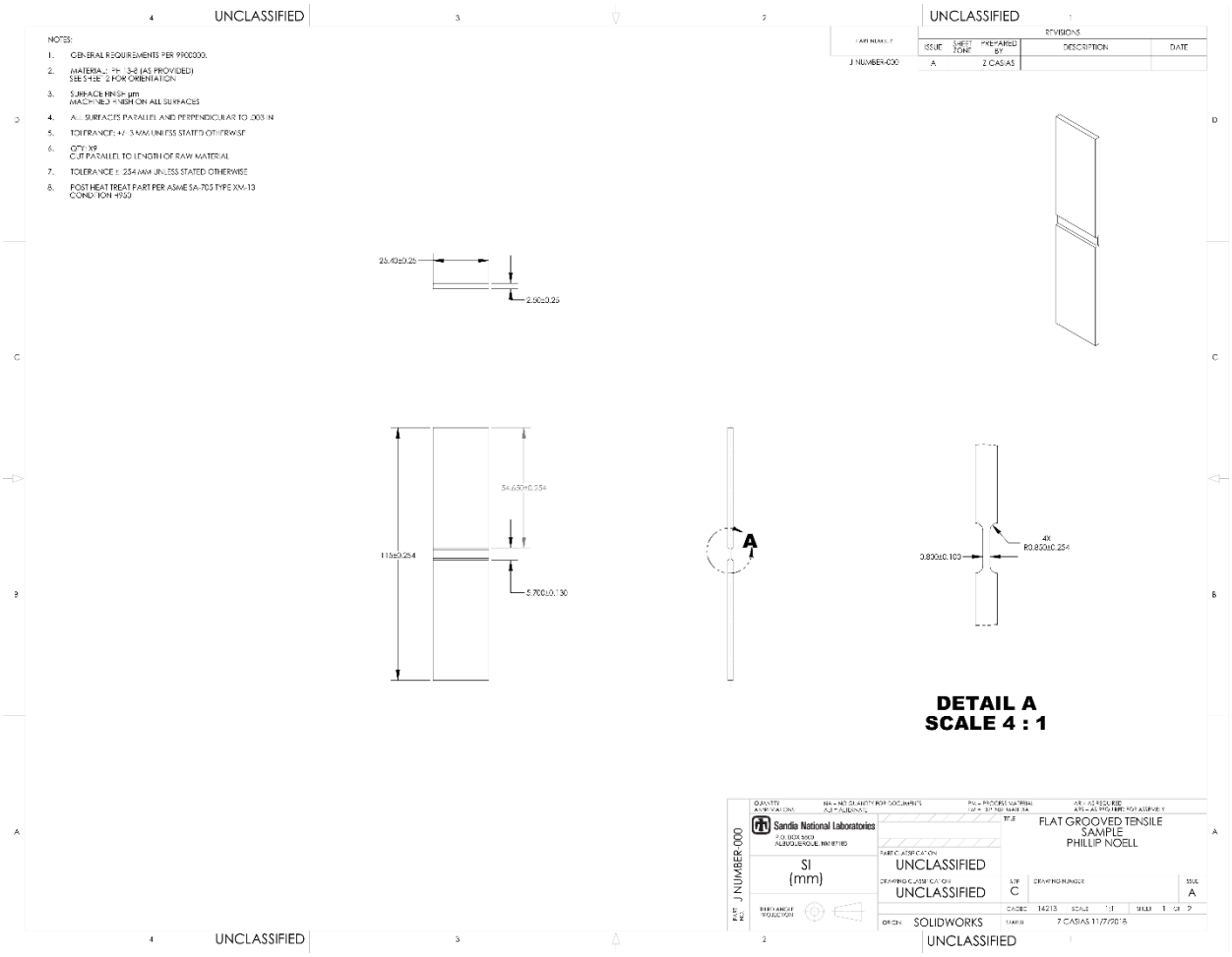

Figure A-1. The engineering drawing used for the flat-grooved plate specimen is shown.

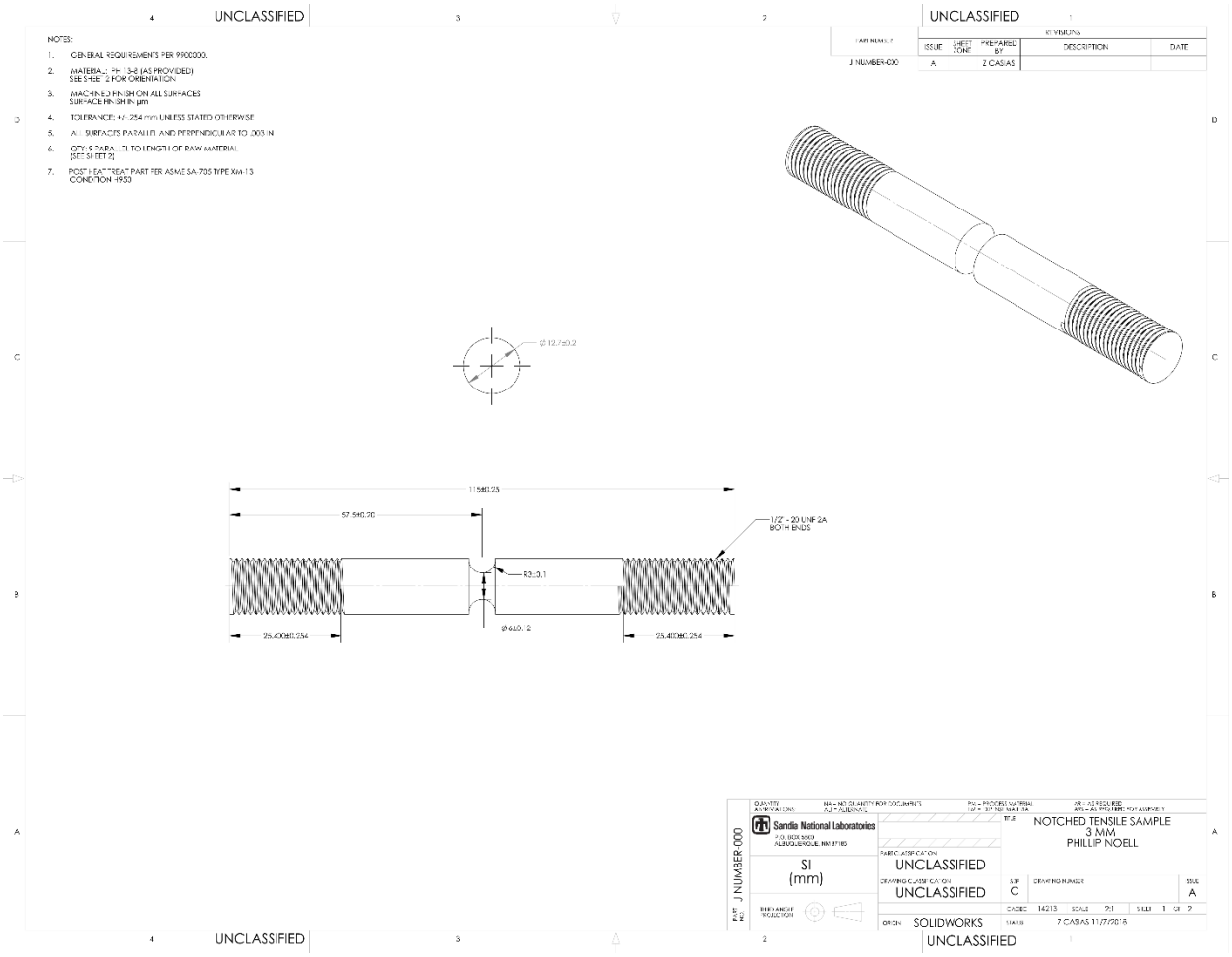

Figure A-2. The engineering drawing used for the 3 mm notched specimen is shown.

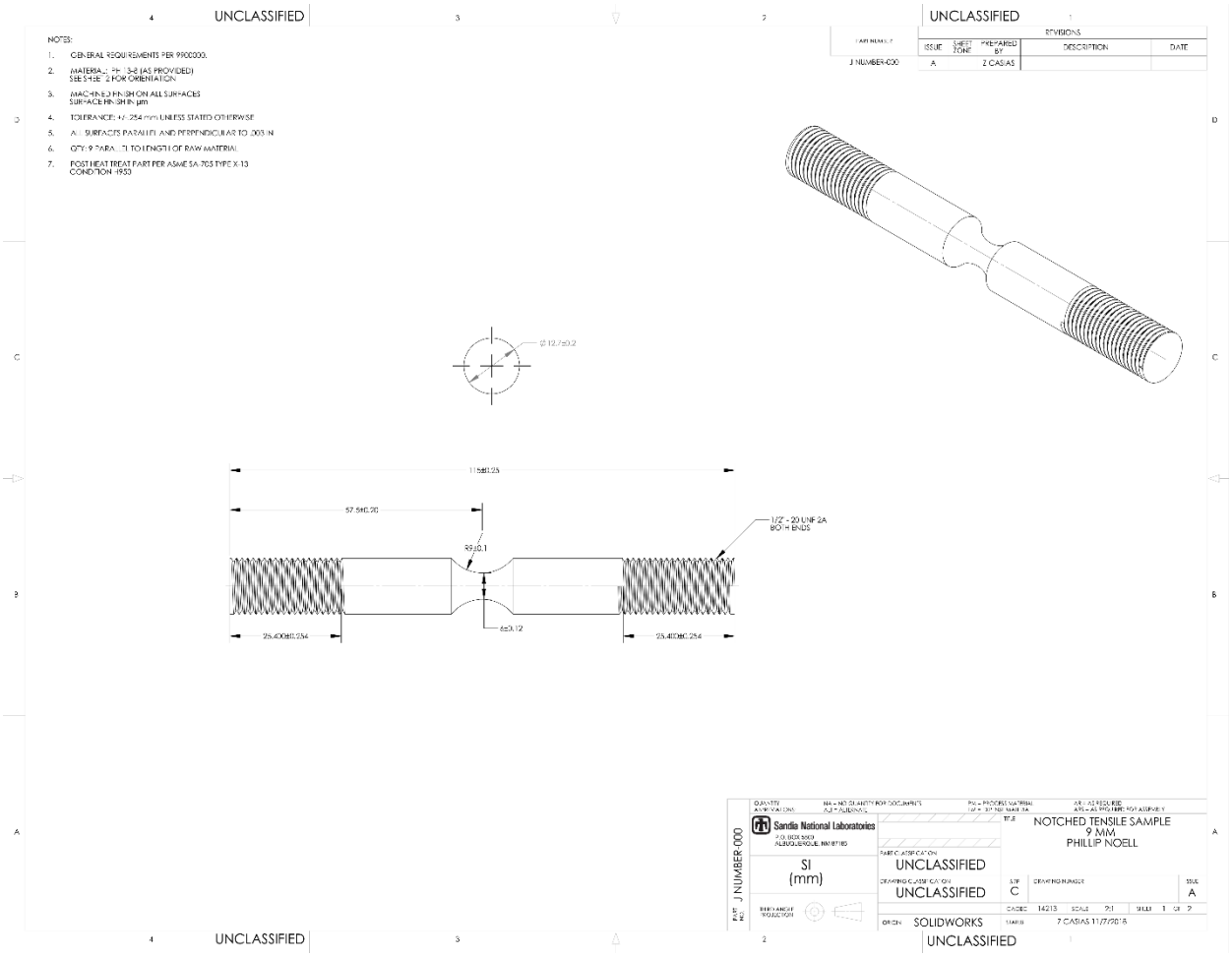

Figure A-3. The engineering drawing used for the 9 mm notched specimen is shown.

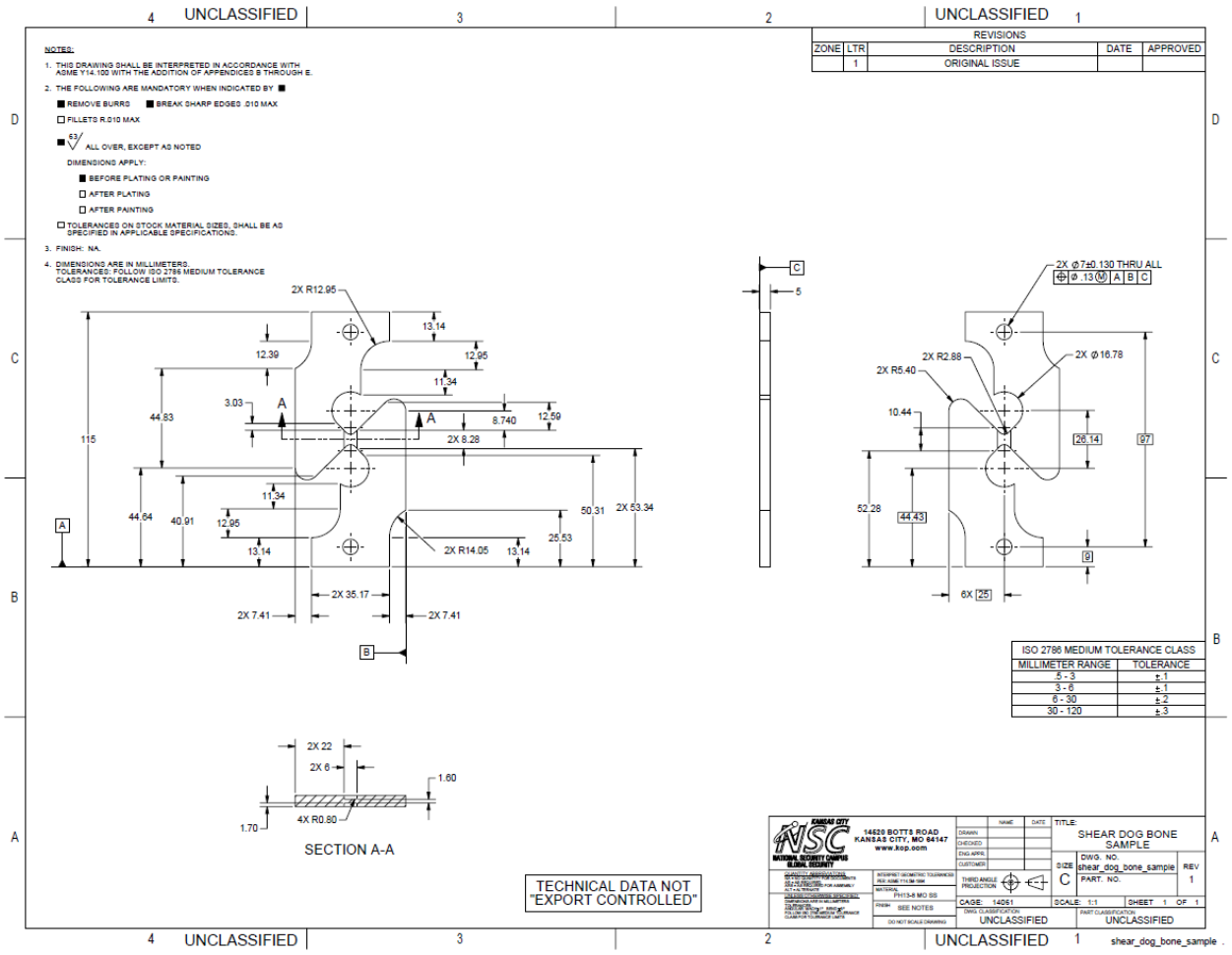

Figure A-4. The engineering drawing used for the shear specimen is shown.

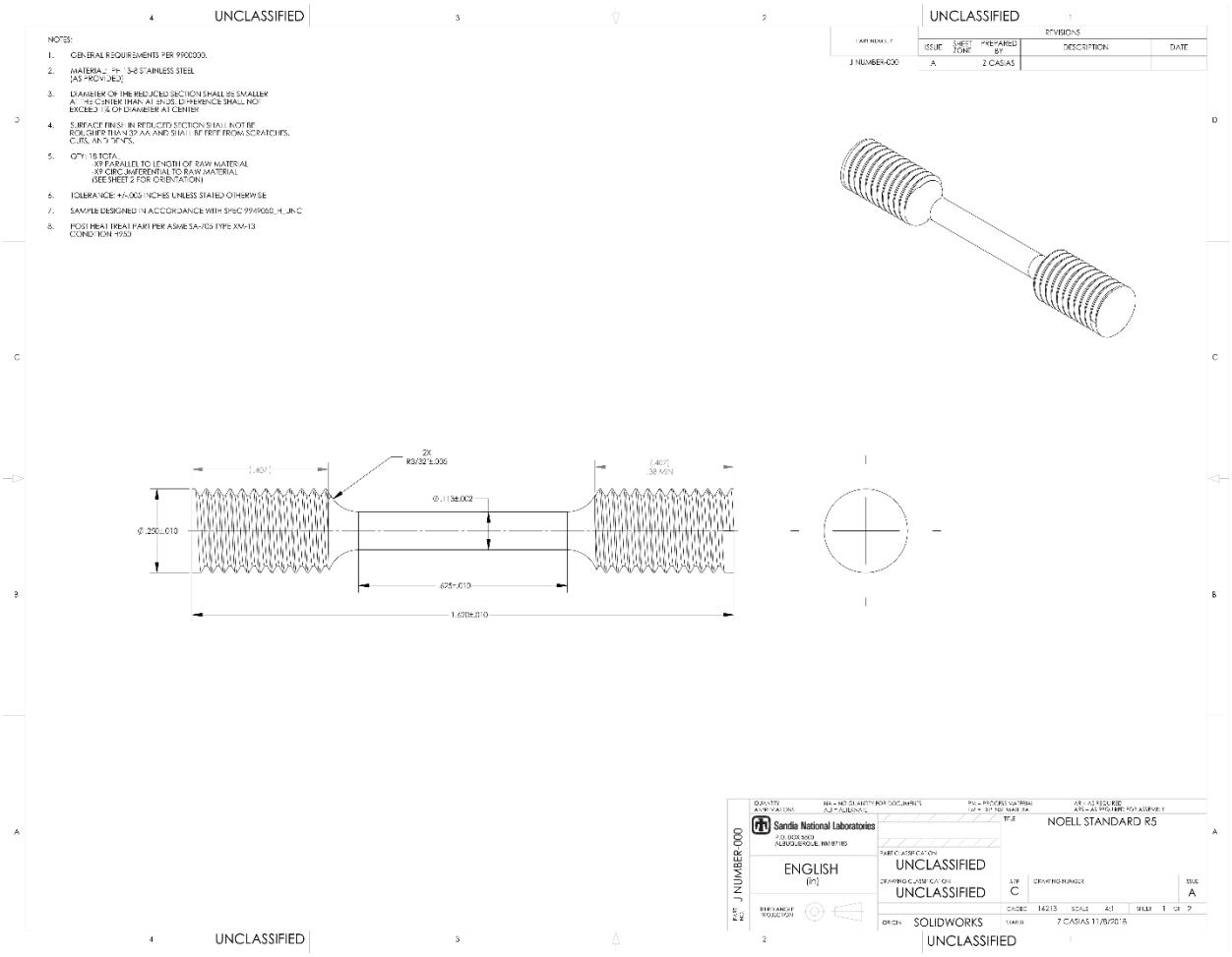

Figure A-5. The engineering drawing used for the R5 specimen is shown.

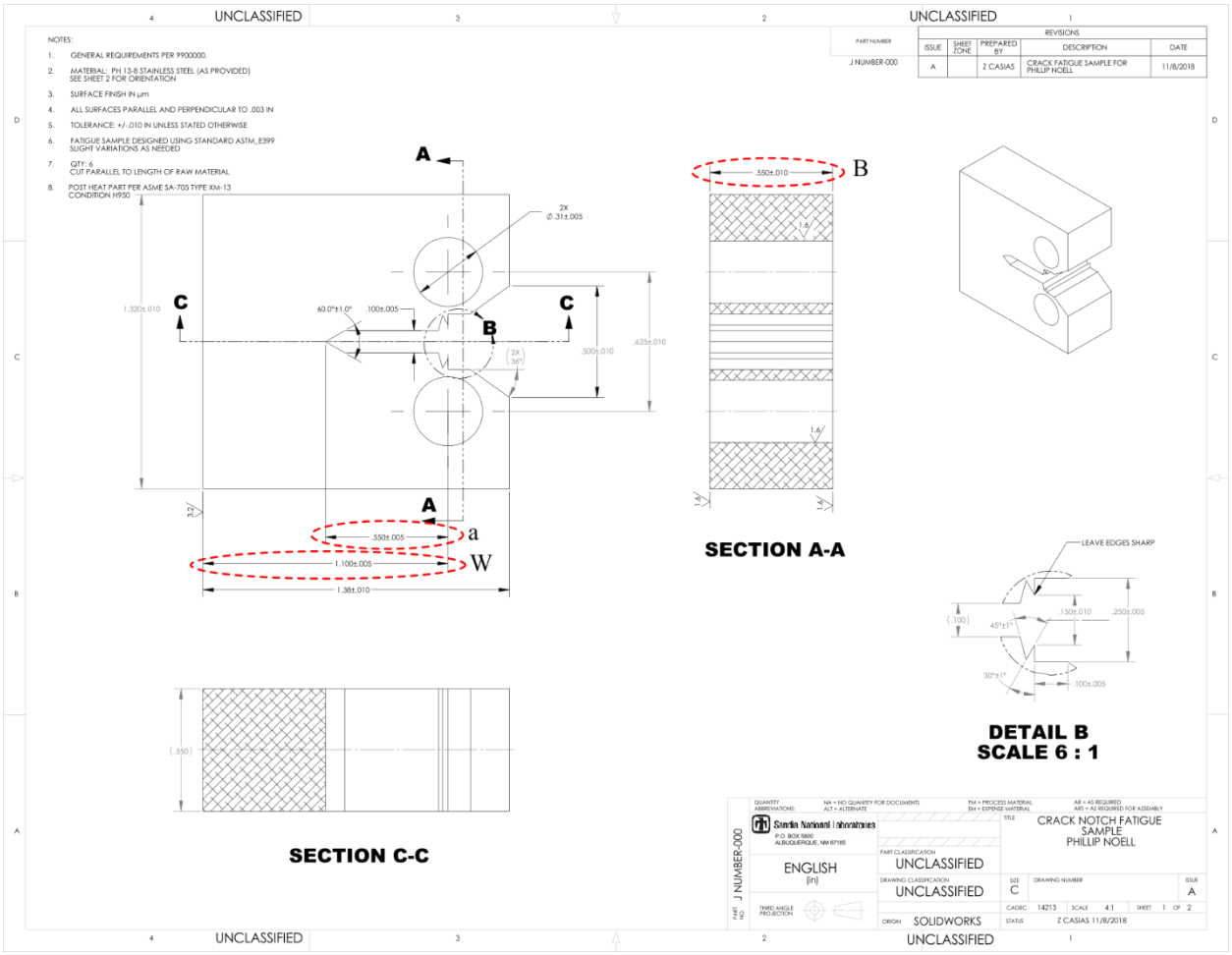

Figure A-6. The engineering drawing used for the compact tension specimen is shown.

APPENDIX B. STRESS VERSUS STRAIN PLOTS FOR SPECIMENS NOT INCLUDED IN BODY OF REPORT

B.1. R5 Parallel Specimens

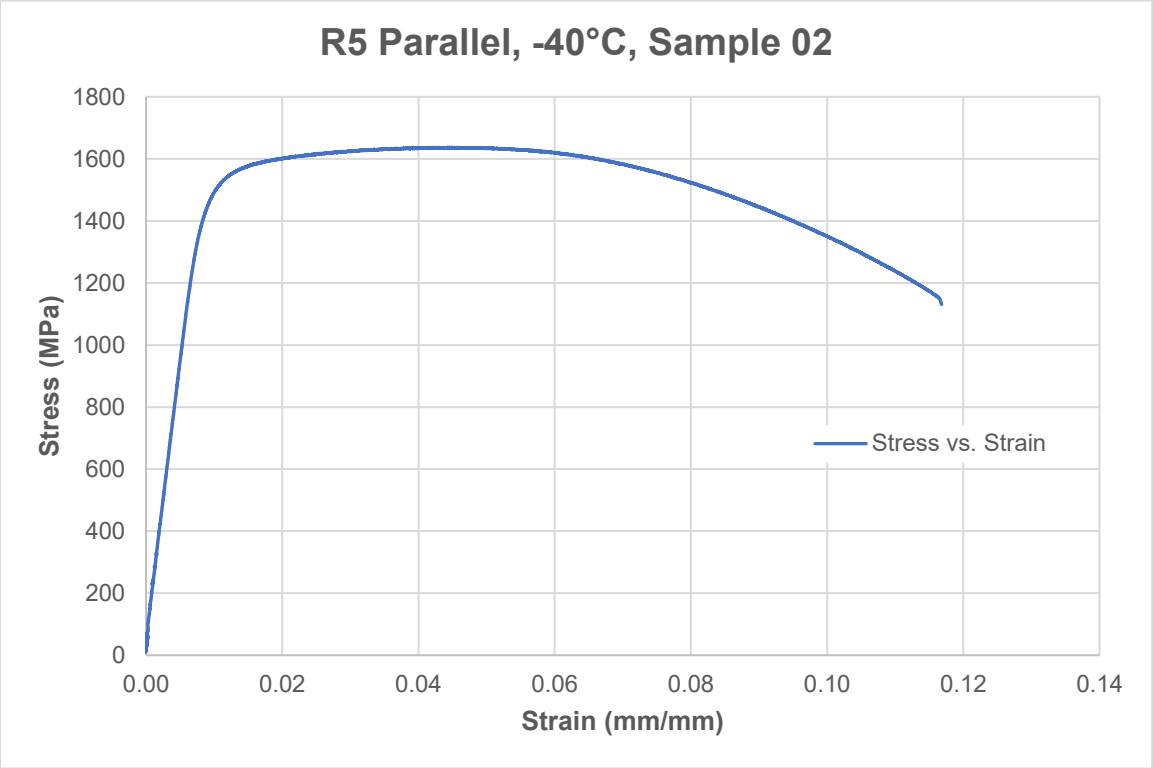

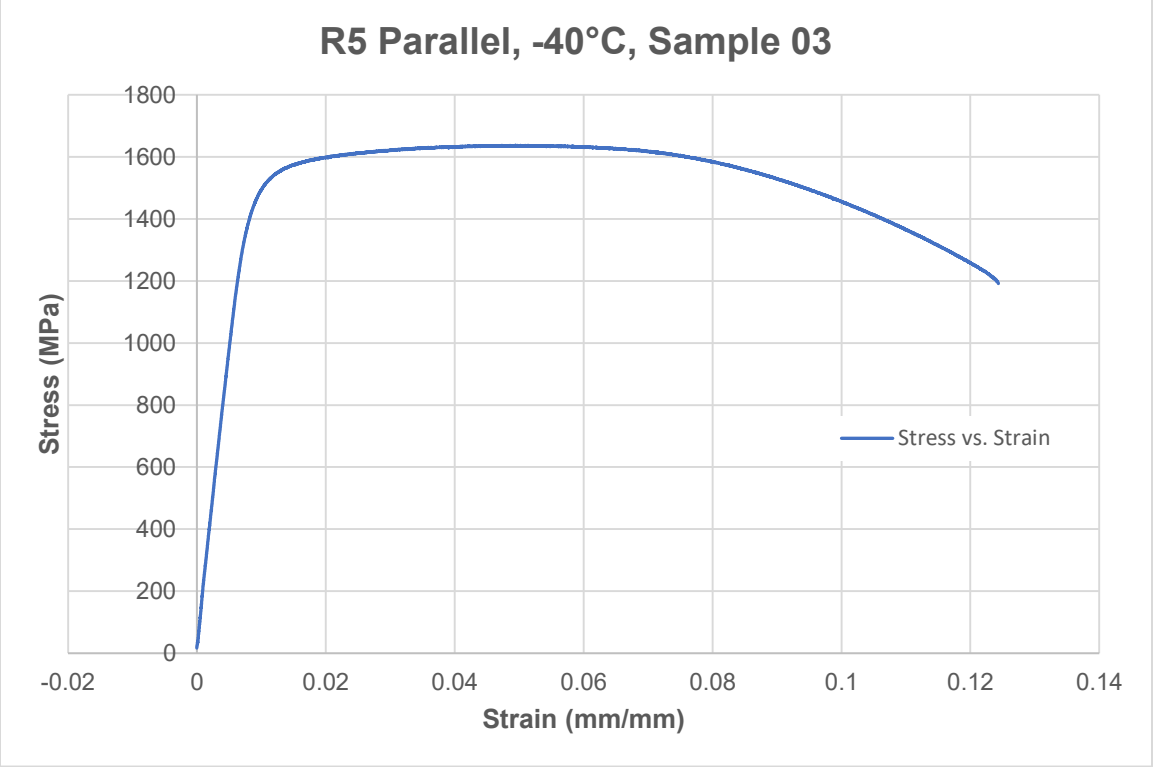

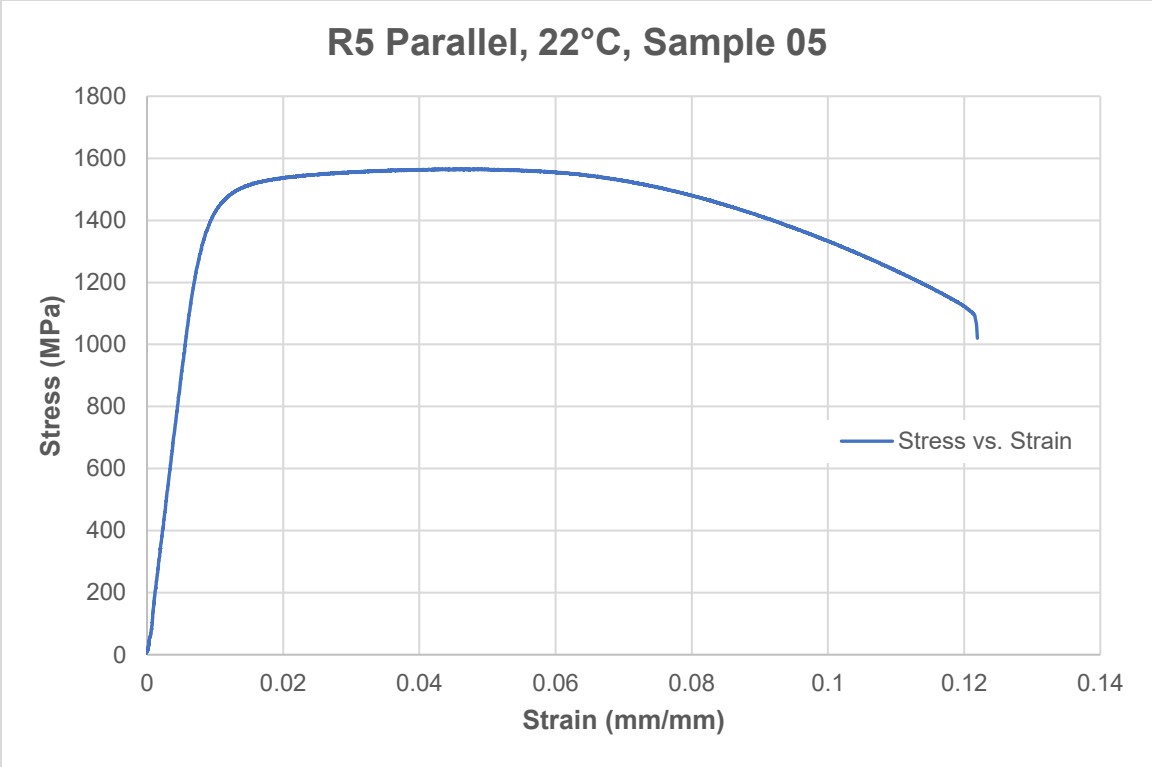
R5 Parallel, 22°C, Sample 05
Stress (MPa)
1800
1600
1400
1200
1000
800
600
400
200
0
0
0.02
0.04
0.06
0.08
0.1
0.12
0.14
Strain (mm/mm)
Stress vs. Strain

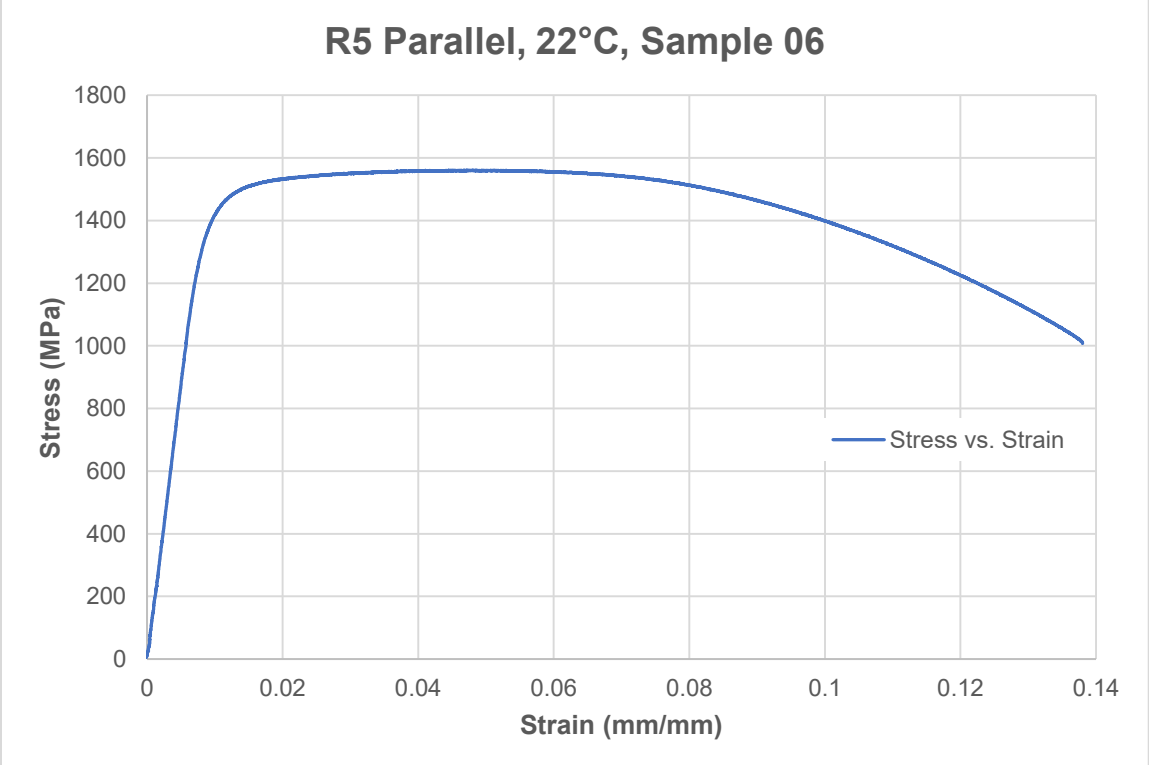
R5 Parallel, 22°C, Sample 06
Stress (MPa)
1800
1600
1400
1200
1000
800
600
400
200
0
0
0.02
0.04
0.06
0.08
0.1
0.12
0.14
Strain (mm/mm)
Stress vs. Strain

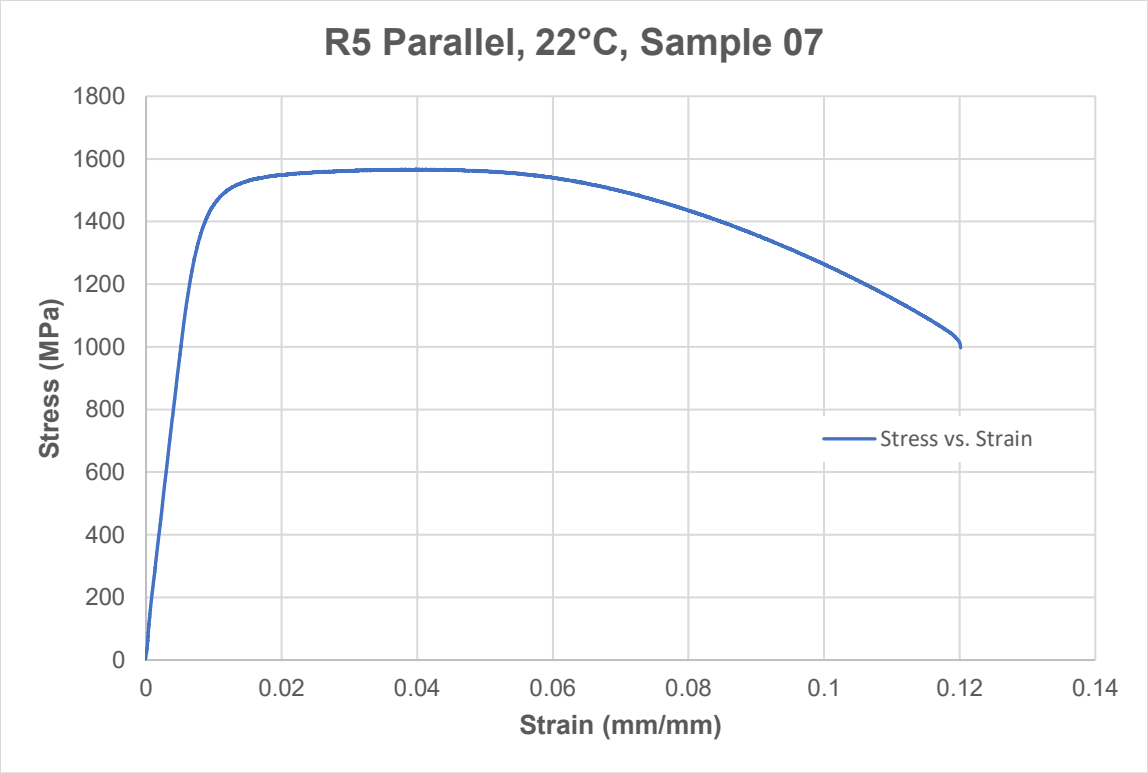

B.2. R5 Radial Specimens

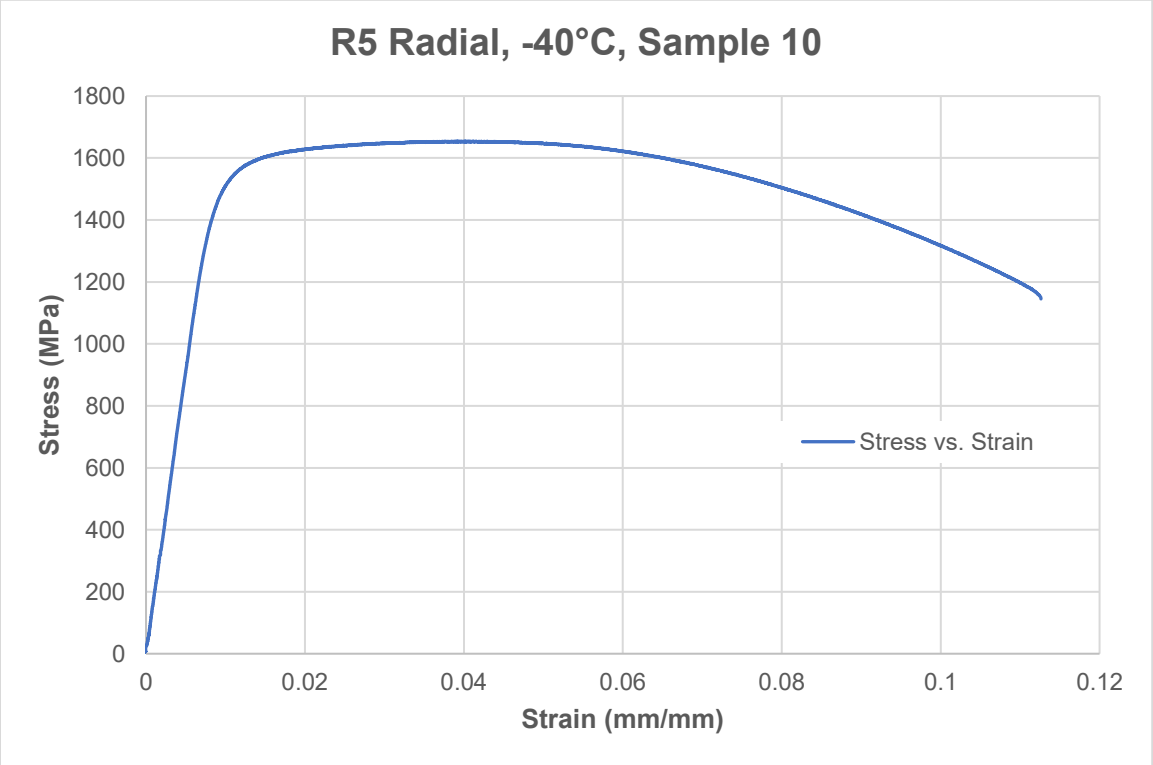

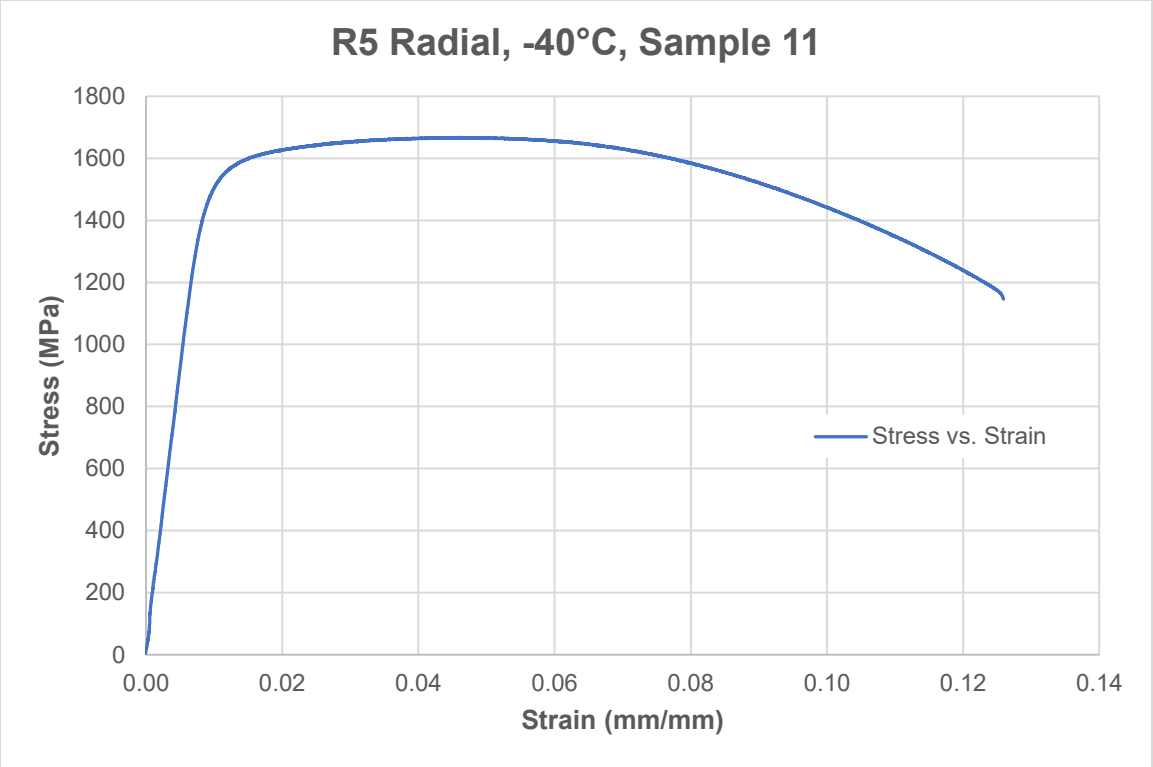
R5 Radial, -40°C, Sample 11
Stress (MPa)
1800
1600
1400
1200
1000
800
600
400
200
0
0.00
0.02
0.04
0.06
0.08
0.10
0.12
0.14
Strain (mm/mm)
Stress vs. Strain

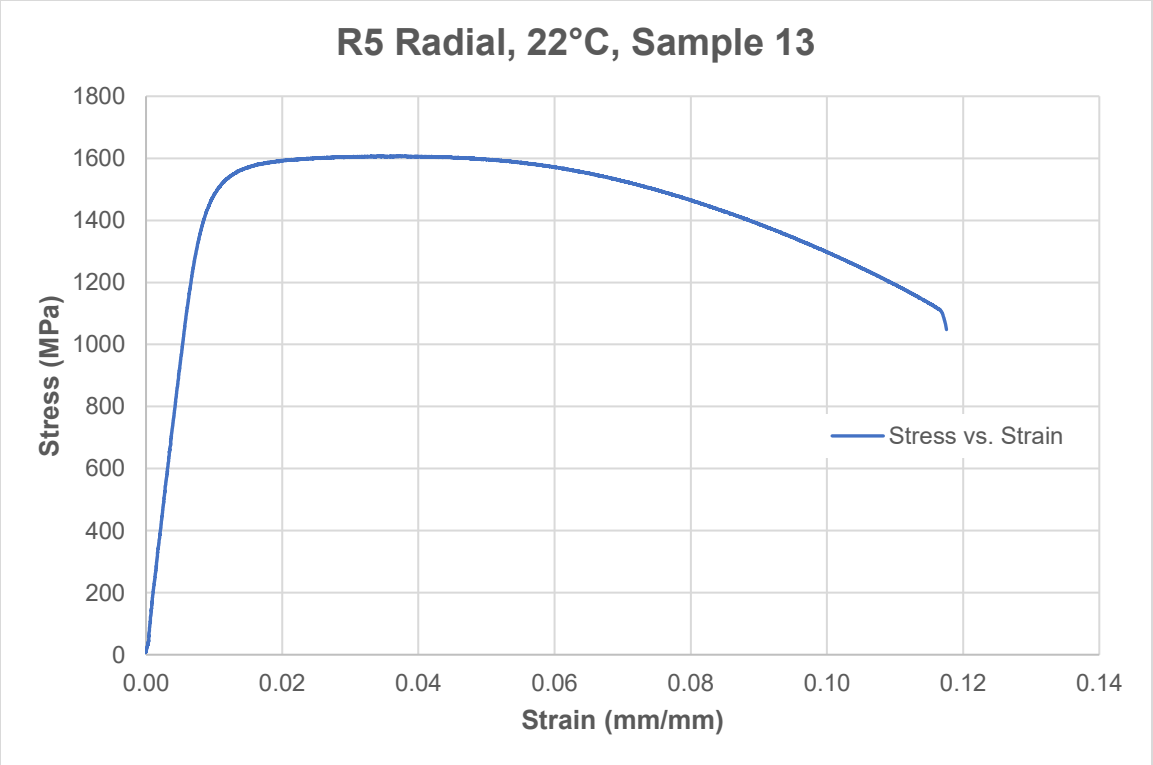
R5 Radial, 22°C, Sample 13
Stress (MPa)
1800
1600
1400
1200
1000
800
600
400
200
0
0.00
0.02
0.04
0.06
0.08
0.10
0.12
0.14
Strain (mm/mm)
Stress vs. Strain

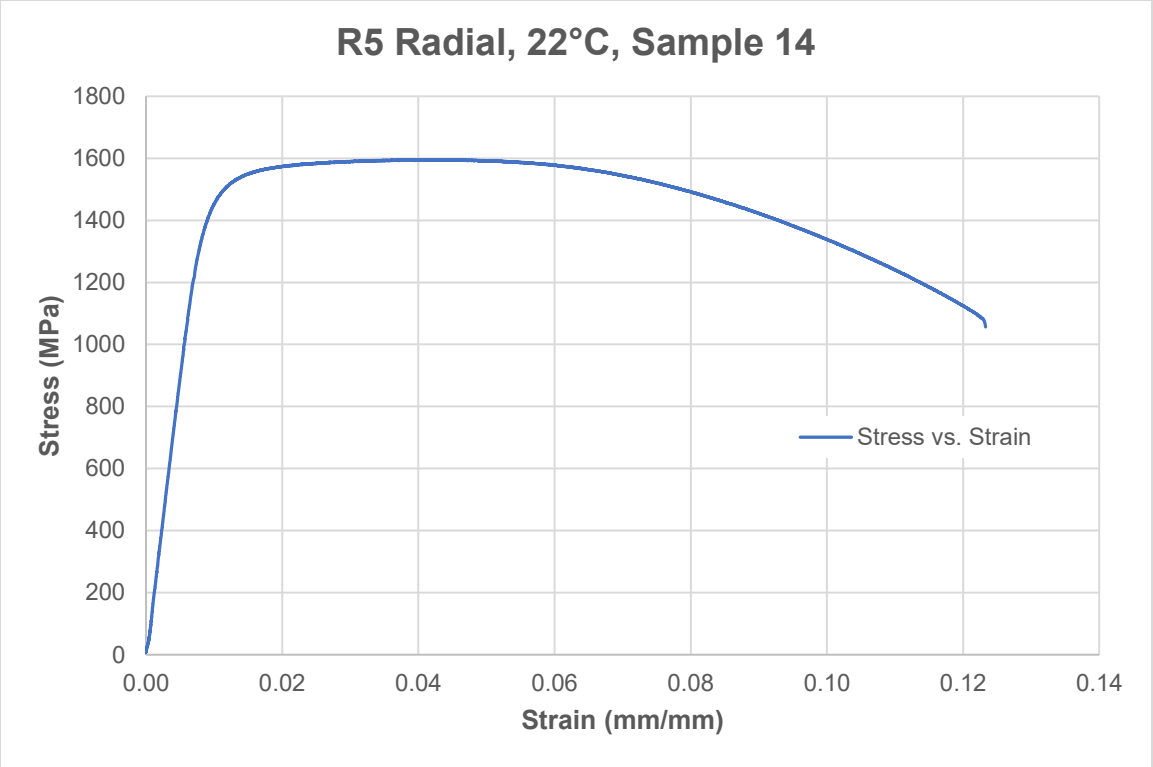

B.3. 3mm Notch Specimens

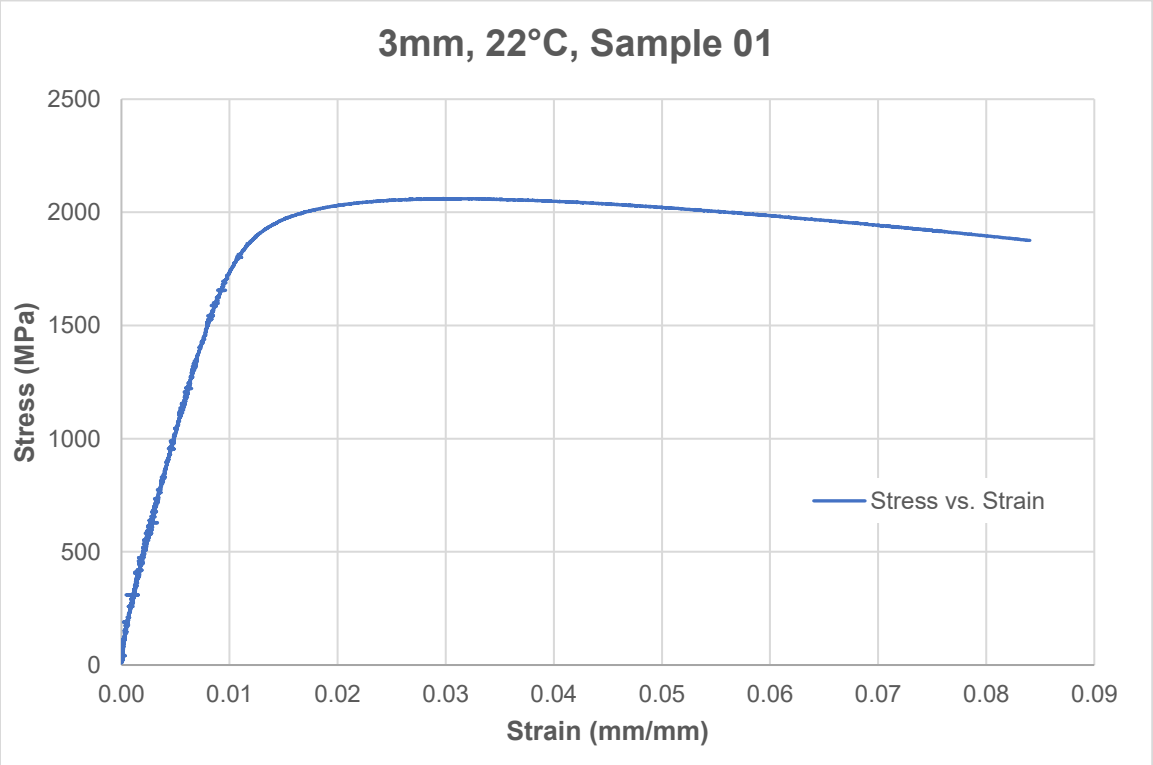

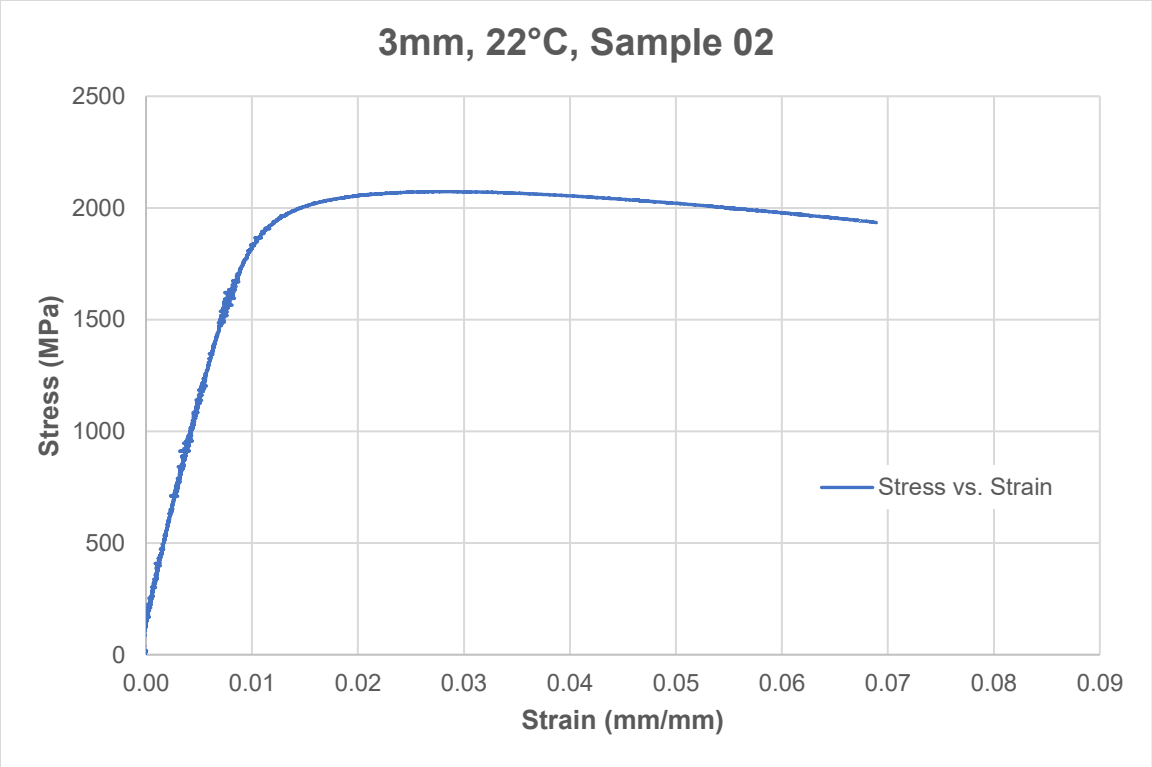
3mm, 22°C, Sample 02
Stress (MPa)
2500
2000
1500
1000
500
0
0.00
0.01
0.02
0.03
0.04
0.05
0.06
0.07
0.08
0.09
Strain (mm/mm)
Stress vs. Strain

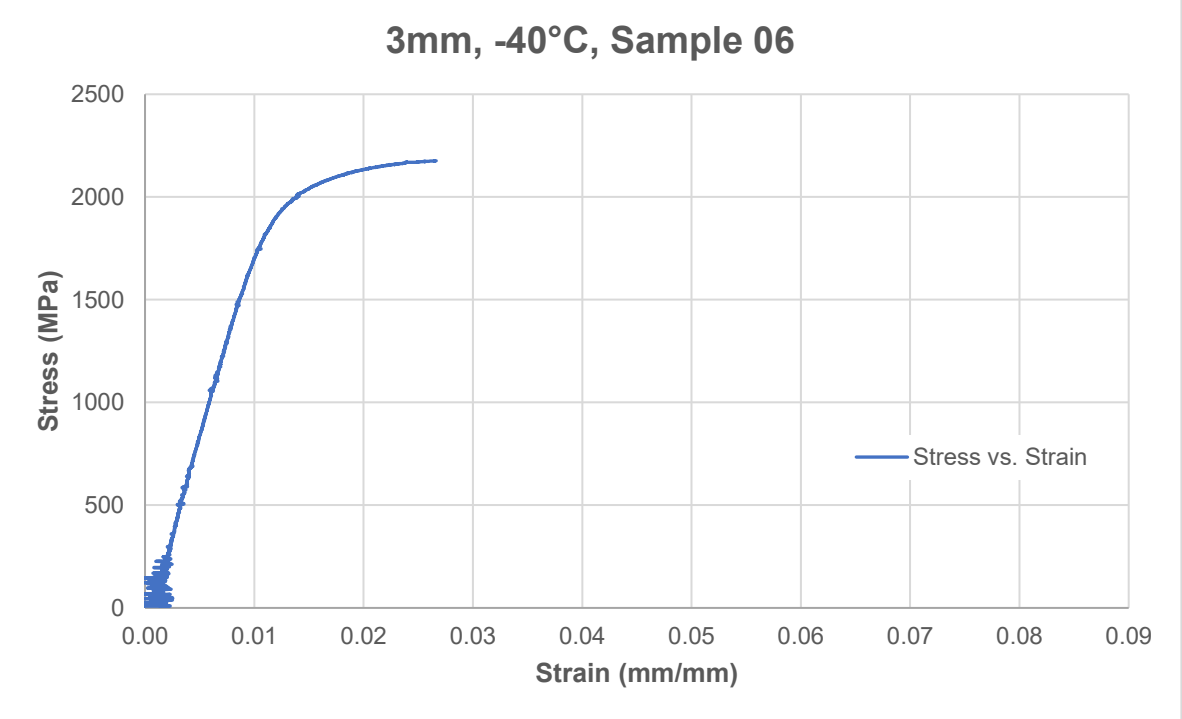
3mm, -40°C, Sample 06
Stress (MPa)
2500
2000
1500
1000
500
0
0.00
0.01
0.02
0.03
0.04
0.05
0.06
0.07
0.08
0.09
Strain (mm/mm)
Stress vs. Strain

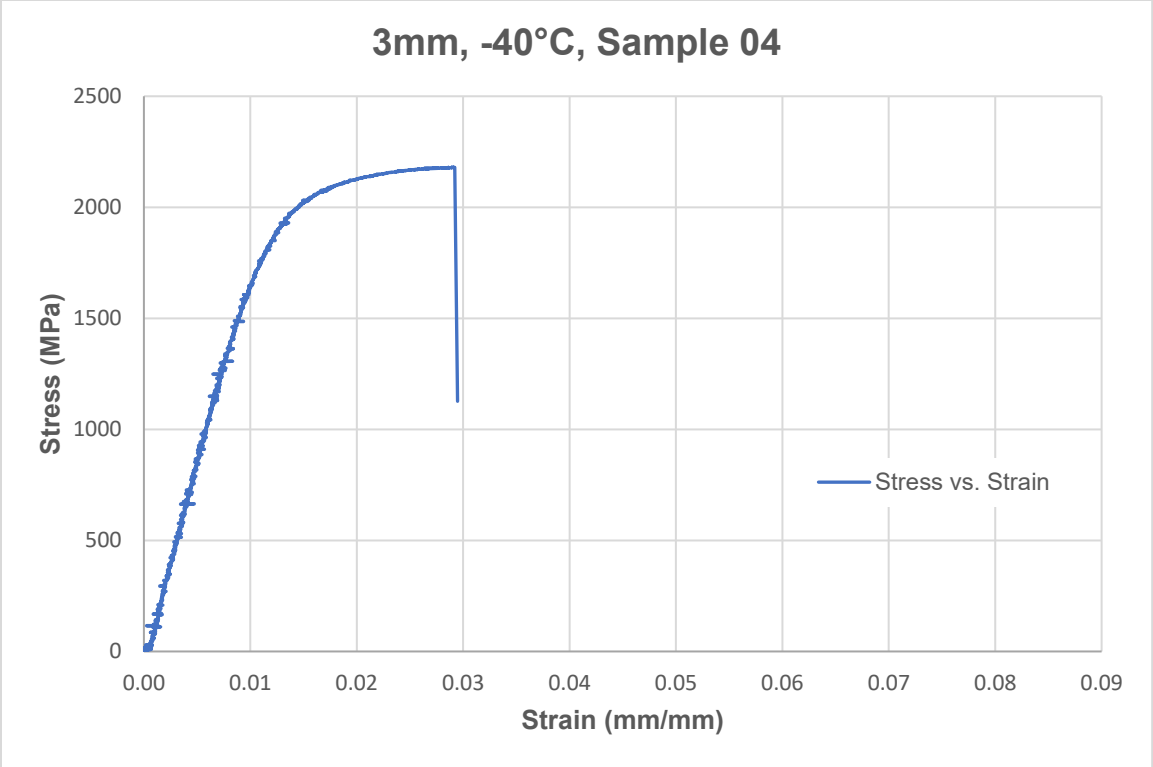
3mm, -40°C, Sample 04
2500
2000
1500
1000
500
0
Stress (MPa)
0.00
0.01
0.02
0.03
0.04
0.05
0.06
0.07
0.08
0.09
Strain (mm/mm)
Stress vs. Strain

B.4. 9mm Notch Specimens

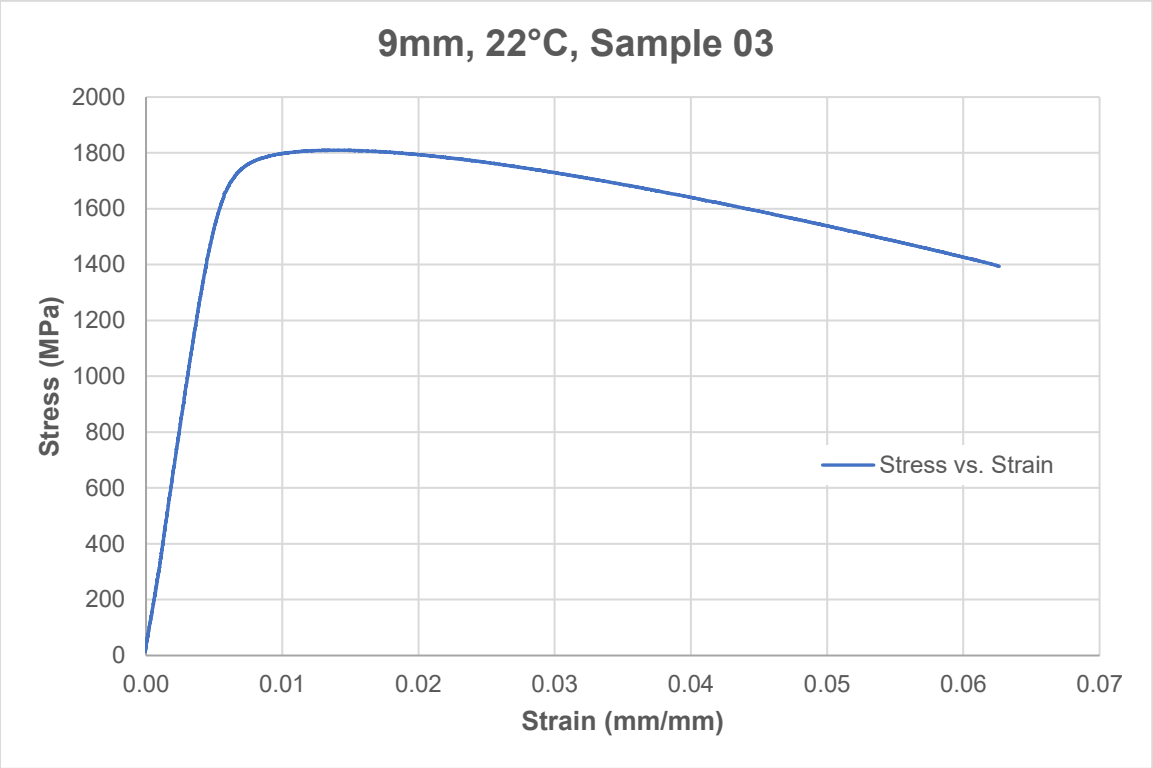

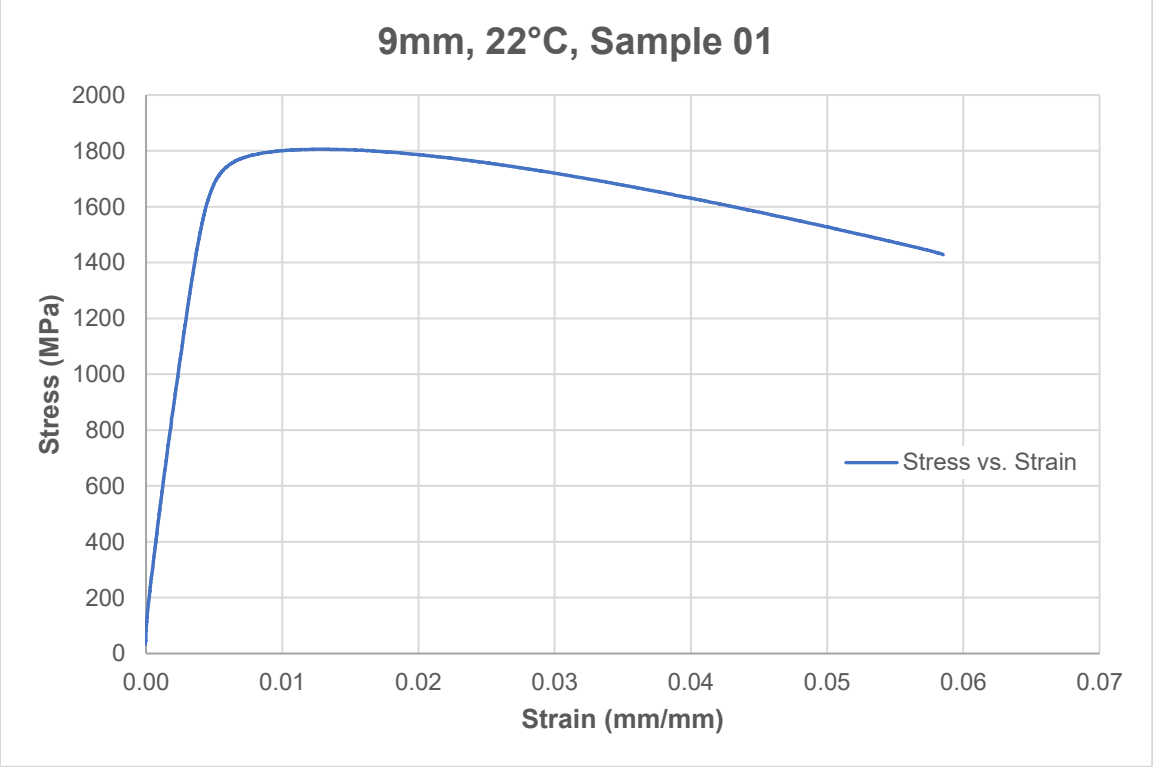

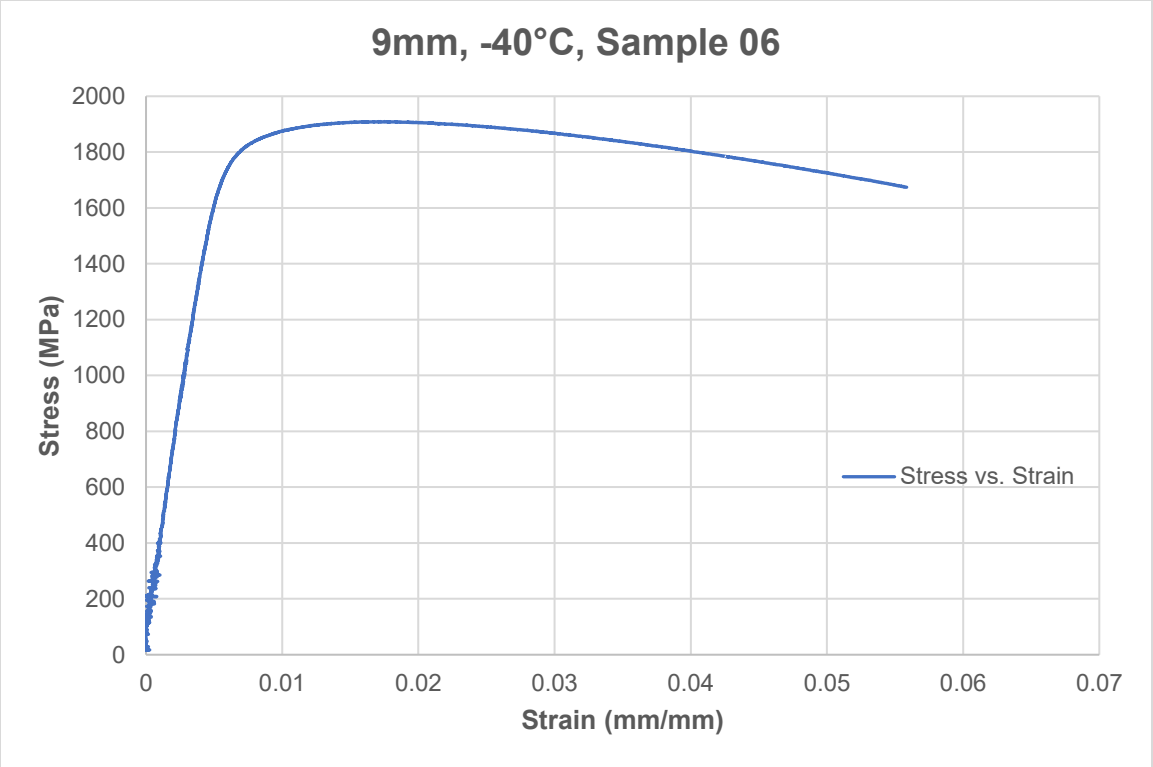
9mm, -40°C, Sample 06
Stress (MPa)
2000
1800
1600
1400
1200
1000
800
600
400
200
0
0
0.01
0.02
0.03
0.04
0.05
0.06
0.07
Strain (mm/mm)
Stress vs. Strain

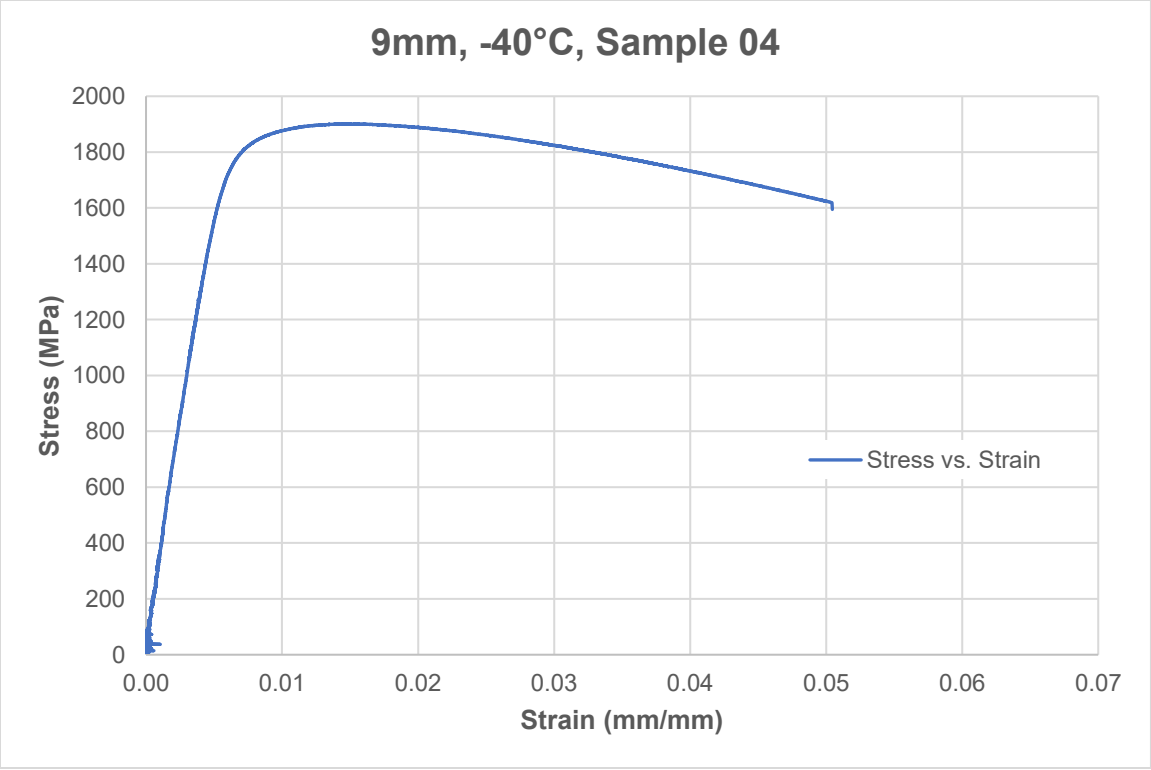
9mm, -40°C, Sample 04
Stress (MPa)
2000
1800
1600
1400
1200
1000
800
600
400
200
0
0.00
0.01
0.02
0.03
0.04
0.05
0.06
0.07
Strain (mm/mm)
Stress vs. Strain

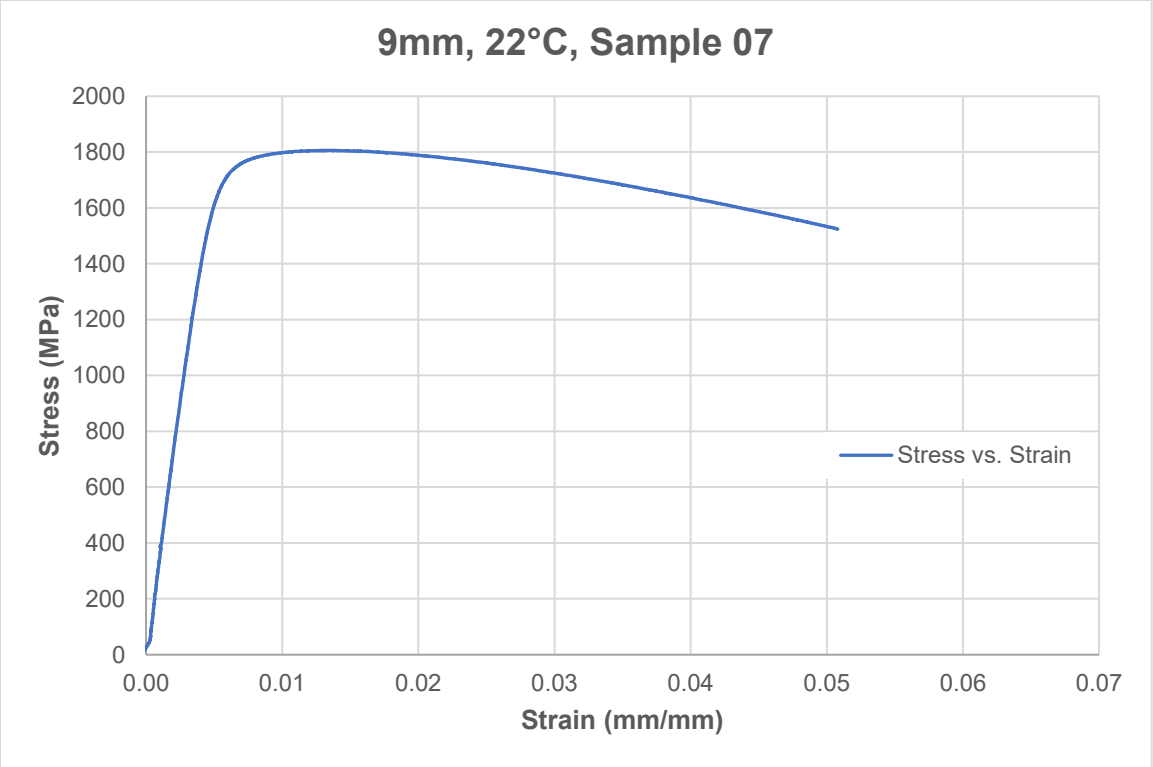

B.5. Flat-Grooved Plate Specimens

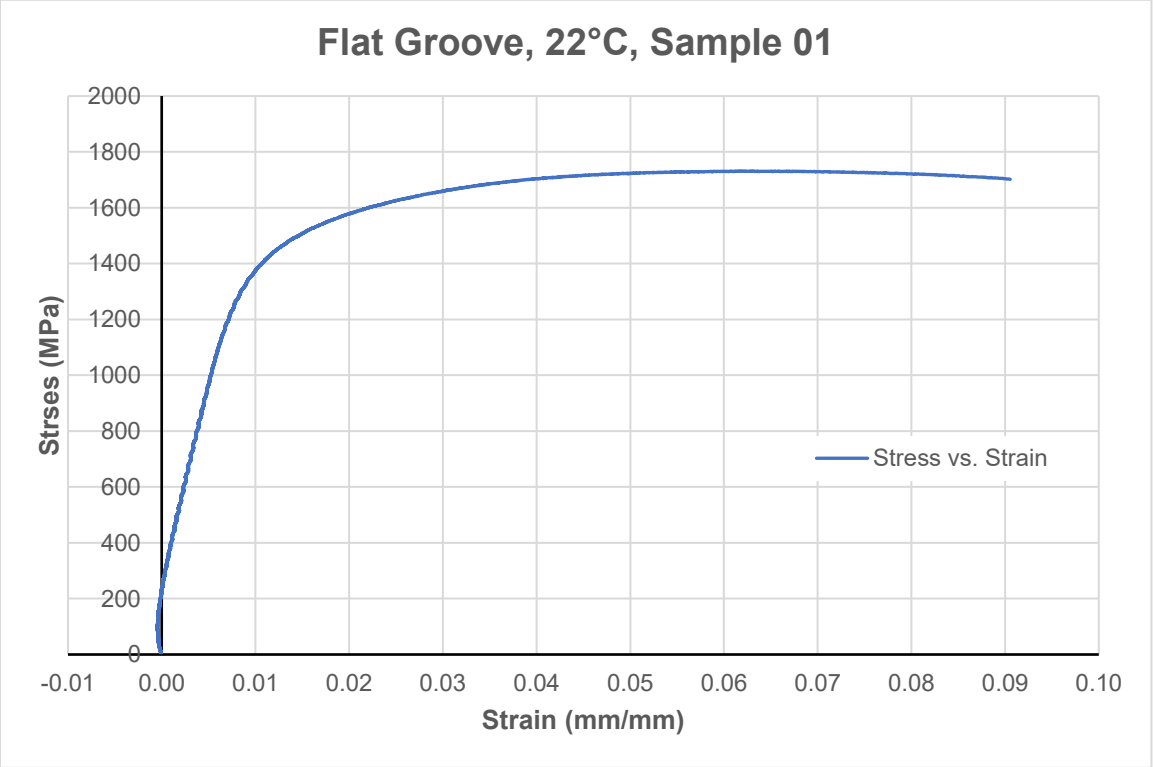

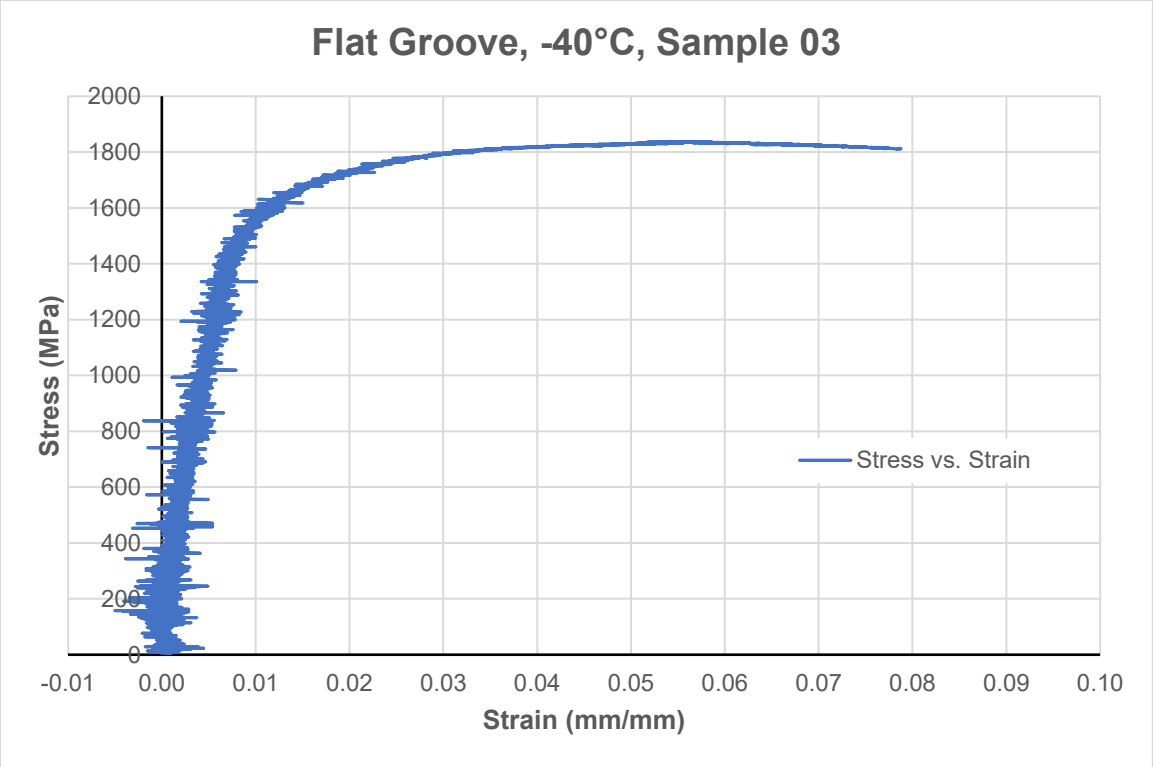
Flat Groove, -40°C, Sample 03
Stress (MPa)
2000
1800
1600
1400
1200
1000
800
600
400
200
0
-0.01
0.00
0.01
0.02
0.03
0.04
0.05
0.06
0.07
0.08
0.09
0.10
Strain (mm/mm)
Stress vs. Strain

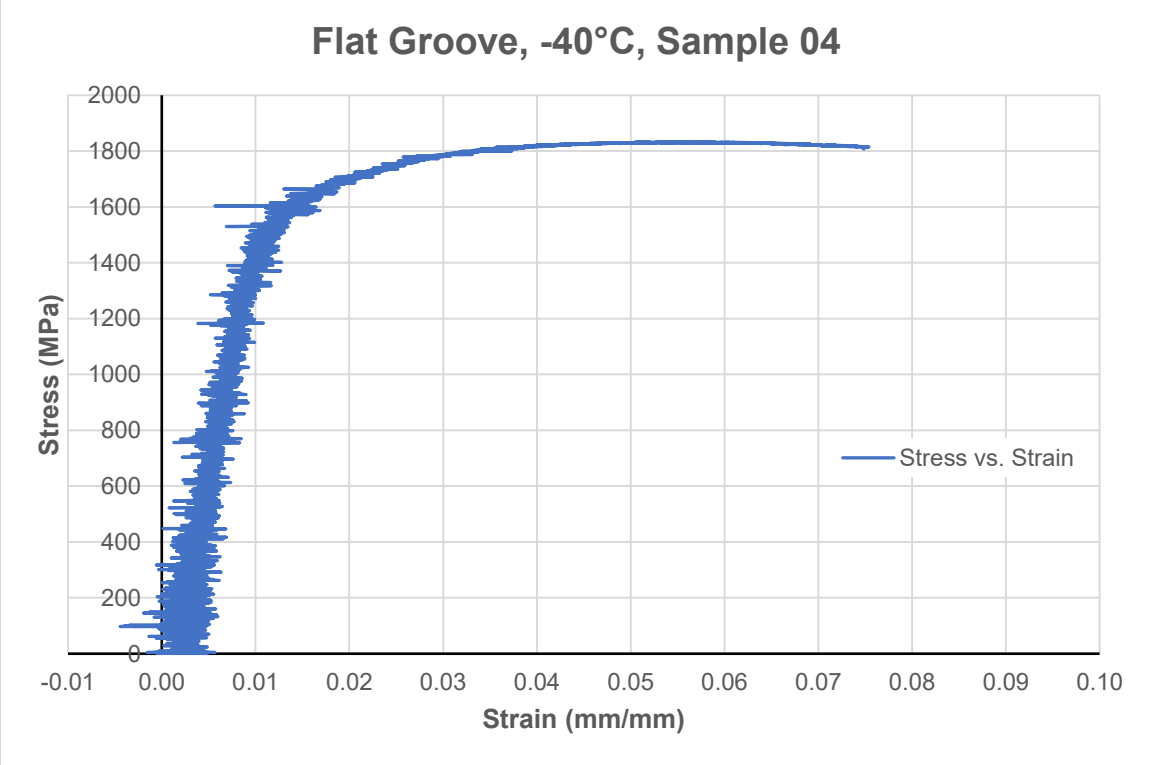
Flat Groove, -40°C, Sample 04
Stress (MPa)
2000
1800
1600
1400
1200
1000
800
600
400
200
0
-0.01
0.00
0.01
0.02
0.03
0.04
0.05
0.06
0.07
0.08
0.09
0.10
Strain (mm/mm)
Stress vs. Strain

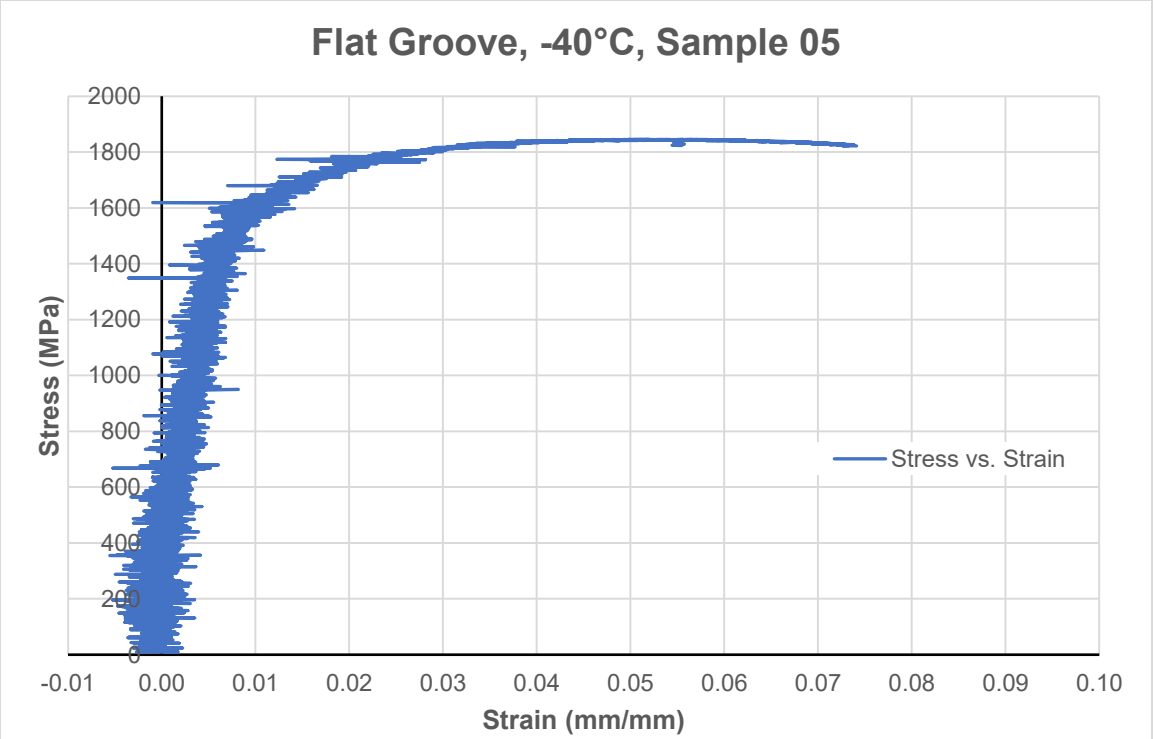

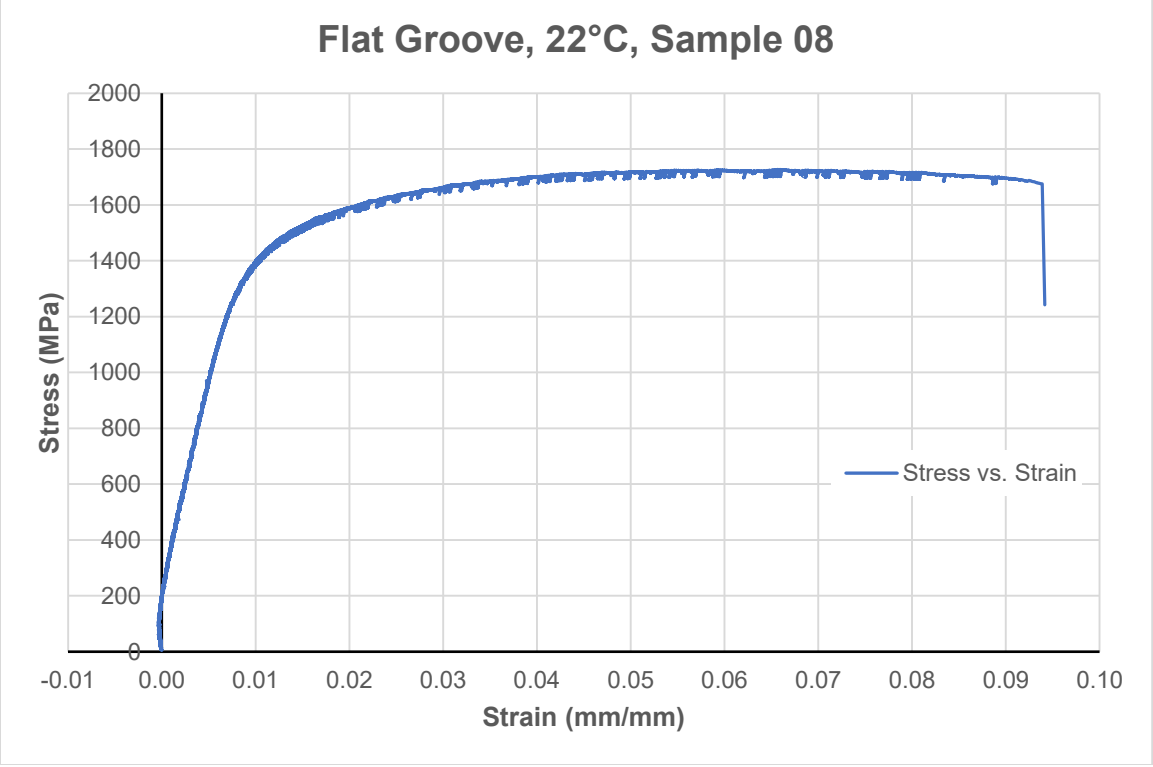

B.6. Shear Specimens

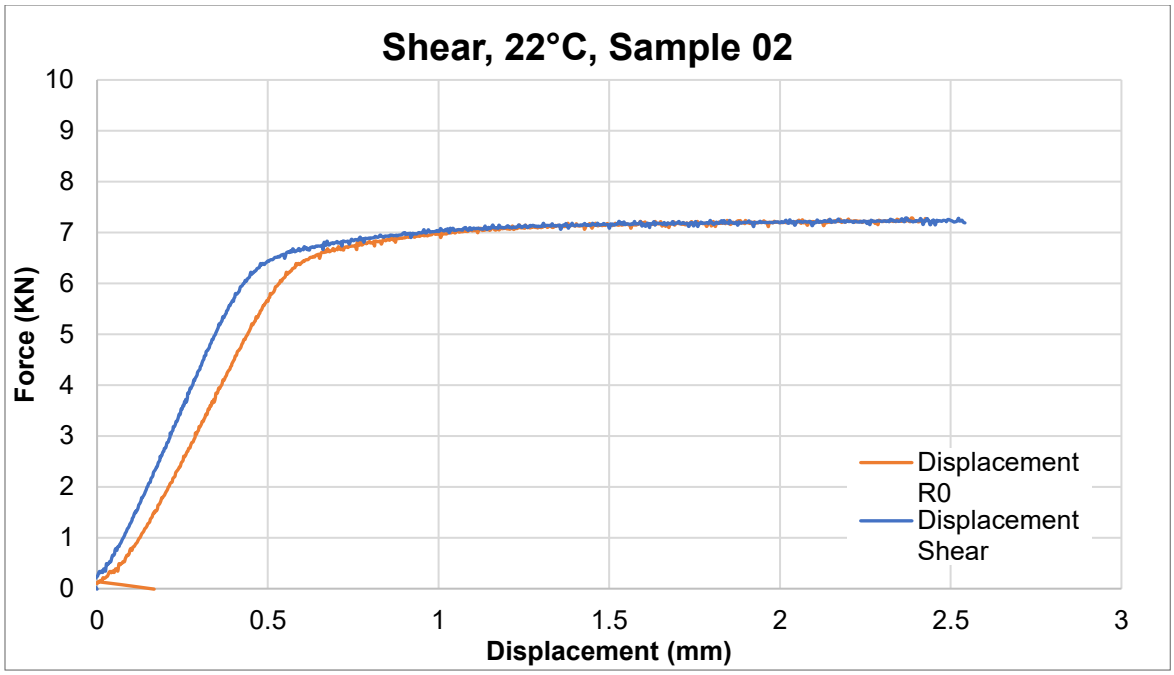
Shear, 22°C, Sample 02
Force (KN)
Displacement (mm)
Displacement R0
Displacement Shear

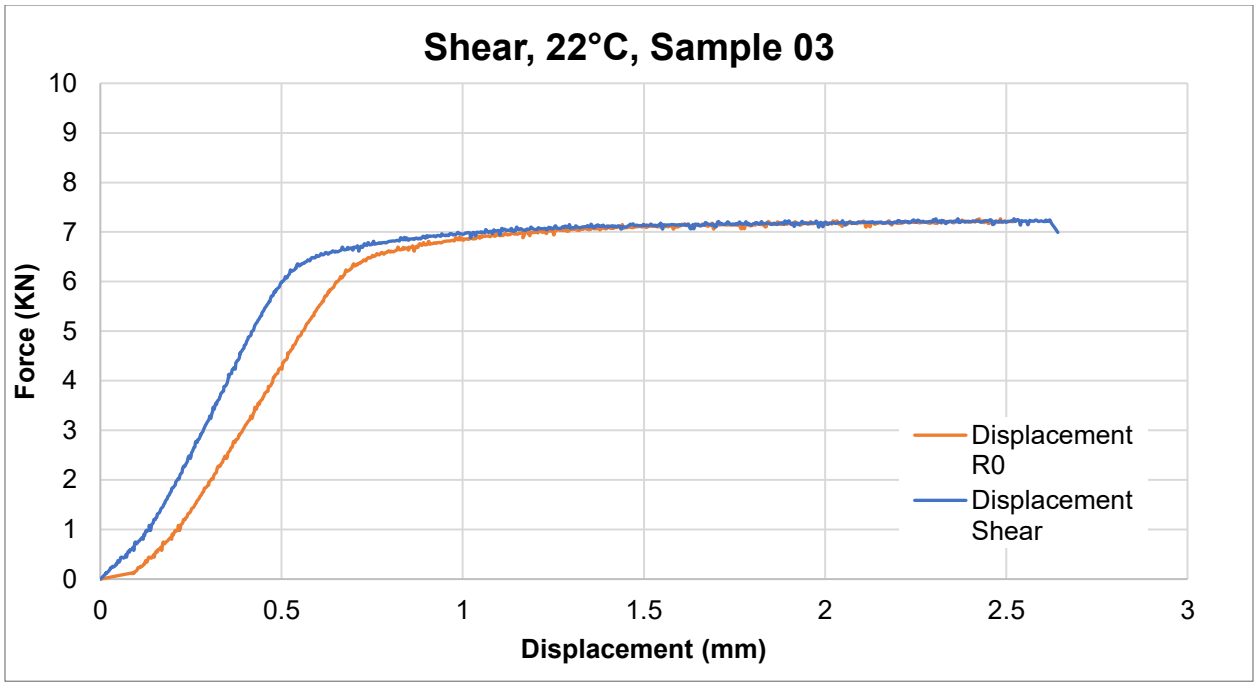
Shear, 22°C, Sample 03
Force (KN)
Displacement (mm)
Displacement R0
Displacement Shear

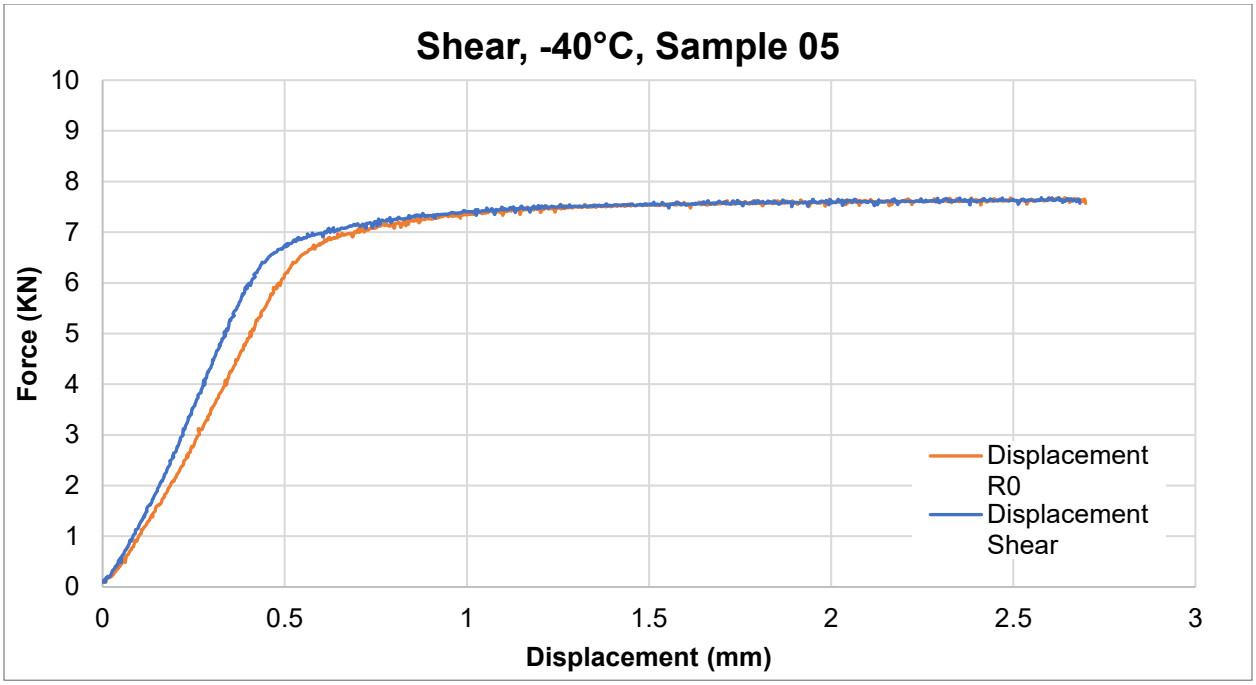
Shear, -40°C, Sample 05
Force (KN)
Displacement (mm)
Displacement R0
Displacement Shear

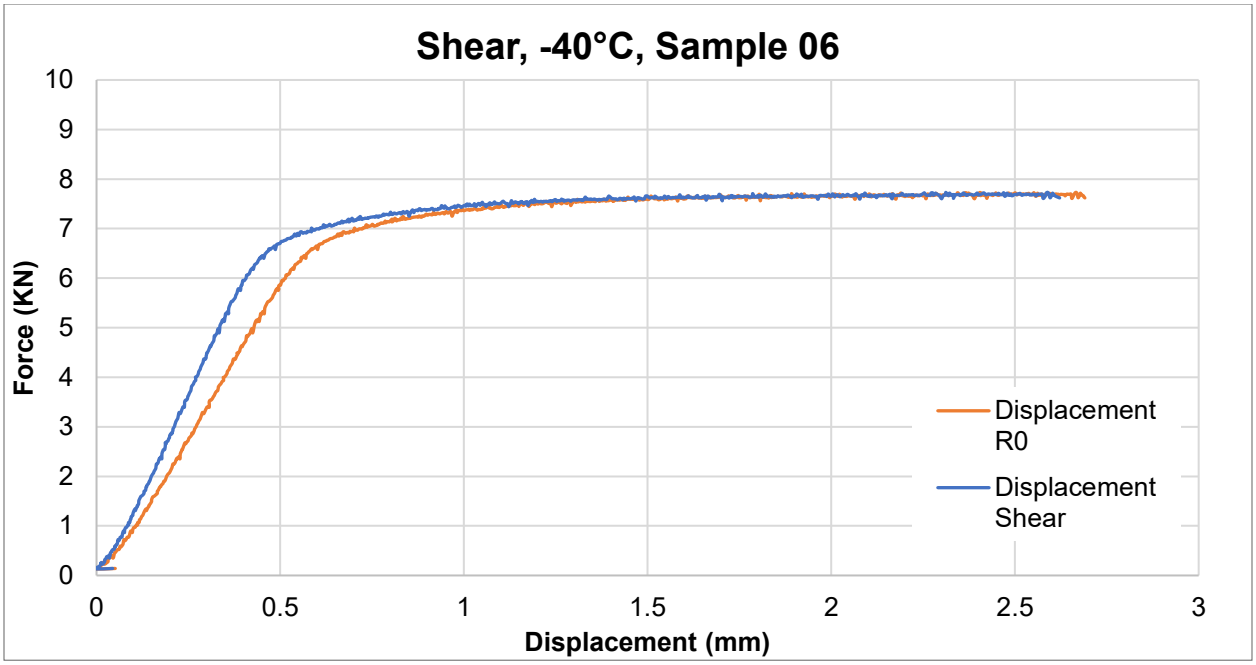
Shear, -40°C, Sample 06
Force (KN)
Displacement (mm)
Displacement R0
Displacement Shear

APPENDIX C. SEM AND OPTICAL IMAGES OF FRACTURED SPECIMENS

C.1. R5 Specimens

Figure A-7. Fracture Surface – R5 Parallel, 22°C, Sample 04

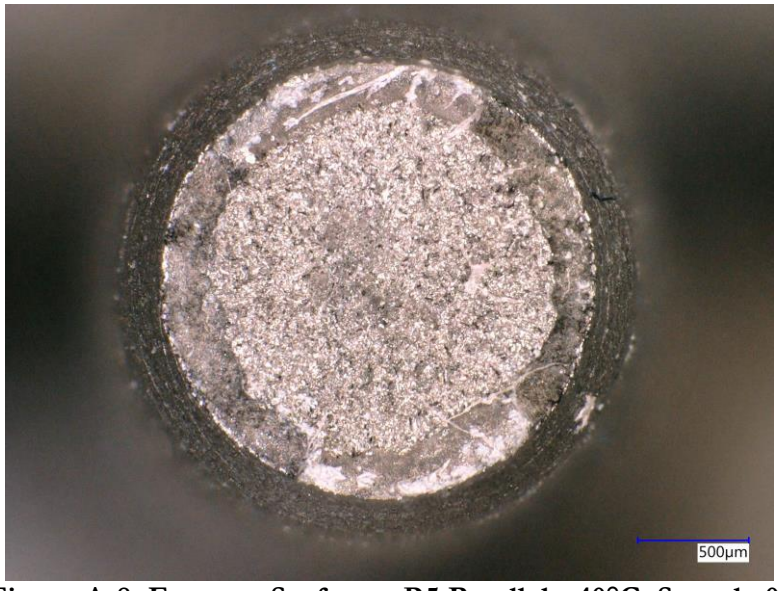

Figure A-8. Fracture Surface – R5 Parallel, -40°C, Sample 01

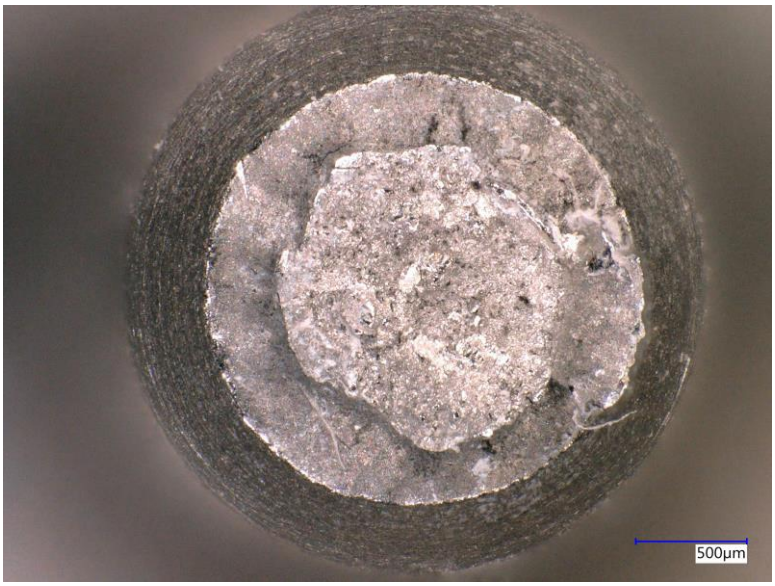

Figure A-9. Fracture Surface – R5 Radial, 22°C, Sample 15

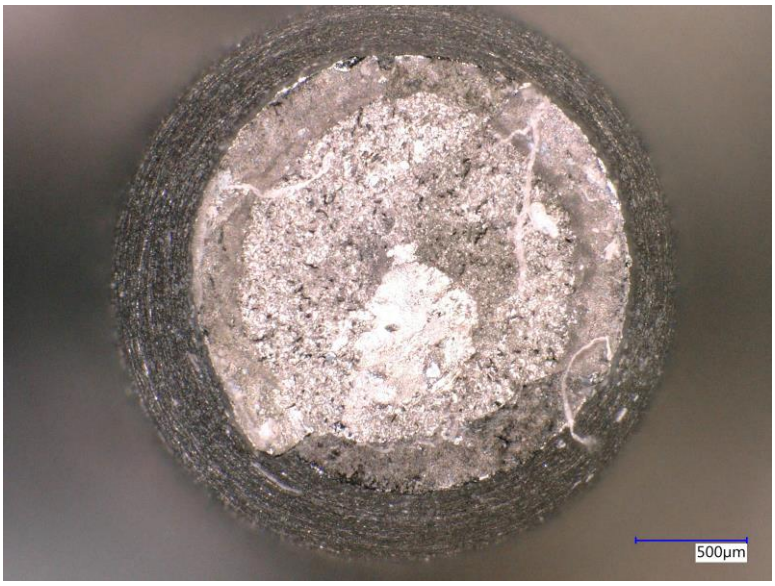

Figure A-10. Fracture Surface – R5 Radial, -40°C, Sample 12

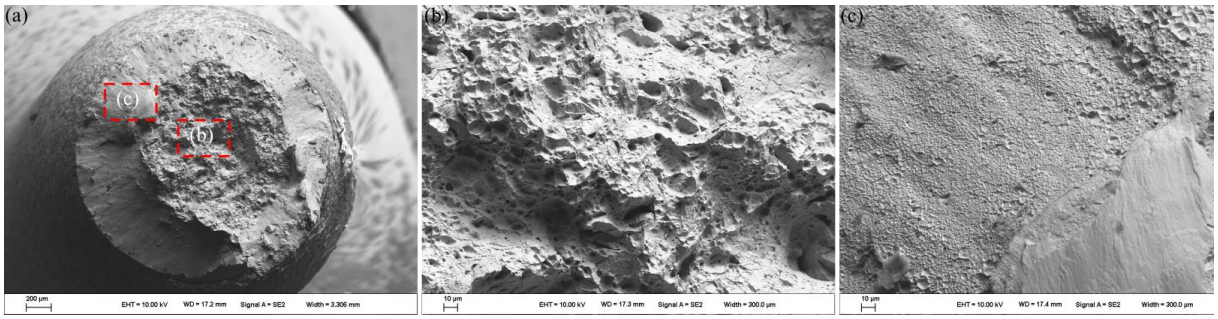

Figure A-11. Secondary electron images of the fracture surface of a R5 parallel sample tested at 22C are provided. A low-magnitude image of the entire fracture surface is show in (a). High-magnification images of the center (b) and shear lip (c) are also provided.

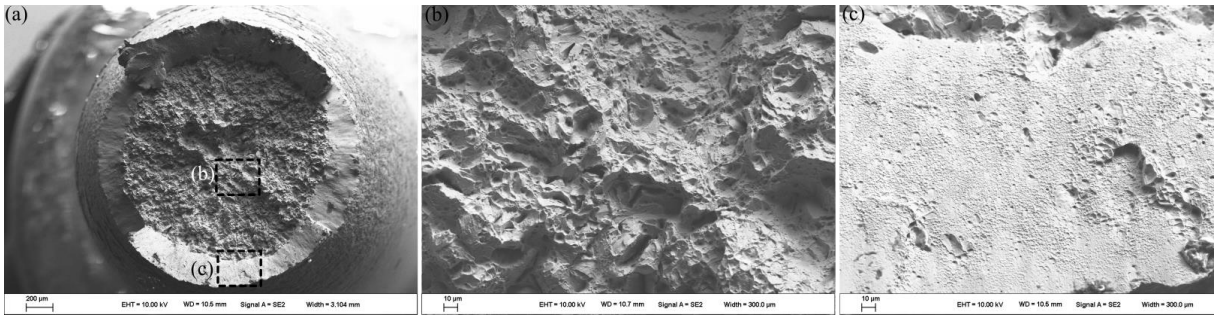

Figure A-12. Secondary electron images of the fracture surface of a R5 parallel sample tested at -40C are provided. A low-magnitude image of the entire fracture surface is show in (a). High-magnification images of the center (b) and shear lip (c) are also provided.

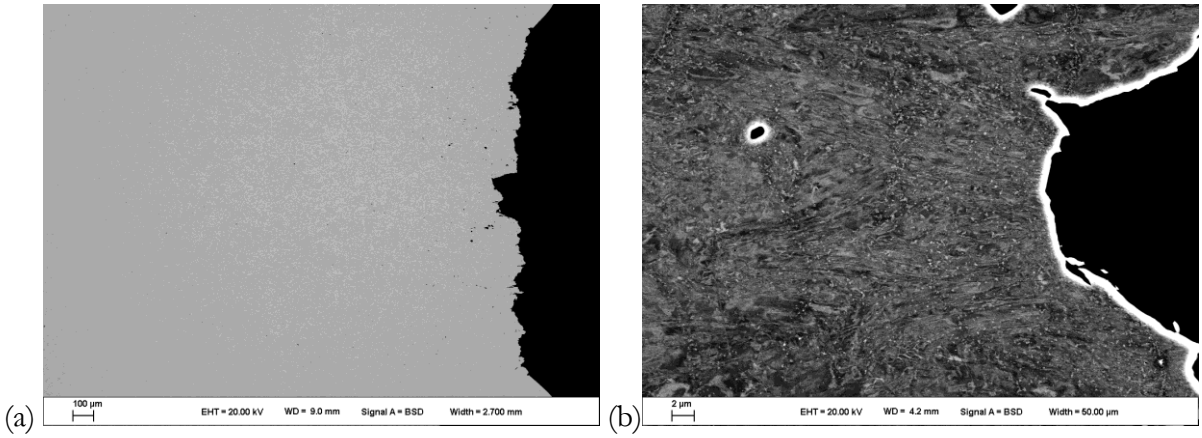

Figure A-13. ECCI images of a cross-sectioned R5 radial sample tested at -40C are provided. The fracture surface can be seen on the right side of both images. (a) shows a low magnification image (the image width is 2.7 mm) and (b) shows a high magnification image (the image width is 0.05 mm). Voids near the fracture surface can be seen in both images.

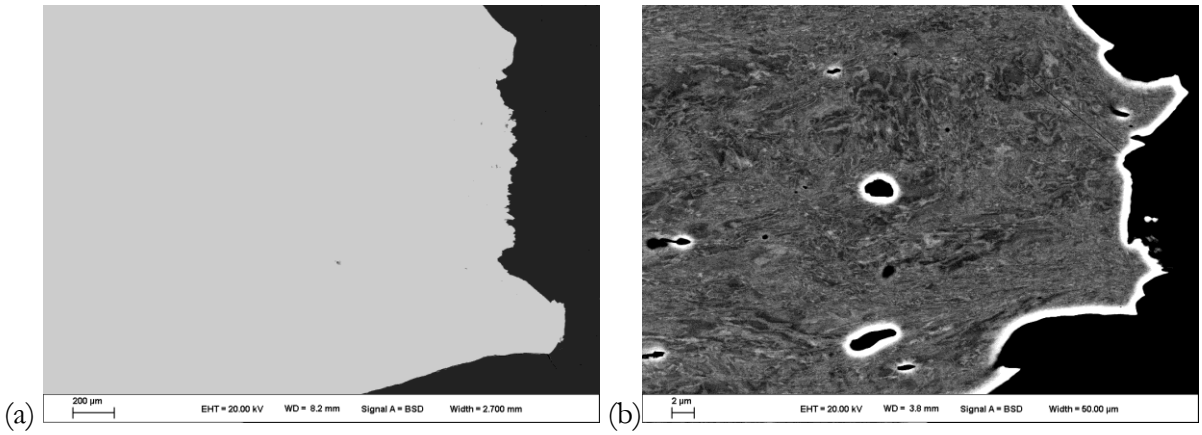

Figure A-14. ECCI images of a cross-sectioned R5 parallel sample tested at 22C are provided. The fracture surface can be seen on the right side of both images. (a) shows a low magnification image (the image width is 2.7 mm) and (b) shows a high magnification image (the image width is 0.05 mm). Voids near the fracture surface can be seen in both images.

C.2. 3mm Notch Specimens

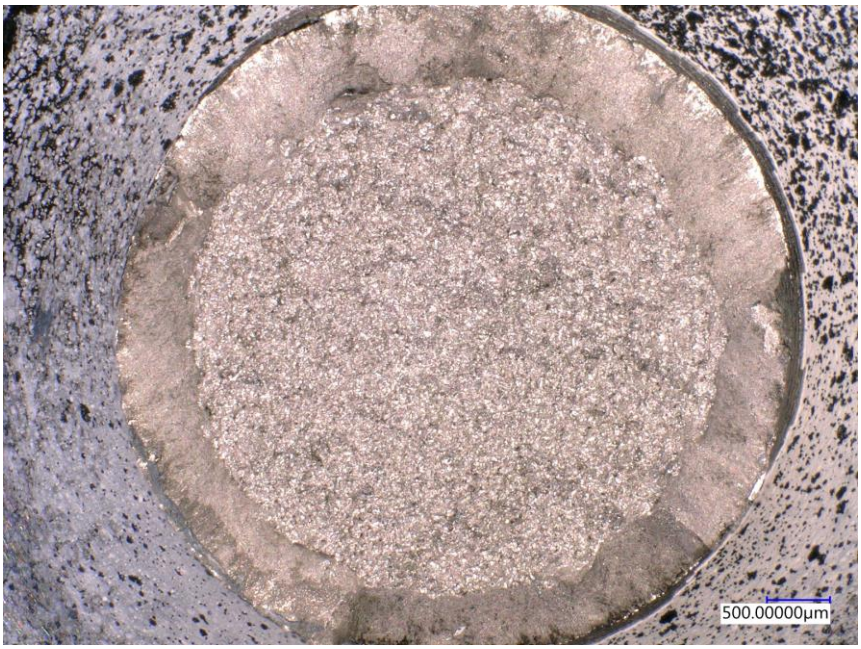

Figure A-15. Fracture Surface – 3mm, 22°C, Sample 01

Figure A-16. Fracture Surface – 3mm, -40°C, Sample 04

C.3. 9mm Notch Specimens

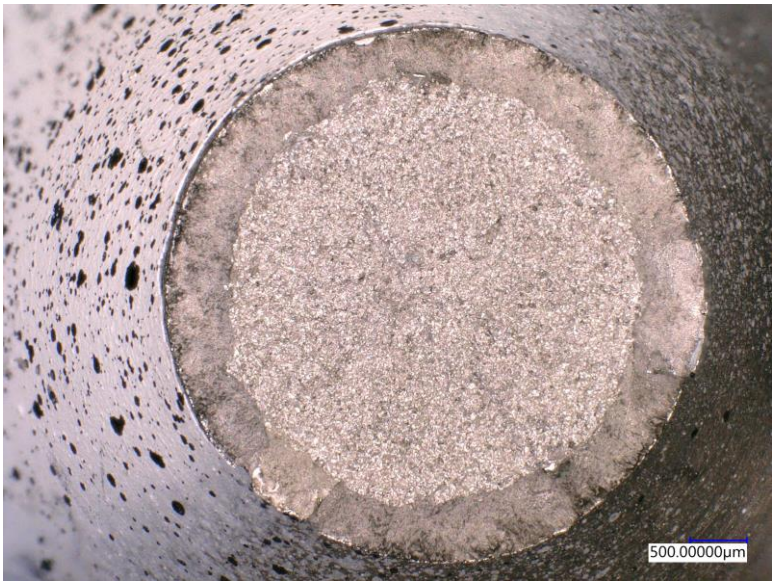

Figure A-17. Fracture Surface – 9mm, 22°C, Sample 01

Figure A-18. Fracture Surface – 9mm, -40°C, Sample 04

C.4. Flat Groove Specimens

Figure A-19. Fracture Surface – Flat Groove, 22°C, Sample 01

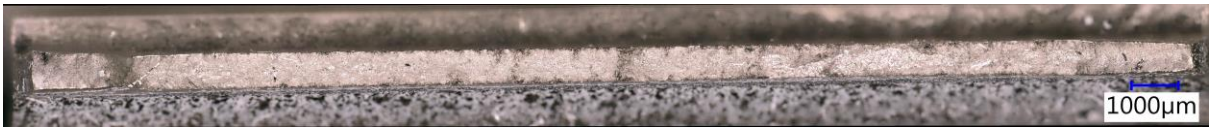

Figure A-20. Fracture Surface – Flat Groove, -40°C, Sample 03

C.5. Shear Specimens

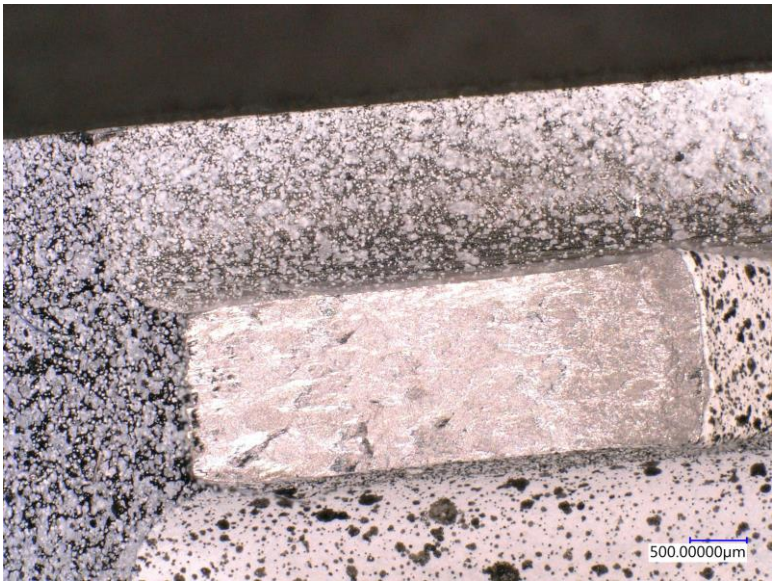

Figure A-21. Fracture Surface – Shear, 22°C, Sample 01

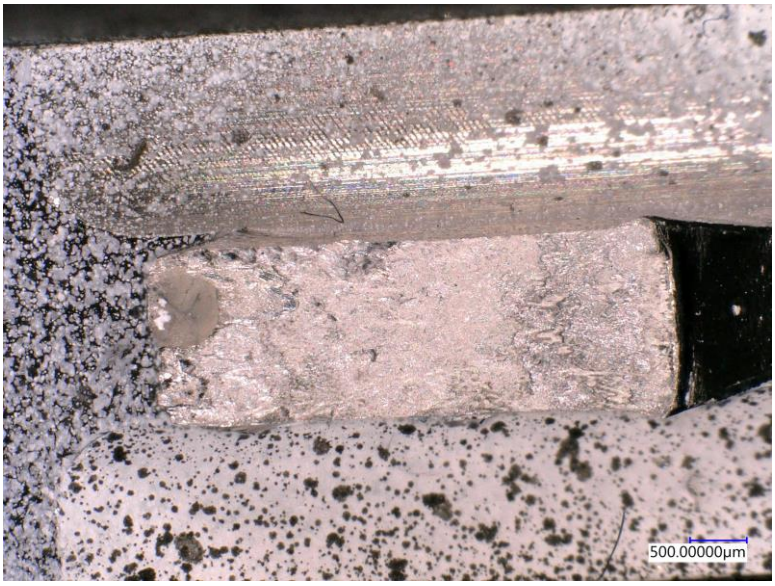

Figure A-22. Fracture Surface – Shear, -40°C, Sample 04

APPENDIX D. REPRESENTATIVE PLOTS OF FORCE DISPLACEMENT

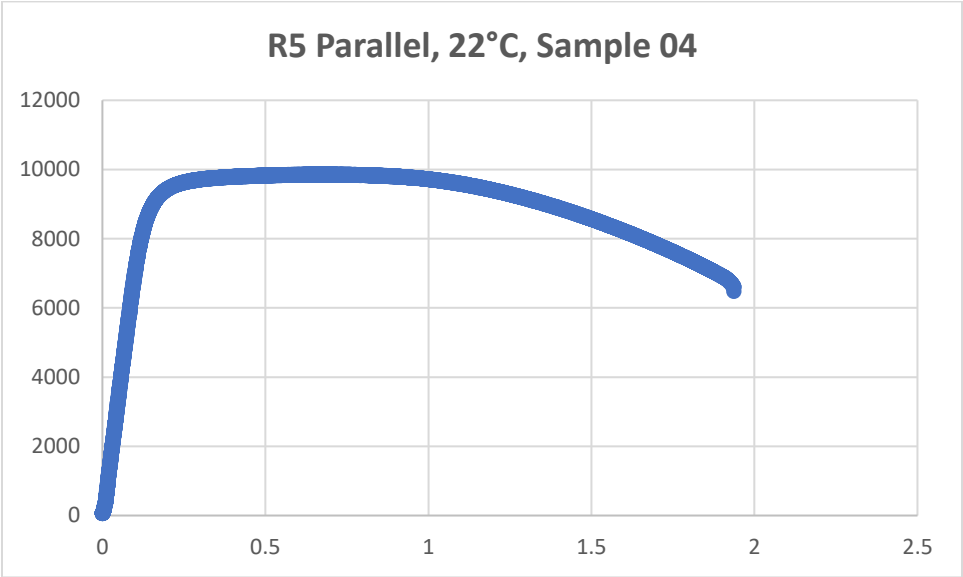

Figure A-23. R5 parallel, 22°C, Sample 04.

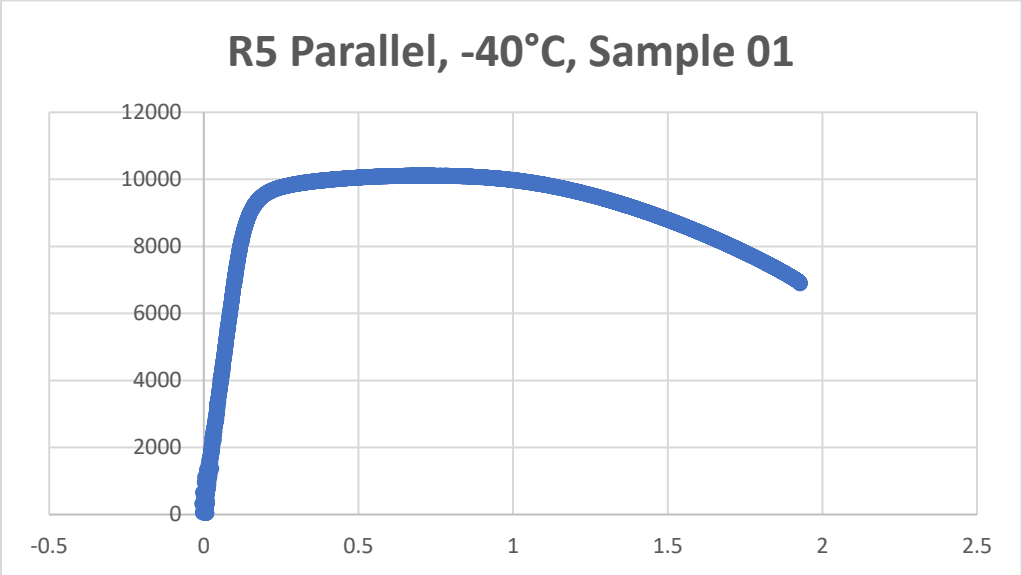

Figure A-24. R5 parallel, -40°C, Sample 01.

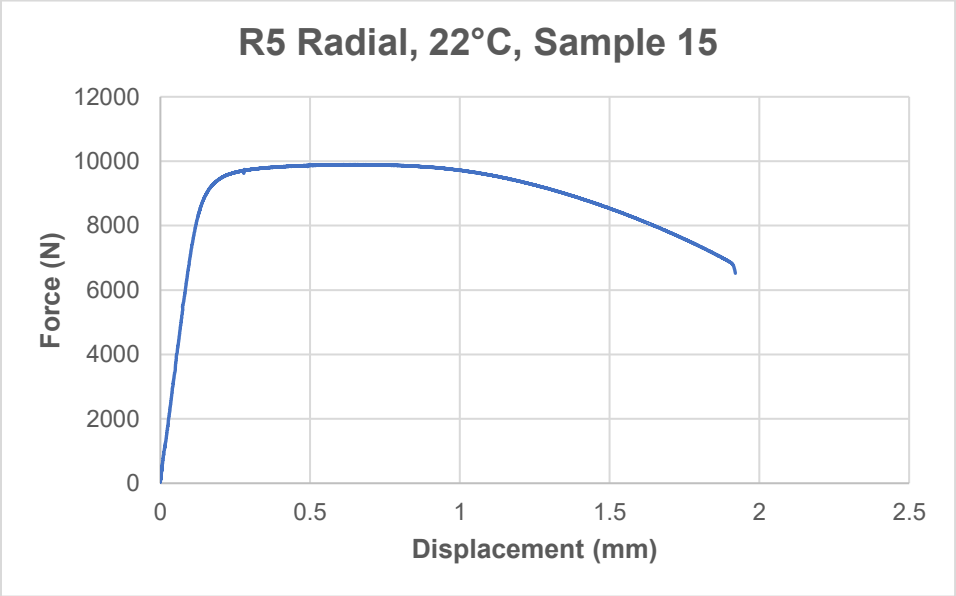

Figure A-25. R5 radial, 22°C, Sample 15.

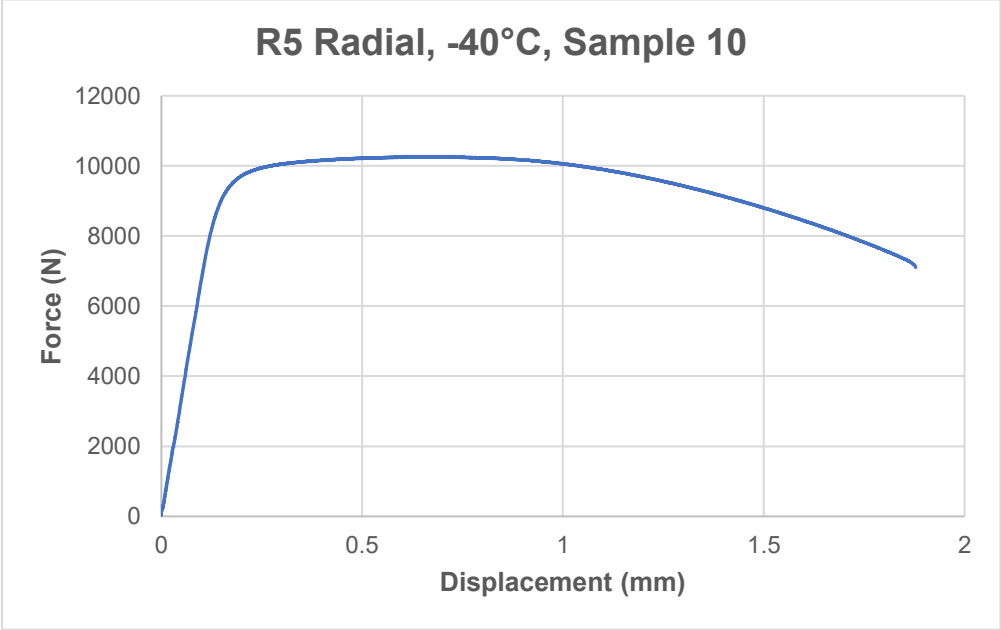

Figure A-26. R5 radial, -40°C, Sample 10.

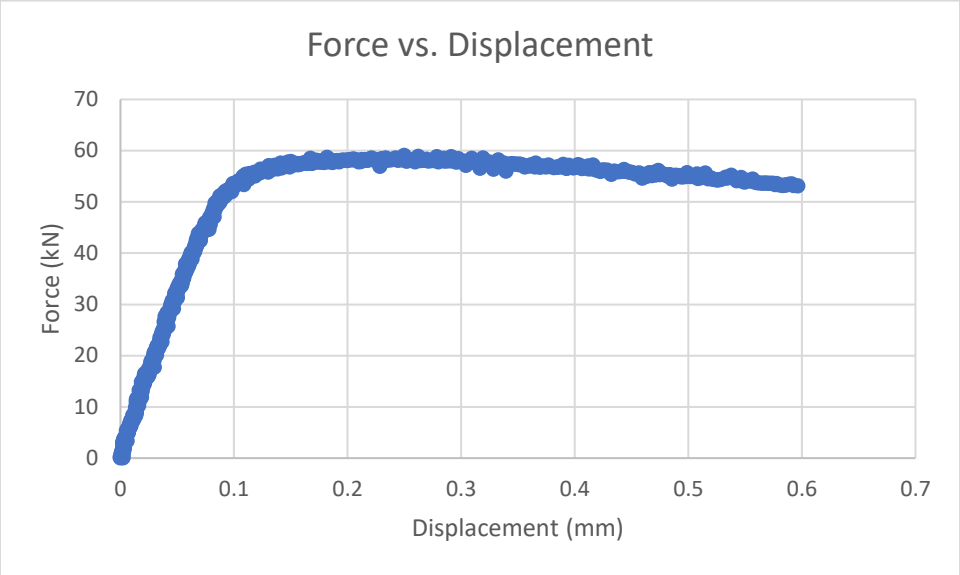

Figure A-27. 3mm, 22°C, Sample 01.

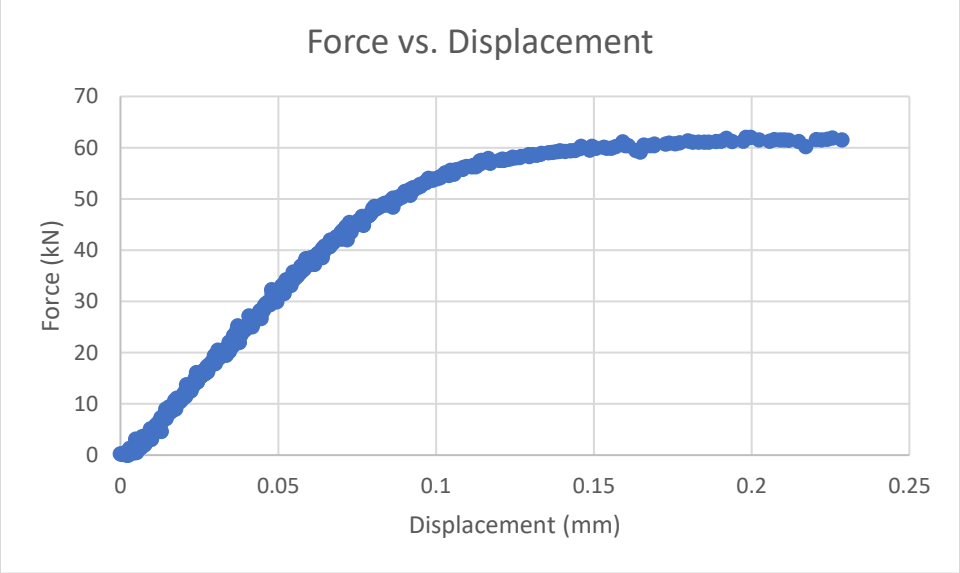

Figure A-28. 3mm, -40°C, Sample 04.

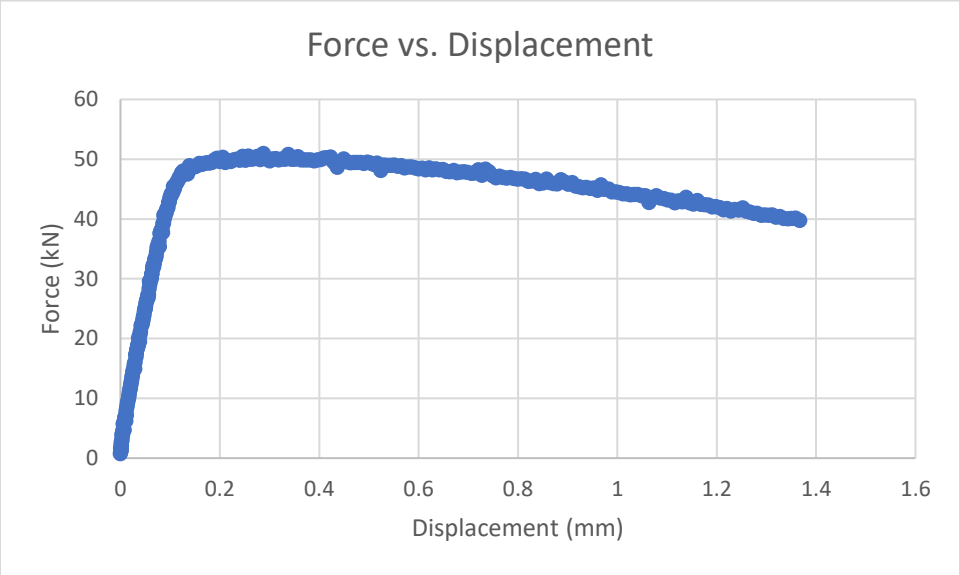

Figure A-29. 9mm, 22°C, Sample 01.

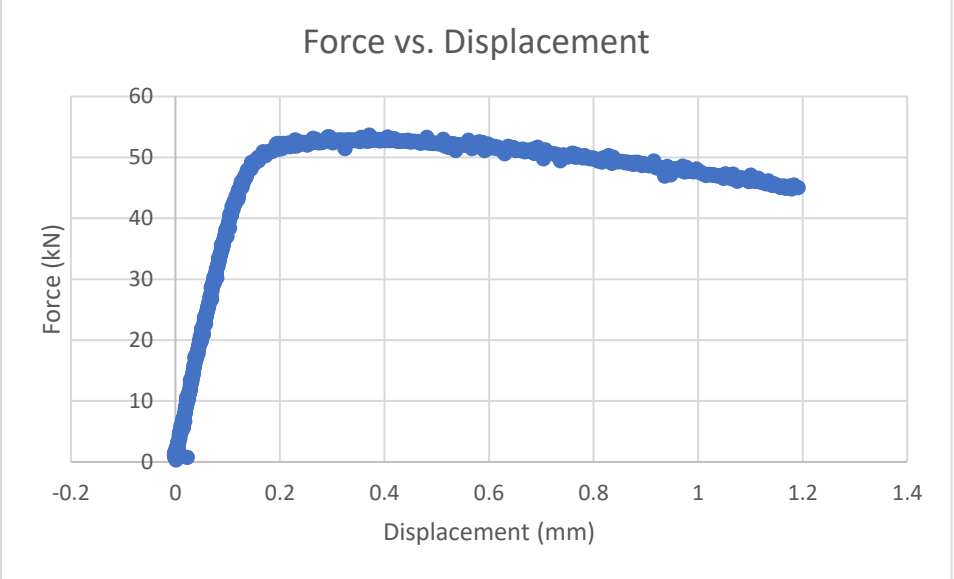

Figure A-30. 9mm, -40°C, Sample 04.

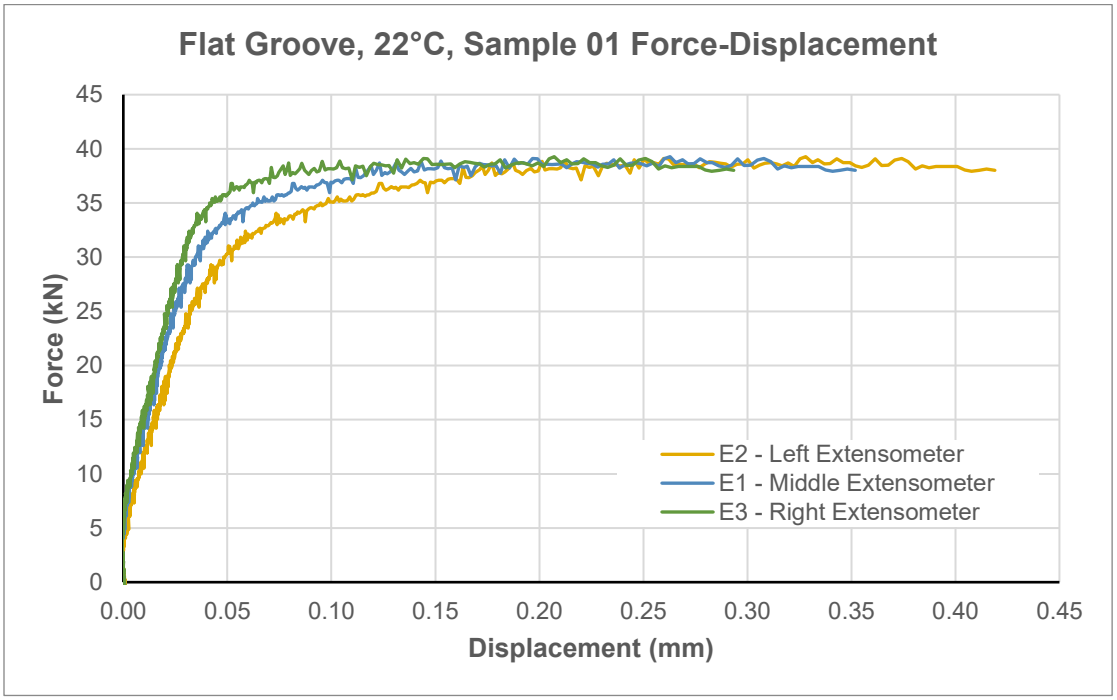

Figure A-31. Flat Groove, 22°C, Sample 01. Displacement values measured relative to the three extensometers shown in Figure 2-7 are reported.

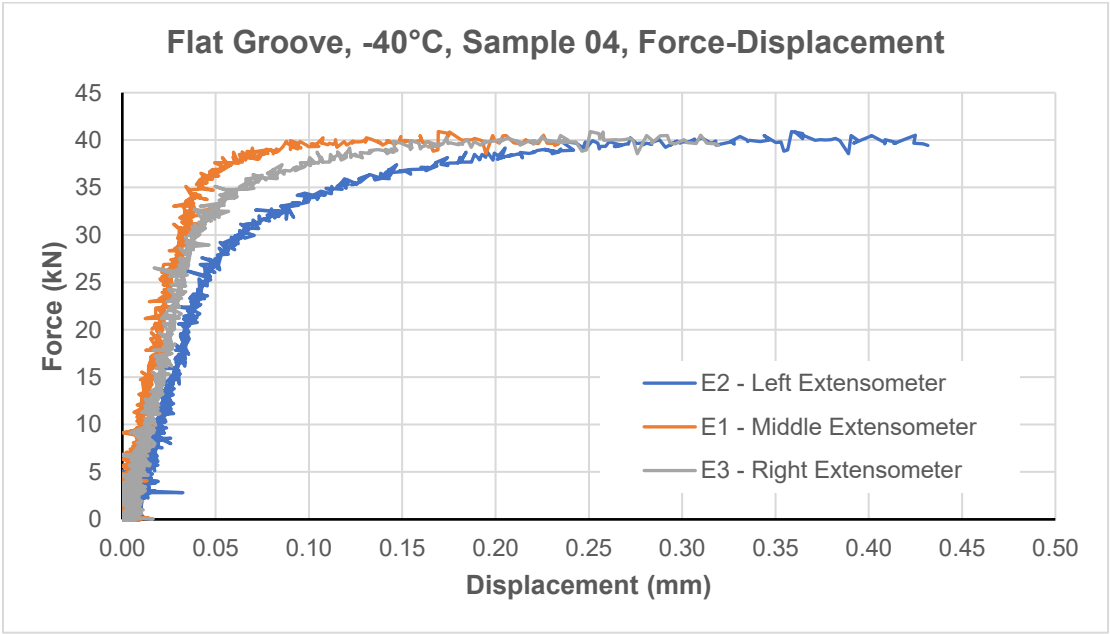

Figure A-32. Flat Groove, -40°C, Sample 04. Displacement values measured relative to the three extensometers shown in Figure 2-7 are reported.

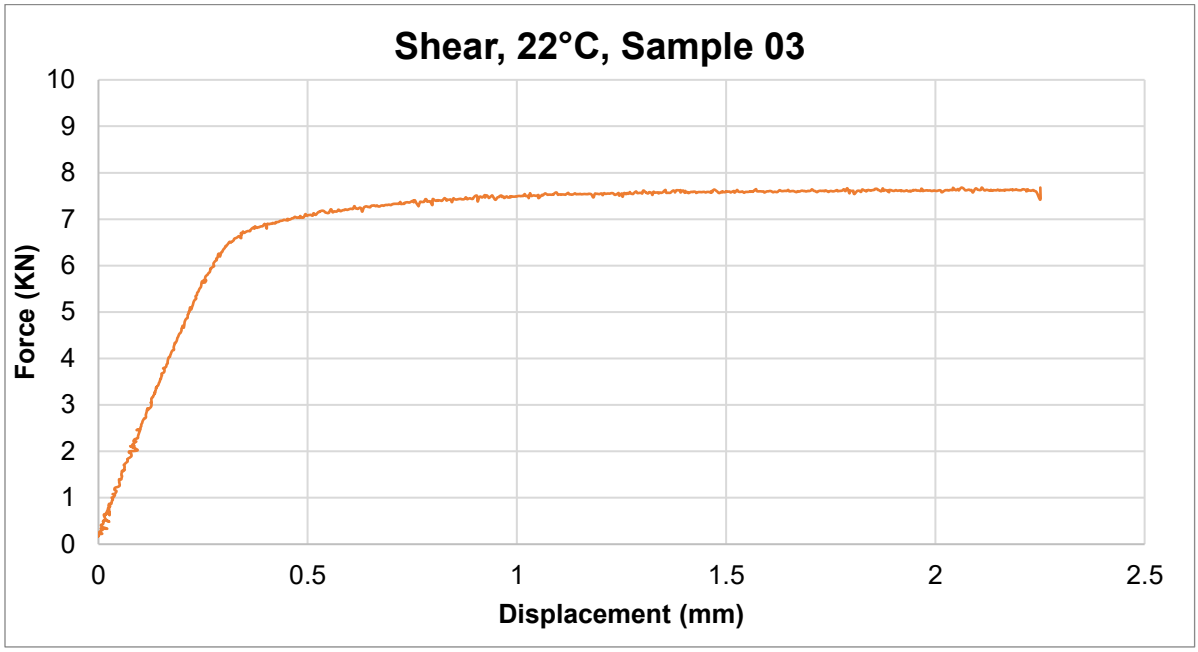

Figure A-33. Force-displacement curve, Shear, 22°C, Sample 03.

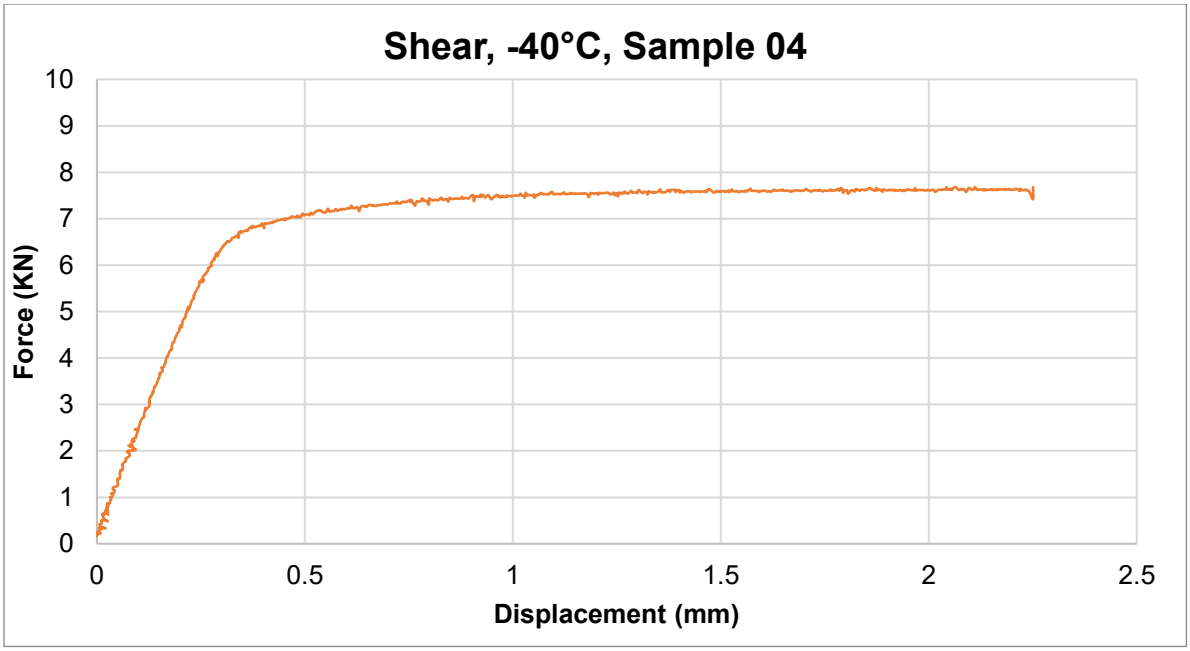

Figure A-34. Force-displacement curve, Shear, -40°C, Sample 04.

This page left blank

This page left blank

DISTRIBUTION

Email—Internal

Name	Org.	Sandia Email Address
Robert Kalan	08854	rjkalan@sandia.gov
Technical Library	01977	sanddocs@sandia.gov

This page left blank

Sandia National Laboratories

Sandia National Laboratories is a multimission laboratory managed and operated by National Technology & Engineering Solutions of Sandia LLC, a wholly owned subsidiary of Honeywell International Inc. for the U.S. Department of Energy's National Nuclear Security Administration under contract DE-NA0003525.